

UNIVERSITÄTSKLINIKUM HAMBURG-EPPENDORF

Zentrum für Experimentelle Medizin

Institut für Experimentelle Pharmakologie und Toxikologie

Prof. Dr. med. Thomas Eschenhagen

**Characterization of a novel interaction between
four-and-a-half-LIM domains 2 and
cardiomyopathy-associated protein 5 in cardiac
myocytes**

Dissertation

zur Erlangung des Grades eines Doktors der Medizin
an der Medizinischen Fakultät der Universität Hamburg.

vorgelegt von:

Josef Schnittger

aus Parchim

Hamburg 2019

Angenommen von der
Medizinischen Fakultät der Universität Hamburg am:
05.11.2020

Veröffentlicht mit Genehmigung der
Medizinischen Fakultät der Universität Hamburg.

Prüfungsausschuss, der/die Vorsitzende:
Prof. Dr. Friederike Cuello

Prüfungsausschuss, zweite/r Gutachter/in:
PD Dr. Diana Lindner

Table of contents

1 Introduction	5
1.1 Heart failure	5
1.2 The heart	6
1.3 β -adrenoceptor signaling in the heart	7
1.4 β -adrenoceptor signaling in heart failure	10
1.5 Scaffolding proteins	12
1.6 Cardiomyopathy-associated protein 5	15
1.7 Four and a half LIM proteins	16
1.7.1 FHL1 in cardiac (patho-)physiology	17
1.7.2 FHL2 in cardiac (patho-)physiology	18
1.8 Aim	20
2 Materials and methods	21
2.1 Materials	21
2.1.1 Chemicals and reagents	21
2.1.2 Buffers	23
2.1.3 Kits	26
2.1.4 Antibodies	26
2.1.5 Consumables and equipment	27
2.2 Methods	31
2.2.1 Comprehensive methods	31
2.2.1.1 Sodium dodecyl sulfate polyacrylamide gel electro- phoresis (SDS-PAGE)	31
2.2.1.2 Western immunoblotting	31
2.2.2 Analysis of human heart samples	32
2.2.2.1 mRNA expression analysis	32
2.2.2.2 Protein expression analysis via SDS-PAGE and western immunoblotting	32
2.2.3 PCR cloning and protein expression of recombinant <i>CMYA5</i> moieties	33
2.2.3.1 Reverse transcription	33
2.2.3.2 Polymerase chain reaction (PCR)	33
2.2.3.3 Directional cloning and transformation	34
2.2.3.4 Protein expression and purification of recombinant	

CMYA5 moieties	36
2.2.3.5 Protein expression and purification of recombinant GST-FHL2	38
2.2.4 Investigation of the FHL2-CMYA5 interaction	39
2.2.4.1 Pull-down assay	39
2.2.4.2 Peptide array	39
2.2.5 Analysis of adult rat ventricular myocytes	41
2.2.5.1 Immunocytochemistry and confocal microscopy	41
2.2.5.2 Duolink [®] assay	42
2.2.6 Cell size measurement of stimulated neonatal rat ventricular myocytes pre-treated with disrupting peptide	43
3 Results	44
3.1 Analysis of mRNA and protein levels of CMYA5 in human left ventricular heart tissue samples	44
3.1.1 mRNA expression levels	44
3.1.2 Protein expression levels	45
3.2 PCR cloning and protein expression of recombinant CMYA5 moieties	46
3.2.1 PCR	46
3.2.2. Cloning of <i>CMYA5</i> cDNA moieties into Champion [™] pET 151 D-TOPO vector and transformation into One Shot [®] TOP10 chemically competent <i>E. coli</i>	48
3.2.3 Recombinant protein expression	49
3.3 Investigation of the FHL2-CMYA5 interaction	51
3.3.1 Pull-down assays	51
3.3.2 Identification of the FHL2 binding sites of CMYA5 by peptide array	53
3.4 Subcellular localization of CMYA5 and FHL2 in ARVM	56
3.5 Analysis of CMYA5 and FHL2 co-localization of CMYA5 and FHL2 by Duolink [®] technology	59
3.6 Cell surface area measurements of neonatal rat ventricular myocytes exposed to peptides in order to disrupt the FHL2-CMYA5 interaction in response to neurohumoral stimulation	62

4 Discussion	64
4.1 FHL2 expression is downregulated in end-stage heart failure, while CMYA5 expression is upregulated	64
4.2 FHL2 and CMYA5 expression is upregulated by pro-hypertrophic stimuli	66
4.3 FHL2 and CMYA5 are associated with sarcomeric structures of cardiac myocytes	67
4.4 CMYA5 is an intrinsically disordered protein (IDP) and could be a flexible linker	67
4.5 FHL2 and CMYA5 are interaction partners in cardiac myocytes.....	70
4.6 FHL2-CMYA5 interaction occurs near the sarcomeric Z-disc of cardiac myocytes	71
5 Conclusions	73
I Abstract/Zusammenfassung.....	75
II List of abbreviations	76
III List of figures	79
IV List of tables	80
V Bibliography	81
VI Appendices	88
Acknowledgements	97
Curriculum vitae	98
Eidesstattliche Versicherung	99

1 Introduction

1.1 Heart failure

Heart failure (HF) is defined as the inability of the heart to circulate blood effectively enough to meet the body's metabolic needs¹. The clinical staging is based on the New York Heart Association's classification, with the phenotype varying from no or mild symptoms during physical activity in early stages (class I-II) to severe disabilities and bedriddenness for late or end stage HF (class III-IV)².

In 2012, diseases of the circulatory system were considered the leading cause for hospitalization in Germany with a rising in-patient morbidity rate for HF³ (Figure 1).

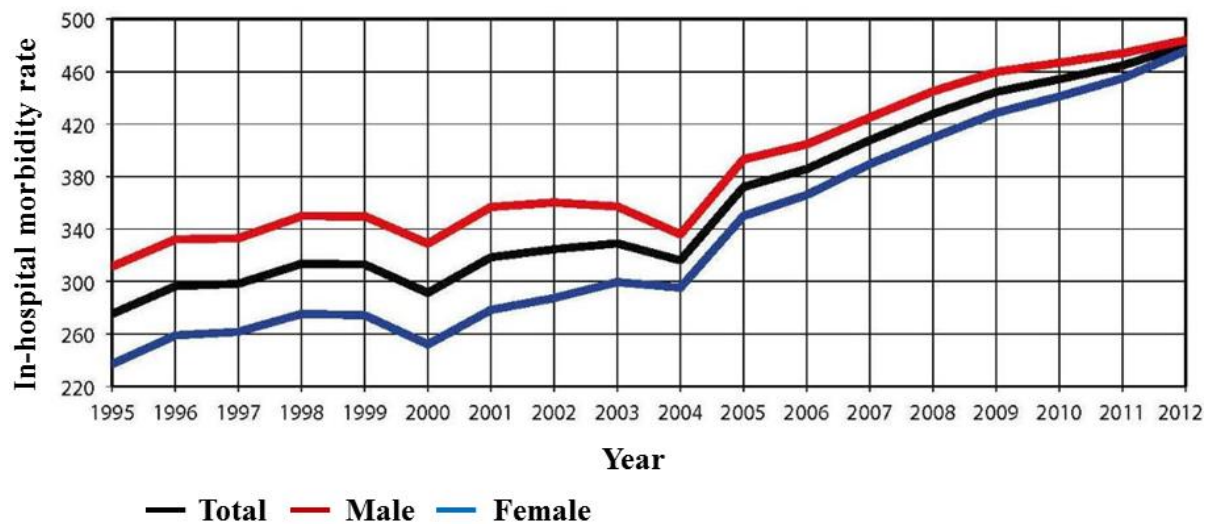


Figure 1: Development of the in-hospital morbidity rate of HF in Germany from 1995 – 2012

Data from the Federal Statistical Office of Germany (Statistisches Bundesamt; Modified from Deutscher Herzbericht 2014)³.

Associated lifestyle components, such as physical inactivity^{4, 5} or smoking⁶, and the current demographic development are causes of the rising prevalence⁷ and incidence⁸ of this disease in the industrialized world and require extensive investigation of its underlying pathology and treatment strategies. Therefore, understanding the molecular signal transduction pathways of cardiac myocyte function would allow inspiration of novel treatment strategies to fight heart disease.

1.2 The heart

The heart is a muscular organ, which pumps blood through blood vessels of the circulatory system¹. Blood distributes oxygen and nutrients through the body as well as assists in the removal of metabolic waste. The heart is divided into four chambers: upper left and right atria; and lower left and right ventricles. It receives blood low in oxygen from the systemic circulation, which enters the right atrium from the superior and inferior venae cavae and passes it to the right ventricle. From there, it is pumped into the pulmonary circulation through the lungs where it becomes oxygenated. Oxygenated blood then returns to the left atrium, passes through the left ventricle and is pumped out through the aorta to the systemic circulation—where the oxygen is used and metabolized to carbon dioxide⁹. Not only oxygen and nutrients, but also hormones are transported in the blood stream and the heart is not just distributor of those hormones, but also an effector organ.

In order to adapt to an increased demand for tissue oxygenation during exercise, heart rate and blood pressure are upregulated by the sympathetic nervous system. Pro-sympathetic signaling is mainly mediated by catecholamines (i.e. epinephrine and norepinephrine), which bind to adrenoceptors (ARs) located on the cardiac myocyte surface to initiate an intracellular signaling cascade resulting in increased cardiac contraction and relaxation capacities¹⁰. These receptors belong to the family of G-protein-coupled receptors (GPCRs)¹¹. GPCRs are 7-transmembrane proteins involved in the regulation of a vast array of physiological processes including cell growth, metabolism and hormonal homeostasis¹². Extracellular binding of ligands leads to the exchange of G-protein-bound guanosine diphosphate for guanosine-5'-triphosphate (GTP) and the dissociation of the G-protein into active $G\alpha$ -GTP and $G\beta\gamma$ subunits. Based on their function, $G\alpha$ -subunits are classified into four subfamilies – $G\alpha_s$ (stimulator), $G\alpha_{i/o}$ (inhibitory), $G\alpha_{q/11}$ and $G\alpha_{12/13}$ with various effector molecules such as adenylyl cyclase (AC), which is stimulated by $G\alpha_s$ and inhibited by $G\alpha_{i/o}$ or phospholipase C- β , which is activated downstream of $G\alpha_{q/11}$. These effector molecules in turn regulate the concentrations of second messengers in the cell, modulating the activity of a number of different downstream signaling molecules^{13, 14}.

ARs are divided into α - and β -ARs with different subtypes. The α_1 -AR effects are $G_{q/11}$ mediated and the receptor is present in a variety of tissues including vessels and the urinary tract, promoting smooth muscle contraction or leading to secretion from different glands. In cardiac myocytes, it exerts both, positive and negative inotropic effects possibly by different receptor subtypes expressed in the left (positive inotropy) and right (negative inotropy) ventricle¹⁵.

Besides various tissues of the central nervous system, α_2 -ARs are found on vascular pre-junctional terminals, where they inhibit the release of norepinephrine (noradrenaline) in a negative feedback for smooth muscle cells of certain vessels by promoting the $G\alpha_{i/o}$ pathway¹⁶.

The role of α -ARs for a global response in a fight-or-flight situation is thereby mediated mainly through modulation of the smooth muscle tone in vessels and other organs and to a lesser extent by changing cardiac propositions like for instance the heart rate. Therefore, in the following the dissertation will concentrate on β -ARs.

1.3 β -adrenoceptor signaling in the heart

In the heart, β -ARs are necessary in order to adapt to different states of exercise and mediate a fight-or-flight response to physical or psychological stress. Periods of exercise or stress require the short-term adjustment of heart rate and blood pressure as well as long term modifications with respect to transcriptional regulation under prolonged physical exercise^{17, 18}.

There are three subtypes of β -ARs in the heart - The β_1 -AR comprises 75–80% and is predominantly expressed in the heart, the β_2 -AR comprises 20–25% and is additionally expressed in the lungs, the uterus, kidneys and blood vessels. The β_3 -AR is found primarily in adipose tissue, and to a lesser extent in the heart, which is why the focus here will be on β_1 and β_2 . Also, a β_4 -AR has been described, but is considered a low affinity state of β_1 -AR that has not been characterized well¹⁹⁻²¹.

When stimulated by epinephrine and norepinephrine, cardiac myocyte β_1 -ARs initially activate and release $G\alpha_s$ -GTP, which activates AC that generates the second messenger cyclic adenosine monophosphate (cAMP) from adenosine triphosphate (ATP). Elevated cAMP levels activate cAMP-dependent protein kinase (PKA) with four cAMP molecules required to activate a single PKA molecule. This is done by two cAMP molecules binding to each of the two cAMP binding sites in the regulatory subunits of PKA inducing a conformational change of the RI subunits that allows the detachment and exposition of the two catalytic subunits²².

Thereupon, calcium (Ca^{2+}) cycling is enhanced by PKA-mediated phosphorylation of L-type Ca^{2+} channels (LTCC), which promotes Ca^{2+} flux into the cardiac myocyte and the subsequent Ca^{2+} -induced Ca^{2+} release via ryanodine receptor 2 (RyR2). Ca^{2+} binding to cardiac troponin C (cTnC) activates contraction. Simultaneously, Ca^{2+} sensitivity of the sarcomeric apparatus is reduced by phosphorylation of cardiac troponin I (cTnI) and cardiac myosin-binding protein C (cMyBP-C) with resulting positive inotropic and lusitropic effects.

In that aspect, also phospholamban (PLB), leading to disinhibition of the sarco/endoplasmic reticulum Ca^{2+} -ATPase 2a (SERCA2a), is phosphorylated, which results in enhanced Ca^{2+} flux into the sarcoplasmic reticulum (SR) (Figure 2)²³.

The sympathetic nervous system is therefore the main driver of inotropy (contractile force), chronotropy (heart rate), lusitropy (relaxation) and dromotropy (conduction velocity).

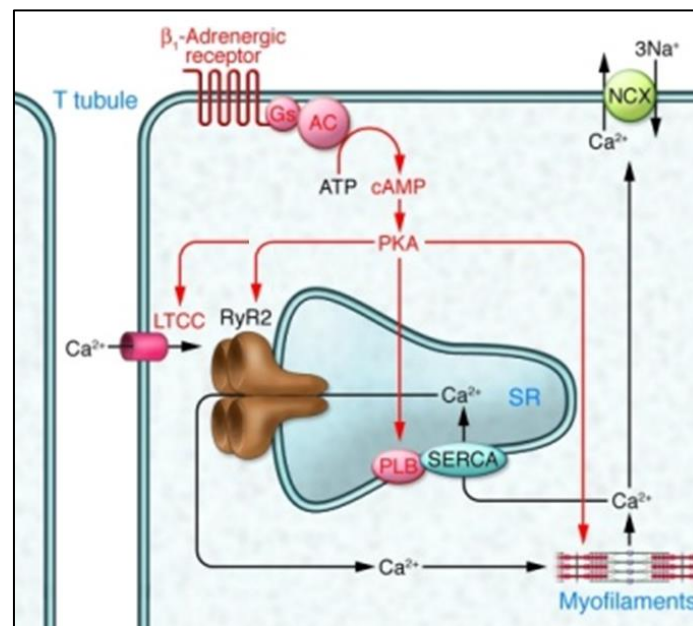


Figure 2: Examples for PKA substrates in cardiac myocytes after β -adrenergic stimulation

Increased cardiac pump function is reached by an increased Ca^{2+} -circulation. Systolic function is promoted by enhanced Ca^{2+} influx through sarcolemmal LTCC and sarcoplasmic RyR2, diastolic function by indirect facilitation of SERCA2a via disinhibition by PLB phosphorylation and reduction of Ca^{2+} affinity of sarcomeric proteins by phosphorylation of cTnI and cMyBP-C (Modified from Eschenhagen T., 2010)²⁴.

The β_2 -AR couples to $G_{\alpha_{i/0}}$. The activated $G_{\alpha_{i/0}}$ subunits inhibit AC activity and therefore antagonise β_1 -AR activity. $G_{\alpha_{i/0}}$ coupling also activates the cytosolic effector molecule phospholipase A2, which causes cAMP-independent enhancement of Ca^{2+} signaling and leads to enhanced cardiac contraction²⁵.

In addition to the acute regulation of excitation-contraction coupling, catecholamines exert profound effects on tissue remodeling, which involves the alteration of specific transcription programs, mainly leading to the development of hypertrophy, but also changes in cell metabolism or survival, all of which participate in the initial adaptation to cardiac stress.

In that respect, the release of the $G\beta\gamma$ subunit contributes to activation of the mitogen-activated protein kinase (MAPK) signaling pathway²⁶. One extensively studied protein kinase of the MAPK family in the context of cardiac hypertrophy is the extracellular signal-regulated

kinase 1/2 (ERK1/2). ERK1/2 is ubiquitously expressed and has diverse cellular and physiological functions, such as the regulation of cell cycle progression, proliferation, cytokinesis, transcription, differentiation, and cell adhesion²⁷.

Typically, growth factors binding to their respective receptor tyrosine kinase (RTK) activate Ras, which recruits and activates Raf (MAP3K) at the plasma membrane. Once activated, Raf phosphorylates and activates MAPK/ERK kinase 1/2 (MEK1/2). MEK1/2 in turn activates ERK1/2 by direct phosphorylation.

But as mentioned before, it can also be activated by β_2 -AR stimulation parallel to the canonical ERK1/2 activation. Binding to $G\beta\gamma$ -subunits released from activated $G\alpha_q$ leads to ERK1/2 dimerization and subsequent autophosphorylation of ERK1/2 on Thr188. This additionally requires the activation and assembly of the entire Raf-MEK-ERK kinase cascade. ERK1/2 then translocate to the nucleus, where phosphorylation of nuclear targets initiate pro-hypertrophic gene expression²⁸ (Figure 3).

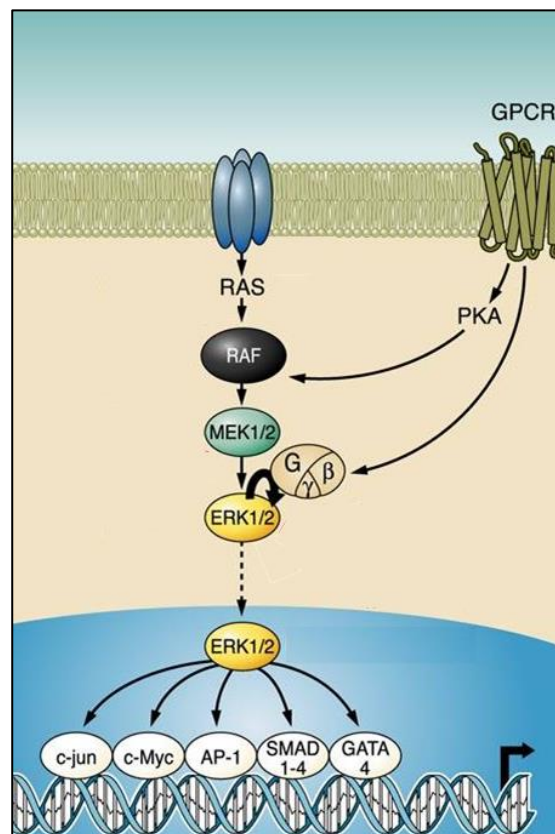


Figure 3: Schematic summarizing ERK1/2 signaling events in the heart.

Not all connections necessarily represent a direct interaction but may rather represent the end product of multiple steps. ERK1/2 is either activated by Ras after ligand binding to RTKs, but can be activated also by the $G\beta\gamma$ subunit of G-proteins. ERK1/2 then translocate to the nucleus and promote pro-hypertrophic gene expression (Modified from Rose BA., 2010)²⁹.

Transgenic mice expressing an activated form of MEK1 showed typical changes in cell morphology observed under conditions of pressure overload, but lacked fibrotic remodeling or sudden cardiac arrest, establishing a role of the MAPK/ERK1/2-pathway in the development of compensated concentric hypertrophy³⁰.

Independent from β -AR activation, attention has been focused on the activation of fetal gene transcription pathways as a consequence of disease development (for instance changes in intracellular Ca^{2+} concentrations), leading to activation of Ca^{2+} -regulated pathways involving signaling components such as calcineurin (CaN) and nuclear factor of activated T cells (NFAT). Specifically, activation of $G\alpha_{q/11}$ downstream of α_1 -ARs plays a pivotal role in resulting in increasing intracellular Ca^{2+} levels. Signaling via the phospholipase C β /diacylglycerol/protein kinase C pathway mobilizes Ca^{2+} release from intracellular stores³¹. CaN, a Ca^{2+} -dependent protein phosphatase, is activated by sustained elevation of intracellular Ca^{2+} concentrations, which promotes CaN binding to its downstream effector NFATc4. Under normal conditions NFATc4 is hyperphosphorylated and retained in the cytoplasm, but translocates to the nucleus in response to CaN-mediated dephosphorylation, acting as a transcription factor (TF) for several genes involved in cardiac development, such as heart and neural crest derivatives expressed 1 (HAND1)³², or as a co-factor for GATA-binding factor 5 (GATA5)³³ and thus, in essence, promotes cardiac hypertrophy development³⁴. Cardiac myocytes isolated from CaN transgenic mice show cardiac myocyte disarray and profound hypertrophy³⁵. Inhibition of the CaN/NFAT signaling has vice versa been shown to reduce pathological cardiac hypertrophy after pressure overload or chronic β -adrenergic stimulation³⁶.

1.4 β -adrenoceptor signaling in heart failure

The mechanisms of adaptation described above are physiological during short times of exercise or in the form of physiological hypertrophy observed in athletes, but during chronic cardiac stress conditions, often caused by sustained hypertension, after myocardial infarction or valvular heart disease, the initial compensatory effects fuel a vicious cycle^{37, 38}: Persistence of these effects and the changes in transcriptional activity as described above cause long term alterations of cardiac myocyte morphology and function^{39, 40} and changes in the composition of the extracellular matrix with enhanced fibrosis^{41, 42}, so called cardiac remodeling. An increase in energy demand in order to maintain the function of the hypertrophic heart and the hearts inability to meet this demand, leads subsequently from initial compensation via

compensated hypertrophy to a mechanical impairment of the heart and therefore to the onset of HF¹.

As one major component for the regulation of the cardiovascular system, the β -AR signaling pathway emerges as a key actor during the progression of HF. Pathological changes in β -AR signaling include a reduction of β_1 -AR protein levels of up to 50%, whereas β_2 -AR protein levels remain unchanged. Also $G\alpha_{i/o}$ protein levels increase during heart failure development whilst $G\alpha_s$ remains unchanged⁴³.

Desensitization as a response to overstimulation is achieved independently of total β -AR levels in two ways⁴⁴. Firstly, it is mediated by second messenger and PKA-dependent signaling. PKA desensitizes β -ARs by phosphorylation of LTCC and intracellular Ca^{2+} -regulatory proteins as negative feedback. Secondly, a ligand-mediated desensitization involves the phosphorylation of β -AR by G-protein-coupled receptor kinases and the subsequent binding of β -arrestin-regulatory proteins^{45, 46}. The binding of β -arrestin to the AR complex initiates the formation of protein complexes, which are consequently removed from the cell surface and relocated to the nucleus, called internalization⁴⁷. Taken together, these changes serve to protect the heart from overstimulation by catecholamines and a subsequently increased oxygen demand⁴⁸.

One model of β -AR signaling in HF suggests that chronic stimulation of β -ARs leads to chronic G-protein activation, and therefore the desensitization represents a (patho-)physiologically adaptive mechanism that attempts to decelerate progressive HF. In line with this model are studies of exaggerated β -AR signaling. For instance, β_1 -AR overexpressing mice developed dilated cardiomyopathy (DCM) and HF at young age, which is a model to investigate high levels of catecholamines⁴⁹. The beneficial effects of desensitization are also taken into account in pharmacological HF therapy, which includes therapeutic application of β -AR inhibitors at an early disease stage, which might seem counterintuitive due to the already reduced cardiac function, but has been shown to reduce mortality substantially in various clinical studies⁵⁰.

However, desensitization is adaptive only in the short term. In the long term it is maladaptive and results in the dysregulation of Ca^{2+} handling and other cellular effects, leading to further progression of myocardial failure.

Generally, chronic stimulation of adrenergic signaling and the subsequent desensitization of signal-transduction mechanisms lead to an increase in the intracellular Ca^{2+} concentration during diastole. This in turn fuels adverse long term changes caused by enhancing pro-hypertrophic gene transcription.

One aspect leading to impaired Ca^{2+} cycling is the hypo-phosphorylation of established PKA-substrates, which in turn leads to reduced contractile function for instance through enhanced PLB-mediated SERCA2a inhibition. The lack of phosphorylation of PLB might be due to the desensitization-related reduction in cAMP, an increase in protein phosphatase 1 and 2 activity, or both⁵¹. The induction of a fetal gene expression program as highlighted above, ultimately results in pathologic hypertrophy^{52,53}.

Additionally, gene-expression studies performed in failing human hearts suggest that β_1 -ARs are also coupled to the induction of fetal gene expression of the contractile proteins, consisting of upregulation of the fetal genes β -myosin heavy chain (*β -Mhc*), slow *cTnI* and atrial natriuretic peptides, and a downregulation of the adult genes *α -Mhc* and *Serca2a*^{52,54}.

1.5 Scaffolding proteins

It is well established that signal transduction pathways are compartmentalized in cardiac myocytes. This is achieved by different mechanisms, for instance, β -ARs have distinct cell surface localizations. In various studies, the β_1 -AR subtype was evenly distributed, whereas the β_2 -AR subtype was more localized in vicinity of deep transverse tubuli^{55,56}.

Also, their downstream effectors are part of larger signalosomes, which might differ between the β_1 -AR and the β_2 -AR subtype. These signalosomes rely on multiple binding abilities of scaffolding proteins⁵⁷. Clustering members of a certain pathway to a specific cellular compartment ascertains signal specificity and also faster and efficient signal transduction⁵⁸.

The most prominent members of these scaffolds in β -AR signaling are A-kinase anchoring proteins (AKAPs). Binding of PKA to AKAPs is in most cases established by a domain that interacts with the type II regulatory subunit (RII) of PKA^{59,60}, and various additional target domains present in different AKAPs specify diverse substrate binding⁶¹.

One example for AKAPs present in cardiac myocytes is muscle specific AKAP (mAKAP, AKAP6). It is known to form a multi-enzyme complex to locate signal cascades that can positively or negatively modulate cAMP induced signal transduction events⁶². A recent study shows that mAKAP participates in hypertrophic gene expression via a mechanism involving activation of the pro-hypertrophic TF NFATc1⁶³. Also, Ca^{2+} cycling or cardiac myocyte contractility are potentially modulated by AKAPs, via AKAP7^{64,65}.

The HUGO Gene Nomenclature Committee lists 31 different AKAPs⁶⁶ of which at least eleven are expressed in cardiac myocytes⁶⁷ (Table 1).

Table 1: Gene Family - A-kinase anchoring proteins

(additional data from UniProt)

Symbol	Name	Most abundant tissue Expression	PKA subunit binding for cardiac AKAPs
ACBD3	acyl-CoA binding domain containing 3	testis and ovary	
AKAP1	A-kinase anchoring protein 1	thymus, prostate, testis, ovary, colon and small intestine	
AKAP2	A-kinase anchoring protein 2		
AKAP3	A-kinase anchoring protein 3		
AKAP4	A-kinase anchoring protein 4		
AKAP5	A-kinase anchoring protein 5		
AKAP6	A-kinase anchoring protein 6	heart, skeletal muscle, brain	RII subunit
AKAP7	A-kinase anchoring protein 7	brain, heart, lung, pancreas and skeletal muscle	unknown
AKAP8	A-kinase anchoring protein 8	heart, liver, skeletal muscle, kidney and pancreas	RII subunit
AKAP9	A-kinase anchoring protein 9	skeletal muscle, pancreas	
AKAP10	A-kinase anchoring protein 10		
AKAP11	A-kinase anchoring protein 11	heart, brain, lung, liver, kidney, testis, ovary	RII subunit
AKAP12	A-kinase anchoring protein 12	endothelial cells, cultured fibroblasts, osteosarcoma	
AKAP13	A-kinase anchoring protein 13	heart, hematopoietic cells, skeletal muscle, lung, breast ductal epithelium	holoenzyme and RII subunit
AKAP14	A-kinase anchoring protein 14	cilia (trachea and testis)	
AKAP17A	A-kinase anchoring protein 17A	heart, brain, lung, liver, skeletal muscle, kidney and pancreas	RI and RII subunits
AKAP17BP	A-kinase anchoring protein 17B	Pseudogene	
ARFGEF2	ADP ribosylation factor guanine nucleotide exchange factor 2	placenta, lung, brain, kidney and pancreas	

CBFA2T3	CBFA2/RUNX1 translocation partner 3	pancreas, skeletal muscle, spleen, thymus, peripheral blood leukocytes	
CMYA5	Cardiomyopathy-associated 5	heart and skeletal muscle	RII subunit
C2orf88	chromosome 2 open reading frame 88	heart and testis	RI subunit
EZR	ezrin	Brain	
MAP2	microtubule associated protein 2		
MYO7A	myosin VIIA	pigment epithelium, photoreceptor cells of the retina	
MYRIP	myosin VIIA and Rab interacting protein	brain, skin, adrenal medulla, pancreas, intestine, liver, kidney, muscle, testis	
NBEA	neurobeachin	Brain	
NF2	neurofibromin 2	widely expressed	
RAB32	RAB32, member RAS oncogene family	heart, liver, kidney, bone marrow, testis, colon and fetal lung.	RII subunit
SPHKAP	SPHK1 interactor, AKAP domain containing	heart, spleen, ovary, brain	RI subunit
SYNM	synemin	heart, skeletal muscle, bladder	unknown
WASF1	WAS protein family member 1	Brain	

But not only beat-to-beat adaptation pathways require scaffolds, also pathways involved in transcription, like MAPK signaling, are compartmentalized by scaffold proteins in cardiac myocytes. The first identified scaffold protein involved in ERK signaling for instance was the kinase suppressor of Ras, a protein that binds to ERK1/2 and their upstream kinases, forming a high-molecular weight macro-complex, whereby signaling flux through the Ras-ERK cascade was regulated⁶⁸.

Recent studies also suggest that cardiac adriamycin responsive protein is an ERK-associated protein that mediates ERK signaling responses in vicinity to the sarcomere during phenylephrine (PE)-induced hypertrophy⁶⁹. It functions as a transcriptional co-factor and is highly expressed in embryonic cardiac myocytes⁷⁰.

1.6 Cardiomyopathy-associated protein 5

CMYA5, also known as myospryn or genethonin 3, is a protein comprising 4096 amino acids in human (UniProt entry: Q8N3K9) and whose expression is observed exclusively in skeletal and cardiac muscle¹⁰⁵. CMYA5 was initially discovered in 2001 via expression analysis aiming to identify co-expressed cardiomyopathy-associated genes together with four other genes¹⁰⁶. Immunofluorescence analysis of human skeletal muscle cells revealed doublet-appearing bands flanking the Z-disc¹⁰⁷ and, in the case of cardiac myocytes, CMYA5 was furthermore detected in the perinuclear region, in vicinity of intercalated discs and associated to lysosomes as well as the SR¹⁰⁸. CMYA5 expression, like FHL2, is regulated by MEF2¹⁰⁹ and different hypertrophic stimuli, for instance angiotensin II (AngII) or PE infusion were shown to increase its expression¹¹⁰.

The C-terminal 570 amino acids of CMYA5 contain domains known for tripartite motif (TRIM) proteins and therefore CMYA5 is also named TRIM76, although just a B-box coiled-coil, two fibronectin type III-like (FN3) repeats and a SP1A and ryanodine receptor (SPRY) domain are present, lacking the TRIM-typical Really Interesting New Gene (RING) motif¹⁰⁵. All so far established protein interactions of CMYA5 occur at its C-terminus, which might result from an overrepresentation of that region in yeast-2-hybrid libraries after initial discoveries of protein interaction for these motifs, but may also be related to its evolutionary conservation. Contrary to that, the middle region of CMYA5 shows great diversity between different species and is speculated to function as a flexible molecular linker. Interestingly, also part of the N-terminal region (Leu51 – Asp160) is evolutionary conserved but no protein binding has been identified and studied so far¹¹¹.

Identification of CMYA5 as a muscle specific AKAP shows that CMYA5 facilitates PKA localization specifically near the sarcomeric Z-disc in muscle tissue. Like most AKAPs, it binds to the RII α subunit of PKA, whereby three different amphipathic helices near the C-terminus independently facilitate this protein interaction. It was also shown by *in vitro* kinase assays that, in addition to anchoring PKA, CMYA5 itself is a PKA substrate¹¹². The mdx mouse model of Duchenne muscular dystrophy provides functional evidence demonstrating the importance of CMYA5 for PKA signaling. CMYA5 protein expression is reduced and it is mislocated, likely resulting from a disrupted interaction with dystrophin. Consequently, the localization of PKA RII α is abnormal, and PKA activity is reduced¹¹³.

Interactions with titin¹⁰⁷ and the abovementioned dystrophin¹¹³ indicate CMYA5 functions as a costameric scaffold and stabilizer of the cytoskeleton. Also, certain types of muscular dystrophy caused by mutations of titin's C-terminal end display reduced levels and

mislocalization of CMYA5. Dystrophin is also part of Biogenesis of Lysosome-Related Organelles (LRO) Complex 1 (BLOC-1) and additional CMYA5 interactions with the member proteins of this complex dysbindin-1¹⁰⁵ and desmin¹⁰⁸ indicate a potential role for CMYA5 in genesis and localization of lysosomes or its aggregates in muscle cells, where LROs are not known to exist. Especially desmin seems crucial, as desmin knockout mice display severe mislocalization of lysosomes and also a loss of CMYA5's perinuclear localization in neonatal rat ventricular myocytes (NRVM). Hence, it is proposed that proper desmin-CMYA5 interaction might be required for correct lysosome trafficking¹¹⁴.

Physiological roles for CMYA5 are furthermore described in terms of the non-enzymatic inhibition of the CaN/NFAT pathway. In mouse skeletal muscle cells, overexpression of CMYA5's TRIM-like region led to reduced tissue regeneration and slow-fiber transformation. Also regenerating myofiber size of these transgenic mice is smaller, indicating a potential anti-hypertrophic effect on skeletal muscle via CaN inhibition¹¹⁵. A possible connection to similar effects observed for FHL2 in cardiac myocytes has not been investigated yet.

1.7 Four and a half LIM proteins

Besides the abovementioned scaffolding proteins, FHL family members act as important regulatory proteins in multiple subcellular locations of muscle cells. The term LIM derived from three independently analyzed transcription factors that contained sequence homology: *Caenorhabditis elegans*-lineage protein LIN-11, the rat insulin enhancer-binding protein ISL-1 and the TF MEC-3. LIM domains are zinc finger containing structures and provide, in contrast to analogous DNA binding structures, a modular protein binding interface^{71, 72} through which they scaffold proteins and protein complexes to their respective cellular localization (Figure 4).

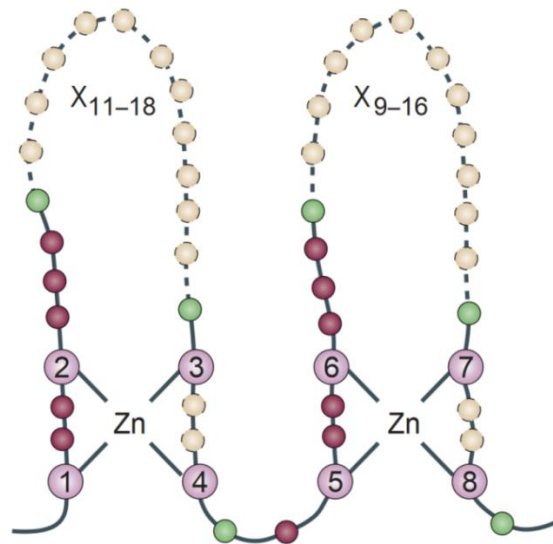


Figure 4: Conserved topology of the LIM domain

Purple circles indicate the zinc-binding cysteines. Semi-conserved aliphatic/bulky amino acid residues are shown as green spheres. Non-conserved residues with invariant spacing are represented as magenta spheres. Dashed yellow circles indicate a variable number of residues (X) that are possible within the sequence (Modified from Kadrmas, JL and Beckerle MC, 2004)⁷³.

The FHL family comprises 5 members, including FHL1-5^{74, 75}. It was shown that FHL1 is expressed predominantly in skeletal muscle and lung tissue, and to a lesser extent in heart, brain and kidney tissue. FHL2 is expressed in the heart and can also be detected in brain and skeletal muscle tissue. FHL3 is highly expressed in skeletal muscle, with very low expression in heart, lung and kidney tissue⁷⁶. FHL4 and 5 are expressed mainly in testis, with no apparent role in cardiac physiology^{77, 78}. This dissertation will concentrate on the current knowledge on FHL1 and 2 in cardiac myocytes.

1.7.1 FHL1 in cardiac (patho-)physiology

To date, more than 25 different protein interactions have been identified for full length FHL1 and these interactions can be mapped to a variety of functional classes. However, FHL1 is expressed predominantly in skeletal muscle. Therefore, most of these protein interactions translate into a multifunctional and integral role for FHL1 in skeletal muscle development, structural maintenance, and signaling⁷⁹. In that aspect, 27 *FHL1* mutations have been identified that relate to different myopathies often in combination with diverse cardiovascular diseases⁸⁰. Also, FHL1 expression is significantly up-regulated in a variety of cardiac disorders, even at the earliest stages of disease onset⁸¹. A two- to threefold increase in FHL1 expression was detected at various time points in three different mouse models of cardiomyopathy, with chronic stimulation of the β -AR signaling pathway. In all three mouse

models, transgenically expressing β_1 -AR, β_2 -AR or PKA, FHL1 was up-regulated at early stages of disease and continued to increase during disease progression⁸².

In cardiac myocytes, FHL1 is part of a complex within the sarcomere that senses the mechanical stress and induces responses leading to cardiac hypertrophy. FHL1 interacts with the N2B region of titin and associates with MAPK cascade components at the sarcomeric I-band, namely Raf1, MEK2, and ERK2. Overexpression of FHL1 caused a significant increase in ERK1/2 phosphorylation compared with control-transduced cardiomyocytes. Also, a link between FHL1 and the $G\alpha_q$ -MAPK was shown when an MAPK/ERK1 inhibitor could completely block PE- and AngII-mediated upregulation of FHL1 expression in cardiomyocytes⁸³.

In line with these pro-hypertrophic effects, *Fhl1*^{-/-} mice were protected when subjected to transverse aortic constriction (TAC) compared to wildtype littermates. They possessed smaller hearts than wild-type mice, including a smaller increase in left ventricular/body-weight ratio, cardiac myocyte cross-sectional area, left ventricular posterior wall thickness and interventricular septal wall thickness. In addition, less reactivation of the fetal gene expression program occurred in those mice, showing a limited hypertrophic response⁸³.

1.7.2 FHL2 in cardiac (patho-)physiology

FHL2 is a 279 amino acid containing^{84, 85}, non-enzymatic protein and the first identified member of the FHL family.

Gene transcription of *Fhl2* is regulated by various TFs, amongst those is p53⁸⁶, serum response factor (SRF)⁸⁷ as well as cardiac lineage factors Nkx2.5⁸⁷ and Ibx1⁸⁸. Also, myocyte-specific enhancer factor 2 (MEF2), a TF playing a pivotal role in determination and differentiation of cardiac and skeletal muscle cells, has been shown to bind to the *Fhl2* promoter region and FHL2 protein levels were decreased in MEF2 deficient NRVM^{89, 90}. Recent findings show FHL2 binding to protein kinase D (PKD), which in turn phosphorylates class II histone deacetylase isoform 5 and thereby promotes MEF2 driven transcription. However, siRNA mediated *Fhl2* knockdown did not alter PKD-mediated MEF2 activity⁹¹.

FHL2 is present in all cellular compartments and exerts distinct functional properties. In the nucleus, it acts as a transcriptional co-factor and modulates the activity of TFs for differential gene expression. For instance, HAND1, a TF playing an important role in cardiac morphogenesis and effector of the CaN/NFAT pathway is repressed⁹².

In the cytosol it forms signaling complexes associated with the myofilament lattice and it functions as a scaffold for multimeric protein complexes and as a molecular link between

different signaling pathways⁷⁵. It binds to titin as well as to metabolic enzymes, namely muscle specific creatine kinase (MM-CK), AC and phosphofructokinase (PFK), thereby scaffolding these enzymes to sarcomeric regions of high energy consumption⁹³. In that aspect, a missense mutation, leading to Gly48Ser in FHL2, was identified in a patient with DCM. Functional analysis demonstrated that the Gly48Ser *FHL2* mutation affected the binding to titin showing that it contributed to the pathogenesis of DCM via impaired recruitment of metabolic enzymes to the sarcomere⁹⁴.

Further scaffolding functions of FHL2 include interactions with various integrins important for cell-adhesion and -migration, but this neither influences attachment of cells to different substrates nor does it induce changes in their migration capacity. It has been shown that this interaction regulates signal transduction pathways from the extracellular compartment into the cell during neurohumoral stimulation^{95, 96}. It was also reported that FHL2 is expressed in endothelial cells and binds to sphingosine kinase 1 (SK1)⁹⁷ and that this interaction inhibits SK1 activity⁹⁸. Under normal conditions SK1 is activated by phosphorylation and subsequently translocates to the cell membrane, where its substrate, sphingosine, is located. Phosphorylated sphingosine acts as a signaling molecule and promotes cell survival, proliferation and differentiation^{99, 100}.

An interaction of FHL2 with minimal potassium (minK), a β -subunit of voltage-gated K⁺ channels, was observed, showing beneficial repolarization in cardiac cells by linking minK to the cytoskeleton¹⁰¹.

Opposite to FHL1, different studies describe an anti-hypertrophic role for FHL2. Although *Fhl2*-targeted knockout mice did not reveal exacerbation of the hypertrophic response subjected to TAC surgery⁷⁶, chronic isoproterenol infusion over seven days resulted in exaggerated cardiac hypertrophy compared to wild type mice¹⁰². In line with these finding is the interaction of FHL2 with ERK2. By masking the binding side responsible for nuclear translocation, FHL2 might prevent nuclear accumulation and thereby the onset of ERK2-dependent pro-hypertrophic gene transcription¹⁰³.

Beyond that, FHL2 exerts various other functions by binding to a variety of different proteins. For a selection of those see table 2, modified from Johannessen M, 2006.

Table 2: FHL2 binding partners⁸⁹

Protein function	Proteins
Receptors	integrins α_{3A} , α_{3B} , α_{7A} , $\alpha_{7\beta}$, β_{1A} , β_{1D} , β_2 , β_{3A} , β_6 , minK, presenilin-2, type IIa Na/P _i cotransporter
Structural proteins	α -actin, titin
Enzymes	AC, calpain, MM-CK, ERK2, PFK, pp125FAK, tumour necrosis factor- α converting enzyme (TACE)
Transcription factors and cofactors	ACT, androgen receptor, β -catenin, CBP, E2F1-4, estrogen receptor, estrogen receptor- α , FHL1, FHL2, FHL3, c-FOS, FOXO1, HAND1, IGFBP-5, c-JUN, myocyte nuclear factor, NCoR, p300, PELP1, PLZF promyelozyt, Runx2/Cbfa1, RXR, SRF, SK1, thyroid hormone receptor, WT1
Splicing factors	hNP220, PTB-associated splicing factor
DNA replication and repair	BRCA1, hCDC47, TACC1
Miscellaneous	AIBP80, BIN1, clathrin assembly, lymphoid myeloid leukemia protein (CALM), TRAF2, TRAF4, TRAF6, TUCAN/CARD8 CARDINAL

Interestingly, another prominent mediator of cardiac hypertrophy, CaN, was also identified as an FHL2 binding partner. CaN as part of the NFAT-dependent pro-hypertrophic gene expression is, similar to ERK2, antagonized by FHL2, possibly by sequestration of CaN at the sarcomere as described for other CaN inhibitors¹⁰⁴.

1.8 Aim

As stated above, diseases of the circulatory system still remain the leading cause for hospitalization in Germany with a rising in-patient morbidity rate for HF³.

Besides large clinical studies, basic research needs to provide new insights into the molecular mechanisms leading to HF to identify potential targets in order to inspire new treatment strategies.

Because of previous work in our group, we are interested in FHL2 and its various cellular functions. Therefore, we aimed to identify novel interaction partners that might be regulated by FHL2. Interestingly, in a yeast-2-hybrid screen, a muscle specific AKAP, cardiomyopathy-associated protein 5 (CMYA5), was identified as a putative FHL2 binding partner. CMYA5 has just been described recently and knowledge of its cardiac functions is scarce.

The primary aim of this work was therefore to verify and characterize the interaction of FHL2 and CMYA5 on a molecular and cellular level to pave the way for further functional analysis of their joint roles in cardiac physiology and pathology.

2 Materials and methods

2.1 Materials

2.1.1 Chemicals and reagents

Table 3: Alphabetical list of chemicals and reagents

Chemicals and reagents	Source	Catalogue #
2-mercaptoethanol	Sigma Aldrich	M6250
2-propanol	Merck Millipore	1096342500
Agar	BD	214010
Agarose UltraPure™	Life Technologies	16500-500
Ammonium persulfate (APS)	Bio Rad	161-0700
Ammonium sulphate	Merck Millipore	168355
Ampicillin trihydrate	Serva	13397.01
Bovine serum albumin	Sigma-Aldrich	A9647
Bromophenol blue	Bio Rad	161-0404
Complete protease inhibitor cocktail tablets	Roche	11697498001
Coomassie Brilliant Blue G-250	Bio Rad	161-0406
Coomassie Brilliant Blue R-250	Bio Rad	161-0436
Developer G150	Agfa	n. a.
Dimethyl sulfoxide	Sigma Aldrich	D8418
Distilled H ₂ O	B. Braun	0082479E
DL-dithiothreitol	Sigma-Aldrich	D0632-10G
DMEM with GlutaMAX™ I, 4500 mg/L D-Glucose, Sodium Pyruvate	Gibco	31966-021
dNTP set, 100 mM solutions	Thermo Fisher Scientific	R0181
DPBS, no Ca ²⁺ , no Mg ²⁺	Life Technologies	14190-144
EagleTaq DNA polymerase	Roche	5206928190
EDTA disodium salt dihydrate	Carl Roth	8043.2
EGTA, molecular biology grade	Merck Millipore	324626-25GM
Ethanol absolute P. A.	Chemsolute	22.461.000
Ethidium bromide, 10 mg/mL UltraPure™	Life Technologies	15585011
Fixer G354	Agfa	n. a.

Gelatin 2% in water, tissue culture grade Type B	Sigma	G1393
GeneRuler 1 kb DNA ladder	Thermo Fisher Scientific	SM0312
GeneRuler 100 bp DNA ladder	Thermo Fisher Scientific	SM0241
Glacial acetic acid	Merck Millipore	1000562500
Glutathione Sepharose 4B	GE Healthcare	17-0756-01
Glycerin EMSURE [®] ACS, Reag. PhEur	Merck Millipore	1040921000
Glycine	Carl Roth	3908.2
Horse serum	Sigma	H-1138
Hydrochloric acid	Carl Roth	N076.1
Imidazole	Merck Millipore	104716
Isopropyl β -D-1-thiogalactopyranoside, dioxane-free	Thermo Fisher Scientific	R0392
L-Glutathione reduced	Sigma Aldrich	G4251
Liquid nitrogen	TMG	n. a.
M199 with Hanks' Salts, L-Glutamine, 25 mM HEPES	Gibco	22350-029
Methanol, HPLC	J. T. Baker	JT9093-03
MgCl ₂ hexahydrate	Merck Millipore	1058331000
MgCl ₂ stock solution	Roche	11699113001
N,N,N',N'-tetramethylethylenediamine (TEMED)	Sigma Aldrich	T9281
NaCl, crystal, BAKER ANALYZED [®]	J. T. Baker	3624-01
NaH ₂ PO ₄ -monohydrate EMSURE [®]	Merck Millipore	106346
NaOH	Carl Roth	K021.1
Ni/NTA agarose	Qiagen	30210
Non-specific goat serum (NGS)	Sigma Aldrich	G9023
N-Propyl gallate	Sigma Aldrich	P3130
Ortho-phosphoric acid	Merck Millipore	100573
PageRuler Plus prestained protein ladder	Thermo Fisher Scientific	26620
Paraformaldehyde 16% solution	Agar Scientific	AGR1026
Phusion High Fidelity buffer	Thermo Fisher Scientific	F-518L
Phusion Hot Start II High-Fidelity DNA polymerase	Thermo Fisher Scientific	F-549L

Powdered milk	Carl Roth	T145.2
Protein assay dye reagent concentrate	Bio Rad	500-0006
ProtoGel (30%)	National Diagnostics	EC-890
QuikSolution	Agilent	200516-51
SDS	Carl Roth	CN30
Taq DNA polymerase PCR buffer (10x)	Life Technologies	18067-017
Triton X-100	Carl Roth	3051.3
Trizma [®] -base	Sigma-Aldrich	T1503
Tryptone	BD	211699
Tween [®] 20	Sigma Aldrich	P9416
Yeast nitrogen base	BD	291940
ZnCl ₂	Merck Millipore	1088160250

2.1.2 Buffers

Table 4: Alphabetical list of buffers and their composition

Buffer	Ingredients	Concentrations / pH
3x reducing Laemmli sample buffer	Trizma [®] -base Glycerol SDS 2-mercaptoethanol Bromophenol blue	187.5 mM (pH 6.8) 30% (v/v) 6% (w/v) 9% (v/v) 0,03% (w/v)
4x SDS-PAGE separating buffer	Trizma [®] -base SDS Adjust with HCl	1.5 M 0.4% (w/v) pH 8.7
4x SDS-PAGE stacking buffer	Trizma [®] -base SDS Adjust with HCl	0.5 M 0.4% (w/v) pH 6.8
Ampicillin selective LB-agar plates	LB-medium Agar Ampicillin trihydrate	100% (v/v) 0.15% (w/v) 0.01% (w/v)
Assay buffer	Trizma [®] -base MgCl ₂ DL-dithiothreitol Triton X-100	30 mM (pH 7.4) 15 mM 1 mM 1% (v/v)

Cellulose solvation solution	Trifluoroacetic acid (TFA)* Trifluoromethanesulfonic acid (TFMSA)* Triisopropylsilyl (TIPS)*	88.5% (v/v) 4% (v/v) 2.5% (v/v)
Coomassie stain SDS-PAGE gel destaining solution	Methanol	20% (v/v)
Coomassie stain SDS-PAGE gel staining solution	Coomassie Brilliant Blue G-250 Ammonium sulphate Ethanol Ortho-phosphoric acid	0.08% (w/v) 8% (w/v) 20% (v/v) 1.6% (v/v)
Coomassie stain PVDF membrane destaining solution	Methanol Glacial acetic acid	50% (v/v) 10% (v/v)
Coomassie stain PVDF membrane staining solution	Coomassie Brilliant Blue R-250 Glacial acetic acid Methanol	0.2% (w/v) 10% (v/v) 45% (v/v)
Dialysis buffer	Trizma [®] -base EDTA Triton X-100 DL-dithiothreitol	50 mM (pH 8.1) 1 mM 0.1% (v/v) 1 mM
Elution buffer	NaH ₂ PO ₄ -monohydrate NaCl Imidazole Adjust with NaOH	50 mM 300 mM 250 mM pH 8.0
Gold buffer	Trizma [®] -base NaCl EGTA MgCl ₂ Adjust with HCl	20 mM 155 mM 2 mM 2 mM pH 7.5
LB medium	Tryptone Yeast nitrogen base Adjust with NaOH	0.1% (w/v) 0.05% (w/v) pH 7.4
Lisbeth's mounting medium	Trizma [®] -base Glycerol N-Propyl gallate	30 mM (pH 9.5) 70% (v/v) 5% (v/v)
Lysis buffer	NaH ₂ PO ₄ -monohydrate NaCl Imidazole Adjust with NaOH	50 mM 300 mM 10 mM pH 8.0

SDS-PAGE reservoir buffer	Trizma [®] -base Glycine SDS	25 mM 192 mM 0.4% (w/v)
Side chain cleavage solution	Trifluoroacetic acid (TFA)* Triisopropylsilyl (TIPS)* Dichloromethane*	80% (v/v) 3% (v/v) 12% (v/v)
SSC buffer	NaCl Trisodium citrate* Adjust with HCl	150 mM 15 mM pH 7.0
TAE 10x	Trizma [®] -base Acetic acid EDTA	40 mM (pH 8.0) 20 mM 1 mM
Transfer buffer	Trizma [®] -base Glycine SDS Methanol	48 mM 38 mM 0.037% (w/v) 20% (v/v)
TTBS 10x	Trizma [®] -base NaCl Adjust with HCl Tween [®] 20	20 mM 137 mM pH 7.6 0.1% (v/v)
Wash buffer	NaH ₂ PO ₄ -monohydrate NaCl Imidazole Adjust with NaOH	50 mM 300 mM 20 mM pH 8.0

* Kindly provided by Prof George Baillie and Jane Findlay (Institute of Cardiovascular and Medical Sciences in Glasgow, United Kingdom)

2.1.3 Kits

Table 5: List of commercial kits

Kit	Source	Catalogue #
High-Capacity cDNA Reverse Transcription Kit	Life Technologies	4368814
High Pure PCR Product Purification Kit	Roche	11732668001
Champion™ pET151 Directional TOPO® Expression Kit with BL21 Star™ (DE3) One Shot® Chemically Competent <i>E. coli</i>	Life Technologies	K151-01
NucleoSpin® Plasmid / Plasmid (NoLid)	Macherey-Nagel	740499.250
Duolink® In Situ Orange Starter Kit Mouse/Rabbit	Sigma-Aldrich	DUO92102
Plasmid Maxi Kit	Qiagen	12163
SV Total RNA Isolation System	Promega	Z3100
Amersham ECL western blotting detection reagent	GE Healthcare	RPN2209

2.1.4 Antibodies

Table 6: List of primary antibodies

Target	Host species	Dilution in WB*	Dilution in IF*	Source	Catalogue #
FHL2	Mouse, monoclonal	1:2000	1:100	MBL	K0055-3
CMYA5 C-terminus	Rabbit	1:2000	1:100	Gift** ¹⁰⁵	n. a.
V5-tag	Mouse, monoclonal	1:5000	n. a.	Life Technologies	R960-25
His ₆ -tag	Rabbit, polyclonal	1:1000	n. a.	Santa Cruz	sc-804
cMyBP-C	Rabbit, polyclonal	n. a.	1:100	Santa Cruz	sc-67354
α -actinin	Mouse, monoclonal	n. a.	1:100	Sigma Aldrich	A7811
Calcineurin (α -subunit)	Mouse, monoclonal	1:2000	n. a.	Sigma Aldrich	C1956

* WB: western immunoblotting IF: Immunofluorescence

** Prof. Derek Blake, MRC Centre for Neuropsychiatric Genetics & Genomics, Cardiff University School of Medicine, United Kingdom

Table 7: List of secondary antibodies for western immunoblotting

Target (species)	Dilution	Source	Catalogue #
Rabbit	1:2000	GE Healthcare	NA934
Mouse	1:2000	GE Healthcare	NA931

Table 8: List of secondary antibodies for immunofluorescence

Target (species)	Max ex/em wavelength	Dilution	Source	Catalogue #
Mouse	588 nm / 519 nm	1:100	Life Technologies	A-11001
Rabbit	556 nm / 571 nm	1:100	AbD Serotec	STAR36D549GA
Nuclear staining (DAPI)	358 nm / 461 nm	1:100	Life Technologies	D1306

2.1.5 Consumables and equipment

Table 9: Alphabetical list of consumables

Consumable	Source	Catalogue #
96-well plates	Sarstedt	83.3924.300
Alleskleber (universal adhesive)	Uhu	n. a.
Amersham Hybond P 0.45 PVDF membrane	GE Healthcare	10600023
Amersham Hyperfilm ECL	GE Healthcare	28-9068-35
Amicon [®] centrifugal filter devices	Millipore	4224
Capillare pistons 250 µl	Glison	F148114
Capillare pistons 50 µl	Glison	F148113
Capped centrifuge tubes 1 ml	Sarstedt	62.515.028
Cell culture dish 100 x 20 mm	Sarstedt	83.3902
Cell culture dish 35 x 10 mm	Sarstedt	83.1800.003
Cell spreaders	VWR	89042-018
Centrifuge bottles	Beckman	356011
Centrifuge tubes 15 ml	Sigma-Aldrich	T1943
Centrifuge tubes 50 ml	Sigma-Aldrich	T2318

Chromatography paper	Thermo Fisher Scientific	3030917
Cotton buds	Beese Medical	n. a.
Coverslips	VWR	631-0174
Filtered pipette tips 10 µl	Eppendorf	22491202
Filtered pipette tips 100 µl	Eppendorf	22491237
Filtered pipette tips 1000 µl	Eppendorf	22491253
Liquid Blocker PAP pen	Ted Pella	22309
Microscope slides	Marienfeld Superior	1000000
Nail varnish	Essence	n. a.
Ni-NTA Superflow columns	Qiagen	30622
Pasteur pipettes	VWR	612_1701
PCR reaction tubes	Sarstedt	72.990.002
Pipette tips 10 µl	Eppendorf	0030 073.207
Pipette tips 1000 µl	Eppendorf	0030 000.919
Pipette tips 200 µl	Eppendorf	0030 000.870
Reaction tubes 1.5 ml	Sarstedt	72688
Reaction tubes 2 ml	Sarstedt	72689
Screw cap tubes 2 ml	Sarstedt	72.694.006
Semi-micro cuvettes	Sarstedt	67.742
Serological pipettes 1 ml	Sarstedt	86.1251.001
Serological pipettes 10 ml	Sarstedt	86.1254.001
Serological pipettes 2 ml	Sarstedt	86.1252.001
Serological pipettes 25 ml	Sarstedt	86.1685.001
Serological pipettes 5 ml	Sarstedt	86.1253.001
Visking dialysis tubes	Medicell Membranes	DTV.12000.02.000

Table 10: Alphabetical list of equipment

Equipment	Source	Catalogue #
A1 ⁺ confocal microscope	Nikon	upon quote request
Accu-jet [®] pro pipette controller	Brand	26300
AF 103 ice flaker	Scotsman	upon quote request
Beckman J2-21 centrifuge	GMI	upon quote request
Beckman J6-B centrifuge	GMI	upon quote request
Benchtop temp. control system WS60	Julabo	n. a.
CFI Apo TIRF 60X H objective	Nikon	MBH76162
Genius analytical balance	Sartorius	n. a.
Heated wire	self-built	n. a.
Humid chamber	self-built	n. a.
JA-14 rotor	Beckman Coulter	339247
JS-5.2 rotor with buckets	Beckman Coulter	339087
Mastercycler [®] pro PCR cycler	Eppendorf	6321 000.515
Microcentrifuge 5415R	Eppendorf	22621408
Microman pipette 250 µl	Gilson	F148505
Microman pipette 50 µl	Gilson	F148503
Milli-Q [®] water purification system	Merck Millipore	upon quote request
Mini-PROTEAN [®] short glass plates	Bio Rad	165-3308
Mini-PROTEAN [®] spacer plates 1.0 mm	Bio Rad	165-3311
Mini-PROTEAN [®] Tetra Cell and PowerPac [™] Basic power supply	Bio Rad	165-8025FC
NanoDrop 1000 spectrophotometer	Thermo Fisher Scientific	n. a.
New Brunswick Scientific C25 Incubator/Shaker	Eppendorf	n. a.
Pioneer [™] Analytical and Precision balance PA512	Ohaus	80251571
Pipette Research [®] 10 µl	Eppendorf	3111 000.122
Pipette Research [®] 100 µl	Eppendorf	3111 000.149
Pipette Research [®] 1000 µl	Eppendorf	3111 000.165
Polymax 2040 shaker	Heidolph	542-40005-00
Primo Maxicell EC 340	Thermo Electron	n. a.

Rotor adapter assembly	Beckman Coulter	339103
Safire ² microplate reader	Tecan	n. a.
SmartSpec™ 3000 spectrophotometer	Bio Rad	170-2501
SONOPULS HD 2200 ultrasonic homogenizer	Bandelin	478
Spinning wheel	self-built	n. a.
TE 77 semi-dry transfer unit	GE Healthcare	0-6211-86
Thermomixer comfort	Eppendorf	n. a.
Ti-E Eclipse microscope	Nikon	upon quote request
Tissue-lyser II	Qiagen	85300
Vertical electrophoresis unit SE600	Hofer	SE600
X-ray cassette type G 18 X 24 cm	Rego	n. a.

Table 11: List of software

Method	Software	Version	Company
Office applications	Word	2010	Microsoft
	Excel	2010	
	Power Point	2010	
Statistical analysis	Prism	5.02	GraphPad
Spectrophotometry	ND-1000	3.8.1	Thermo Fisher Scientific
Densitometry	GeneTools	4.2.3.0	Syngene
Agarose gel imaging	GeneSnap	7.12.01	Syngene
Bradford assay	Magellan	5.0.3.5	Tecan
Microscopy	NIS Elements	4.20	Nikon
Referencing	Endnote X7	7.10.2	Thomson Reuters

2.2 Methods

2.2.1 Comprehensive methods

2.2.1.1 Sodium dodecyl sulfate polyacrylamide gel electrophoresis (SDS-PAGE)

Polyacrylamide gels were manually casted for protein separation. A protein running gel was immediately covered by 2-propanol and left for polymerization for 20 min. After discarding of 2-propanol, the stacking phase was casted on top. Combs were placed for well formation and left for another 20 min. For compositions of different gels see table 12. The samples were boiled for 5 min at 95 °C before they were loaded into the wells of the stacking gel. A protein standard was also loaded in order to judge the molecular mass of the proteins of interest. Gels were run at constant 200 V in electrophoresis chambers filled with 1x SDS-PAGE reservoir buffer.

Table 12: Composition of SDS-PAGE gels with different polyacrylamide concentrations.

Amounts account for 10 ml gel preparation.

	Stacking gel	6% (w/v) Running gel	10% (w/v) Running gel
4x separating buffer	--	2.5 ml	2.5 ml
4x stacking buffer	2.5 ml	--	--
ProtoGel 30%	1.16 ml	2 ml	3.33 ml
APS (10%)	10 µl	10 µl	10 µl
TEMED	100µl	100 µl	100 µl
ddH ₂ O	6.33 ml	5,4 ml	4,07 ml

2.2.1.2 Western Immunoblotting

For western immunoblot analysis, we performed a semi-dry transfer of proteins from SDS-PAGE gels onto PVDF membranes. Per gel, a blotting sandwich comprised of one PVDF membrane and 6 filter papers was used. Before the transfer, the PVDF membrane was activated in methanol for 20 sec and, along with the filter papers, equilibrated in transfer buffer. A transfer sandwich consisting of gel and membrane in between two layers of three filter papers each on top and at the bottom was assembled as required in a semi dry transfer cell and blotting was performed under constant current of 1 mA/cm² for 2 h.

Blocking of nonspecific binding sites of the membranes was achieved by incubation in 10% (w/v) non-fat milk powder in TTBS for 30 min. After a quick wash with TTBS, the

membranes were incubated overnight with primary antibody solution (prepared in 1% [w/v] milk in TTBS) at 4°C on a shaker.

The next day, the membranes were washed four times 15 min in TTBS before incubation with 20 ml secondary antibody solution (prepared in 1% [w/v] milk in TTBS) for 1 h on a shaker at room temperature. After another four times of 15 min washes the membranes were incubated in 2 ml ECL detection reagent mixture for 2 min under minimal light exposure. In a dark room, the membranes were exposed to photographic films in a closed cassette for different time periods before 2 min development, a 30 sec wash in 5% (v/v) acetic acid, 5 min fixation and washing with tap water.

After drying of the films, protein standard lines were labelled according to their position on the membranes. The PVDF membranes were Coomassie stained for 1-3 h and subsequently destained (50% (v/v) methanol, 10% (v/v) glacial acetic acid) on a shaker.

For quantification of blotting results, the GeneTools software was used to determine band densities and GraphPad Prism 5 was used for subsequent statistical analysis.

2.2.2 Analysis of human heart samples

2.2.2.1 mRNA expression analysis

RNA purification was achieved with the Promega SV Total RNA Isolation System Kit according to the manufacturer's instructions. Analysis of mRNA expression for the proteins of interest was kindly performed by Angelika Piasecki from our working group. Visualization and testing of significance were done by GraphPad Prism.

2.2.2.2 Protein expression analysis via SDS-PAGE and western immunoblotting

Failing and non-failing human left ventricular heart tissue was kindly provided by Prof. Thomas Eschenhagen. Tissue samples were prepared as 10% (w/v) homogenates in 100 mM Tris (pH 7.4) and supplemented with protease inhibitors (Complete, Roche), after homogenization for 2 min in a Qiagen Tissue-lyser II.

Large scale (14 cm x 8.5 cm), two-phase 1.5 mm thick polyacrylamide (6% [w/v]) gels were casted for protein separation. The samples were mixed 2:1 with 3x sample buffer and boiled for 5 min at 95 °C before 20 µl of each sample as well as 15 µl of protein standard were loaded onto the gel. Gels were run for 3-4 h at constant 200 V in an electrophoresis chamber filled with SDS-PAGE reservoir buffer. For FHL2 protein analysis, SDS-PAGE was performed with standard mini gels (8.5 cm x 5.5 cm; 1 mm thickness; 5 µl protein standard; 10 µl samples).

Transfer, immunostaining and –detection and statistical analysis were performed as described in the according sections above. The data was acquired by Prof. Friederike Cuello and Dr. Konstantina Stathopoulou.

2.2.3 PCR cloning and protein expression of recombinant *CMYA5* moieties

2.2.3.1 Reverse transcription

Reverse transcription was used to generate cDNA from human non-failing ventricular heart tissue RNA samples for PCR amplification of the gene of interest, *CMYA5*. This was performed with the High-Capacity cDNA Reverse Transcription Kit according to the manufacturer's instructions. Specifically, 5 µl of a 1:10 dilution of non-failing human heart RNA, with an initial concentration of 31.85 ng/µl were kindly provided by Lisa Krämer from our institute, and added to 5 µl master mix (1 µl 10x RT buffer, 0.4 µl 25 mM dNTPs, 1 µl 10x RT Random Primers, 2.1 µl RNase-free distilled water, 0.5 µl MultiScribe™ Reverse Transcriptase). A one-step cycling with annealing at 25 °C for 10 min, elongation at 37 °C for 2 h and inactivation of the reverse transcriptase at 85 °C for 5 min before cooling down to 4 °C was performed.

2.2.3.2 Polymerase chain reaction (PCR)

Eight individually designed primer pairs were synthesized by Eurofins Genomics in order to amplify eight non-overlapping DNA portions of *CMYA5*. The primers were selected so as the amplified DNA segments would be suitable to be used for cloning and transformation of DNA using the Champion™ pET151 Directional TOPO® Expression Kit (see Table 13). Each forward primer starts with the directional cloning sequence CACC and each reverse primer with the reverse complement stop codon motif TCA.

For the PCR reaction, the Phusion Hot Start II DNA polymerase was used. Each reaction mixture contained 0.2 µl polymerase, 11.8 µl ddH₂O, 4 µl 5x Phusion HF Buffer, 0.4 µl of 10 mM dNTPs, 0.6 µl DMSO, 1 µl of a 10 pM primer stock solution and 1 µl cDNA or ddH₂O as control. According to the manufacturer's instructions, a three-step cycling protocol was established consisting of a 30 sec initial denaturation at 98 °C, followed by 35 cycles of 5 sec denaturation at 98 °C, 30 sec annealing at 63 °C and 80 sec extension at 72 °C. Final extension was performed at 72 °C for 7 min after which the reaction was put on hold at 4 °C until further processing.

In order to verify the size of the amplified PCR products, 5 µl of each PCR product were mixed with 10 µl of 50% (v/v) glycerol, loaded onto a 1.5% (w/v) agarose in TAE gel

containing 0.005% (v/v) ethidium bromide and run for 45 min at 120 V in electrophoresis chambers filled with TAE. Images were acquired using the Chemi Genius 2 Bio Imaging System and GeneSnap 7.12.01 by SynGene.

If the expected fragment size was amplified, DNA purification was performed using the Roche High Pure PCR Product Purification Kit according to the instructions with an additional dry spin after washing. Elution was done in 50 µl ddH₂O.

The DNA concentration was determined using a NanoDrop spectrophotometer.

Table 13: Primers for directional cloning of *CMYA5* moieties

Moiety	Bp	Forward primer	Reverse primer
#1	1-1500	CACCATGGCGAGCCGCGA TAGCAAC	TCACATTAGAGGTTTCAGA AAGAGA
#2	1501-3000	CACCTTAGAAGAACCAGA GAAAGAAGAA	TCATGGAGAGAACAGTTC CGCTTC
#3	3001-4500	CACCGACTCAGCATCACA AGTTTCAATC	TCAAGAAAATAAAAAGATC TTGTTTGTC
#4	4501-6000	CACCACAGTCTGTGACTCT GAACGTTTG	TCATACATTTCCAGCTAGG ACTAAAGAC
#5	6001-7500	CACCGAGAGAAACATAGC AGAGGGGAAG	TCAAGATCCAAGTGTAATT TGTGTCTTC
#6	7501-9000	CACCAGATCTACTGAACT GAAAGAATC	TCAACAAGCAACTGTTTCA CTATCATC
#7	9001-10500	CACCCATAAAACATTTAAA GAGCAGG	TCATGCCTTTTTCAGTTACT ACCTC
#8	10501-12207	CACCCAAAAAGAGCTGAA AAAGTCCCAG	TCACTTGTGCCTTACAGAA TCCG

2.2.3.3 Directional cloning and transformation

Directional cloning was performed using the Champion™ pET151 Directional TOPO® Expression Kit. This TOPO vector carries a polyhistidine (His₆)- as well as a V5-tag after its start codon upstream of the directional cloning site that ensures fusion with a corresponding N-terminal protein tag in the correct reading frame for analysis. Furthermore, a lac operon site upstream of the start codon enables IPTG driven protein expression. A detailed depiction of the vector is shown in Figure 5. 2 µl of fresh PCR product were incubated with 1 µl salt solution, 2 µl ddH₂O and 1 µl vector for 15 min at room temperature. 5 µl of this mixture were used to transform One Shot® TOP10 chemically competent *E. coli* cells following the

manufacturer's instructions. 50 μ l and 200 μ l of transformed cells, respectively, were plated onto ampicillin-selective LB-agar plates and incubated overnight at 37 °C.

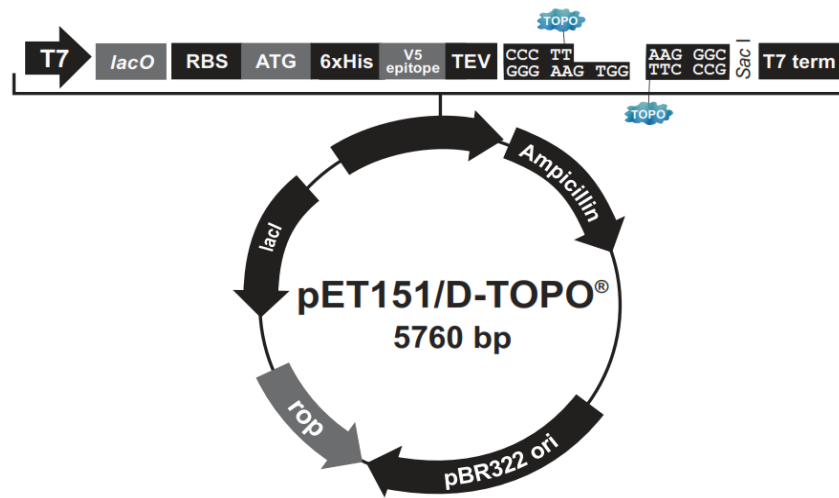


Figure 5: Map of the pET151/D-TOPO[®] vector

T7 promoter: Permits IPTG-inducible expression of recombinant protein in *E. coli* strains expressing the T7 RNA polymerase

T7 promoter priming site: Allows sequencing in the sense orientation

lac operator (lacO): Binding site for lac repressor that serves to reduce basal expression of recombinant protein

Ribosome binding site (RBS): Optimally spaced from the TOPO[®] Cloning site for translation of PCR product.

Initiation ATG: Start codon

Polyhistidine (6xHis) region: Permits purification of recombinant fusion protein on metal-chelating resin (Ni-NTA). In addition, allows detection of recombinant protein with the Anti-His₆ Antibodies

V5 epitope: Allows detection of the fusion protein by the Anti-V5 Antibodies

TEV (Tobacco Etch Virus) recognition site: Allows removal of the N-terminal tag from recombinant protein using TEV protease

TOPO[®] cloning site (directional): Permits rapid cloning of your PCR product for expression in *E. coli*

T7 reverse priming site: Allows sequencing of the insert

T7 transcription termination region: Sequence from bacteriophage T7 which permits efficient transcription termination

bla promoter: Allows expression of the ampicillin resistance gene

Ampicillin resistance gene (β -lactamase): Allows selection of the plasmid in *E. coli*

pBR322 origin of replication (ori): Permits replication and maintenance in *E. coli*

ROP ORF: Interacts with the pBR322 origin to facilitate low-copy replication in *E. coli*

lacI ORF: Encodes lac repressor which binds to the T7lac promoter to block basal transcription of the gene of interest and to the lacUV5 promoter in the host chromosome to repress transcription of T7 RNA polymerase

The next day, multiple isolated colonies were selected and grown individually in 5 ml LB medium supplemented with ampicillin (0.01% [w/v]) under shaking at 37 °C overnight.

The following day, 600 µl of the culture were prepared as glycerol (33% [v/v]) stocks for long-time storage at -80 °C for future experiments before continuing.

Plasmid DNA was isolated according to Macherey-Nagel's NucleoSpin® Plasmid/Plasmid (NoLid) kit protocol. Spinning steps were performed using maximum spinning speed and DNA elution was achieved with 30 µl ddH₂O.

Isolated plasmid DNA concentrations were measured spectrophotometrically and a control PCR was implemented in order to verify the molecular size and purity of isolated plasmid DNA. This control PCR was done with the EagleTaq DNA polymerase. 1 µl of plasmid DNA or ddH₂O control, respectively and 0.4 µl of each corresponding 10 pM primer stock solution were added to a PCR master mix (0.4 µl polymerase, 13.8 µl ddH₂O, 2 µl 10x DNA polymerase PCR buffer, 1.2 µl MgCl₂ solution, 0.2 µl 10 mM dNTPs, 1 µl QuikSolution).

A three-step cycling protocol was established consisting of a 3 min initial denaturation at 95 °C, followed by 35 cycles of 30 sec denaturation at 95 °C, 30 sec annealing at 63 °C and 1 min extension at 68 °C. Final extension was performed at 68 °C for 10 min after which the reaction was put on hold at 4 °C until further processing. PCR performance was controlled as described in the corresponding section.

To verify correct cloning of the DNA sequence of interest, plasmid DNA was sent for sequencing to Eurofins Genomics using the T7 promotor for forward sequencing and the reverse T7 promotor for reverse sequencing.

For isolation of larger DNA quantities, the HiSpeed Plasmid Maxi Kit was used according to the respective protocol.

2.2.3.4 Protein expression and purification of recombinant CMYA5 moieties

In order to test FHL2 binding to the different recombinant CMYA5 moieties in pull-down experiments, the vectors were transformed into One Shot® BL21 Star™ (DE3) chemically competent *E. coli* for recombinant protein expression. 10 ng of plasmid DNA were used for transformation. Shaking was done with maximum speed, before 50 µl and 200 µl of the transformation reaction were plated onto ampicillin-selective LB-agar plates.

The following day, multiple colonies were picked and separately grown overnight in 5 ml LB medium containing ampicillin (0.01% [w/v]) at 37 °C under mild shaking.

Bacterial glycerol stocks were prepared as described above. Before large-scale induction of recombinant protein expression, small-scale inductions were performed in order to identify

most efficient protein-producing clones. For each selected colony, 100 µl of culture were added to 900 µl fresh LB medium containing ampicillin (0.01% [w/v]) and incubated on a heat block at 37 °C for 1 h under mild shaking. To induce protein expression, 5 mM IPTG were added and the cells were left for 3 h at 37 °C and 1400 rpm. Non-induced cultures of the respective clones were used to assess the degree of recombinant protein expression. The cultures were centrifuged for 1 min at maximum speed, the supernatant was discarded and the pellets containing the bacterial cells were resolved in 150 µl 3x reducing sample buffer each. SDS-PAGE was performed as described above, using 1 mm polyacrylamide (10%) gels. The gels were subsequently stained overnight with Coomassie SDS-PAGE gel staining solution and destained (50% (v/v) methanol, 10% glacial acetic acid) the next day.

For large scale protein expression and purification of the recombinant CMYA5 moieties, small amounts of the frozen bacterial stocks of the selected clones were added to 30 ml ampicillin (0.01% [w/v]) selective LB medium and incubated at 37 °C overnight under mild shaking.

The following day, this culture was used to inoculate 270 ml fresh LB medium containing ampicillin (0.01% [w/v]) and incubated under mild shaking at 37 °C until the optical density at 600 nm (OD_{600}) reached 0.9. Protein expression was induced by adding 5 mM IPTG and cultures were incubated for 5 h at 30 °C. They were subsequently spun down at 4 °C for 20 min at 4000 g, the supernatant was discarded and the pellet was washed with 10 ml ice cold PBS. After a second centrifugation step, the supernatant was removed and the cell pellet was shock frozen in liquid nitrogen and stored at -80 °C overnight.

The next day, cells were thawed on ice and lysed in 10 ml lysis buffer. The lysate was sonicated using five times 25 sec of sonication with 38% power and 20 sec intervals on ice and subsequently clarified by centrifugation at 4 °C for 35 min at 10000 g. Ni/NTA agarose was used for protein purification of recombinant His₆-tagged CMYA5 moieties. Whilst centrifugation of the sonicated lysate, 1 ml Ni/NTA agarose was washed to equilibrate twice with 1 ml lysis buffer before the supernatant was gently added. The mixture was transferred to a polypropylene column and mixed for 1 h at 4 °C on a spinning wheel. Subsequently, the lysate was allowed to empty by gravity through the column and then the Ni-NTA agarose column was washed twice with 10 ml wash buffer at 4 °C. Elution of the recombinant protein was achieved with 4 ml elution buffer and the eluate was transferred into dialysis tubing and dialysed in 1.5 l dialysis buffer under mild stirring at 4 °C overnight.

Protein expression and purification was tested via SDS-PAGE and subsequent Coomassie staining of samples from different stages of the procedure (before induction - after induction -

after sonication - cleared lysate - flow through - wash 1 - wash 2 - eluate - dialysed eluate). The concentration of the purified recombinant proteins was assessed by using the Bradford assay according to protocol. A BSA standard curve was used comprising twelve different concentrations (0 – 2 ng/μl) and three dilutions of the protein of interest (1:1, 1:3, 1:10) were used to estimate the respective concentration of the purified protein.

Since recombinant CMYA5 moiety #8 showed low concentrations, it was subsequently concentrated at 4 °C with a Centricon® centrifugal filter device with a cut-off for proteins with a molecular mass of 30 kDa (YM-30) by centrifugation at 5000 g until about 90% of the dialysed eluate was run through the filter membrane. The recombinant protein was recovered by reversal of the filter device by centrifugation at 5000 g for 10 min.

2.2.3.5 Protein expression and purification of recombinant GST-FHL2

For expression of GST-FHL2, One Shot® BL21 Star™ (DE3) chemically competent *E. coli* cells were grown overnight from a glycerol stock available in our institute and 200 μl of cell culture was plated onto ampicillin-selective LB-agar plates.

The next day one colony was picked and grown in 400 ml LB medium containing ampicillin (0.01% [w/v]) in an Erlenmeyer flask with large indentations until OD₆₀₀ reached 1.5. After cold shocking the bacteria by shaking on ice for 15 min, 100 μM ZnCl₂ was added and protein expression was induced with 0.2 mM IPTG overnight, at room temperature under mild swirling.

The cell culture was centrifuged at 5000 rpm (4 °C, 15 min) and the pellet was washed with 50 ml ice cold PBS before a second spin. Cells were lysed in 5 ml lysis buffer containing 1% (v/v) Triton X-100 in PBS and a Complete protease inhibitor cocktail. This was followed by sonication and centrifugation of the lysate as described in the previous section. For the recombinant protein purification, 1 ml glutathione sepharose 4B slurry was washed twice with 10 ml PBS, equilibrated twice with 10 ml 1% (v/v) Triton X-100 in PBS, mixed with the bacterial lysate supernatant, transferred in a polypropylene column and incubated for 1 h at 4 °C on a spinning wheel. After passing the lysate through the column by gravity, the column was washed twice with 10 ml PBS and elution was achieved with 5 ml 5 mM reduced glutathione in 50 mM Tris (pH 8.0). Dialysis was performed overnight at 4 °C in 2 l 50 mM Tris (pH 8.0).

Control SDS-PAGE for procedure efficiency and purity of the recombinant protein, and a Bradford assay to estimate recombinant protein concentrations were performed as described in the according sections.

2.2.4 Investigation of the FHL2-CMYA5 interaction

2.2.4.1 Pull-down assay

Glutathione Sepharose 4B beads were used as the matrix to bind recombinant GST-FHL2 or GST (as control). 50 µl beads were washed twice with 300 µl ice cold assay buffer (30 mM Trizma[®]-base (pH 7.4), 15 mM MgCl₂, 1 mM DL-dithiothreitol, 1% (v/v) Triton X-100) for 1 min at 1000 g, after which 500 µl assay buffer and 200 pmol recombinant GST-FHL2 or GST were added and mixed under rotation for 1 h at 4 °C. Matrix without any pre-bound protein in assay buffer was used to control for unspecific binding of proteins to the matrix (negative control). Subsequently, 400 pmol recombinant CMYA5 moieties were admixed and incubated under rotation for additional 2 h at 4 °C.

Mixtures were then centrifuged at 1500 g (4 °C, 90 sec) and the supernatants (unbound protein fractions) were transferred into clean tubes, each receiving 250 µl 3x reducing sample buffer. Pellets (bound protein fractions) were washed three times 90 sec with 500 µl assay buffer at 4 °C and 1500 g before being resolved in 70 µl 3x reducing sample buffer. Samples were stored at -20 °C until analysis by SDS-PAGE and western immunoblotting using primary antibodies against the V5- or GST-tag, respectively.

2.2.4.2 Peptide array

In order to narrow down the exact FHL2 binding site on CMYA5, peptide arrays were performed in collaboration with Prof George Baillie and Jane Findlay (Institute of Cardiovascular and Medical Sciences in Glasgow, United Kingdom) as described in previous work of their group and others^{116, 117}. Recombinant CMYA5 moieties #1 and #8 showed increased binding to FHL2 in pull-down experiments and were therefore chosen for the peptide array. These domains were synthesised as overlapping 25 amino acid-containing peptides using the MultiPep Celluspots, an automated multiple peptide synthesiser from INTAVIS Bioanalytical Instruments AG. Peptide synthesis was planned as depicted in Figure 6 and executed according to the manufacturer's instructions.

CMYA5 #1	N-term - MASRDSNHAGESFLGSDGDEEATRELETEEESEGEEDETA... -C-term
Peptide 1	N-term - MASRDSNHAGESFLGSDGDEEATRELETEEESEGEEDETA... -C-term
Peptide 2	N-term - MASRDSNHAGESFLGSDGDEEATRELETEEESEGEEDETA... -C-term
Peptide 3	N-term - MASRDSNHAGESFLGSDGDEEATRELETEEESEGEEDETA... -C-term
Peptide 4	N-term - MASRDSNHAGESFLGSDGDEEATRELETEEESEGEEDETA... -C-term

Figure 6: Exemplary depiction of peptide synthesis for the N-terminal fraction of CMYA5 moiety #1

Peptides were synthesised as 25-mers with 5 amino acid shifts. Red characters indicate the synthesised peptide.

Using fluorenylmethyloxycarbonyl (Fmoc) chemistry, peptides were synthesised on cellulose discs in the robot. A synthesis scale of 2 μ mol and a double coupling protocol were chosen.

Following peptide synthesis, cellulose discs were placed into 96 well plates. Fmoc side chains were removed from the peptides by incubating discs with 150 μ l side chain cleavage solution (80% TFA, 3% TIPS, 5% H₂O, 12% dichloromethane). After 1 h incubation at room temperature, the solution was aspirated off, 250 μ l cellulose solvation solution (88.5% TFA, 4% TFMSA, 2.5% TIPS, 5% H₂O) was added and the plates were incubated overnight at room temperature. 750 μ l ice-cold methyl tert-butyl ether was pipetted into each well and the plates were inverted 10 times before incubation at -20 °C for 1 h and a subsequent spin at 4 °C at 2000 g for 20 min. The ether was tipped off and the procedure was repeated without incubation at -20 °C. The plates were dried upside down in a fume cupboard for 15 min, after which 300 μ l DMSO were added to each well and the plates were left open for 2 h.

To spot the peptides on coated slides, 30 μ l of peptide solution were mixed with 10 μ l 1x SSC buffer and transferred into a 384-well plate. Spotting was performed automatically using the Slide Spotting Robot by INTAVIS Bioanalytical Instruments AG according to its manual.

After spotting, the slides were wetted in TTBS and blocked with 3 ml 5% (w/v) BSA in TTBS for 2 h. The slides were rinsed in TTBS and 0.1 μ mol recombinant GST-FHL2 or GST diluted in 2.5 ml 0.5% (w/v) BSA in TTBS was added. Incubation was done on a shaker overnight at 4 °C.

The next day, the slides were washed three times 10 min with TTBS before addition of the primary anti-GST antibody in 1% (w/v) BSA in TTBS and incubation overnight at 4 °C. The primary antibody was washed off three times 5 min with TTBS and the slides were incubated for 1 h with secondary antibody solution in 1% BSA (w/v) in TTBS followed by three times 10 min washing with TTBS. Incubation with ECL and development was performed as described for western immunoblotting.

2.2.5 Analysis of adult rat ventricular myocytes

2.2.5.1 Immunocytochemistry and confocal microscopy

Fresh cultured adult rat ventricular myocytes (ARVM) from male Wistar rats (body weight: 200-250 g) in single cell culture dishes were kindly prepared by Angelika Piasecki from our group according to a protocol used in previous work¹¹⁸.

Maintenance medium was aspirated from ARVM and the cells were washed with 2 ml PBS. Cells were fixed with 1 ml 4% (v/v) paraformaldehyde in PBS for 10 min and washed three times 5 min with PBS on a shaker. The last wash was not aspirated and cells were stored at 4 °C until further processing.

Fixed cells were permeabilised by incubation with 2 ml 0.2% (v/v) Triton X-100 in PBS for 5 min and subsequently washed with 2 ml PBS for 5 min. The edge of the cell culture dish was dried with a cotton bud and sealed with a wax pen before blocking of non-specific binding sites with 100 µl 5% (v/v) NGS in 1% (w/v) BSA in Gold buffer for 20 min was performed. Cells were incubated with 1% (v/v) primary antibody in 100 µl 1% (w/v) BSA/Gold buffer overnight at 4 °C in a humid chamber with mild shaking.

The following day, cells were washed three times 5 min with PBS on a shaker before incubation with 1% (v/v) secondary antibody and 0.01% (v/v) DAPI in 100 µl 1% BSA in Gold buffer for 3 h in a light-tight humid chamber on a shaker. After three times 5 min washing with PBS under minimal light exposure one drop of Lisbeth's medium was applied and the dish was capped with a cover slip. The walls of the dish were removed with a heated wire and the dish was mounted onto a glass microscopic slide with glue. The cover slip was sealed with nail varnish and the slide was stored deprived of light at 4 °C until examination by confocal microscopy.

Confocal microscopy was performed with the kind help of Nils Mangels (Institute of Biochemistry and Molecular Cell Biology, UKE Hamburg). A TI Eclipse microscope with A1 plus camera, APO TIRF 60X Oil DIC N2 objective and NIS Elements software 4.20 was used to acquire images. The excitation and emission wavelengths of the fluorescent dyes utilised in this study are displayed in Table 14.

Table 14: Dyes and laser settings used in immunofluorescence/Duolink[®] assay

Dye	Targets	Excitation wave-length in nm	Emission wave-length in nm
DAPI	A-T rich regions of DNA (nuclear staining)	405.00	450.00
Alexa488	FHL2, α -actinin	488.00	525.00
Cy3	CMYA5, cMyBP-C, Duolink	561.00	595.00
pinhole radius: 39.59 μ m (IF); 34.48 μ m (Duolink [®])			

2.2.5.2 Duolink[®] assay

Duolink[®] assays are proximity ligation assays (PLA) based on PLA probes that recognise primary antibodies and contain small DNA sequences. If two different targets come in close proximity within a cell, the two different DNA sequences can be ligated and amplified by rolling circle amplification with fluorescently labelled DNA nucleotides. In consequence, the single channel signal indicates similar cellular sublocalisation of the primary targets.

Cell preparation, fixation, permeabilisation, nonspecific binding site blocking and incubation with primary antibodies were performed identical as described for confocal microscopy in the according section. Slides with single primary antibody staining were prepared as negative controls.

Duolink's[®] PLA probes were diluted in 1% (w/v) BSA in Gold buffer and the assay protocol was implemented with preparation of 100 μ l solutions per dish. After incubation with the ligation and amplification solution according to the protocol and application of the cover slip, slide preparation was performed as specified in the previous section.

Slides were stored at -20 °C in the dark and examined within 48 h with the aforementioned hardware setup. All image acquisition was kindly performed by Nils Mangels.

For information regarding the laser settings see Table 14.

2.2.6 Cell size measurement of stimulated neonatal rat ventricular myocytes pre-treated with disrupting peptide

NRVM were isolated from 0-3 days old Wistar rats according to an established protocol in the Institute of Experimental Pharmacology and Toxicology as described in previous publications¹¹⁹.

Cells were resuspended in plating medium (v/v: 63% DMEM, 17% M199, 10% horse serum, 5% fetal bovine serum) supplemented with 1% (v/v) penicillin/streptomycin and plated in 70 mm cell culture dishes for 90 min. In this pre-plating step, the non-myocytes adhere to the bottom of the dish while cardiac myocytes remain floating in the medium. Following this step, the medium with NRVM was collected and cells were plated in 35 mm cell culture dishes pre-coated with 1% gelatin in PBS. After 18 h, cells were washed once with maintenance medium (80% (v/v) DMEM, 20% (v/v) M199) supplemented with 1% (v/v) penicillin/streptomycin to remove dead cells and then kept in maintenance medium.

Pharmacological treatments took place on the following day. Initially, cells were pre-treated for 3 h with vehicle (DMSO) or myristoylated FHL2-CMYA5 interaction disruption peptide for rat (sequence: LQISSNGTVISFSERRRLTEIPSVL; final concentration: 10 μ M) after which time PE was added to a final concentration of 3 μ M and incubated for 48 h. Cells were washed with PBS and fixed in 4% (v/v) PFA as described in the section on immunocytochemistry and confocal microscopy. Then, cells were stained with antibodies against α -actinin and CMYA5. Specimens were imaged by confocal microscopy obtaining images from different areas of the slides so as to have at least 75 cells per dish, which could be used to assess cell surface area. This was achieved using the acquired α -actinin images and Image J software¹²⁰. Statistical analysis was performed using the Student's t-test (P<0.05 was considered significant).

3 Results

Importantly, as obvious from the extensive methods section, this dissertation is based on the establishment of novel tools and sophisticated methods to study protein-protein interactions *in vitro* and *in cellulo*. Therefore, the methods are considered as a proportion of the results chapter and some overlap might exist.

3.1 Analysis of mRNA and protein levels of CMYA5 in human left ventricular heart tissue samples

In order to investigate potential differences in gene expression and protein expression levels of CMYA5 and FHL2 in human heart failure, mRNA and protein levels were analyzed in human left ventricular heart tissue samples from non-failing (NF) donors and patients with end-stage heart failure due to ischemic (ICM) or dilated (DCM) cardiomyopathy.

3.1.1 mRNA expression levels

MRNA levels of *FHL2* and *CMYA5* were investigated by quantitative PCR (RT-qPCR). Analysis of the results revealed no significant difference for *FHL2* mRNA levels in patients compared to NF donors. However, there was a trend towards decreased mRNA levels for *FHL2* in failing heart samples detectable, them not being significant might be due to small n-numbers per group. In contrast, *CMYA5* mRNA levels were significantly increased in ICM samples (see Figure 7).

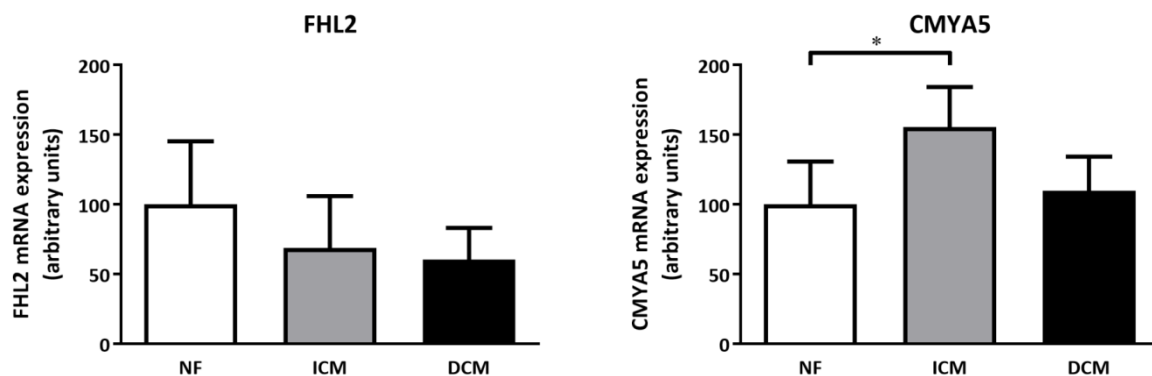


Figure 7: *FHL2* and *CMYA5* mRNA expression analysis in human ventricular cardiac tissue

FHL2 and *CMYA5* mRNA expression levels were measured by RT-qPCR in human left ventricular heart samples from NF donors and patients with ICM or DCM. Bar charts express results as percentage of the average *FHL2* or *CMYA5* mRNA levels in the NF samples. $p < 0.05$, $N = 4$

3.1.2 Protein expression levels

Protein levels of FHL2 and CMYA5 in human heart tissue samples from NF donors or patients with ICM and DCM were evaluated by western immunoblotting. Quantification was achieved by densitometry of the blots and the results were statistically analyzed.

Protein levels of FHL2 were significantly reduced in diseased samples compared to NF samples. CMYA5 protein levels were vice versa increased under disease conditions (see Figure 8).

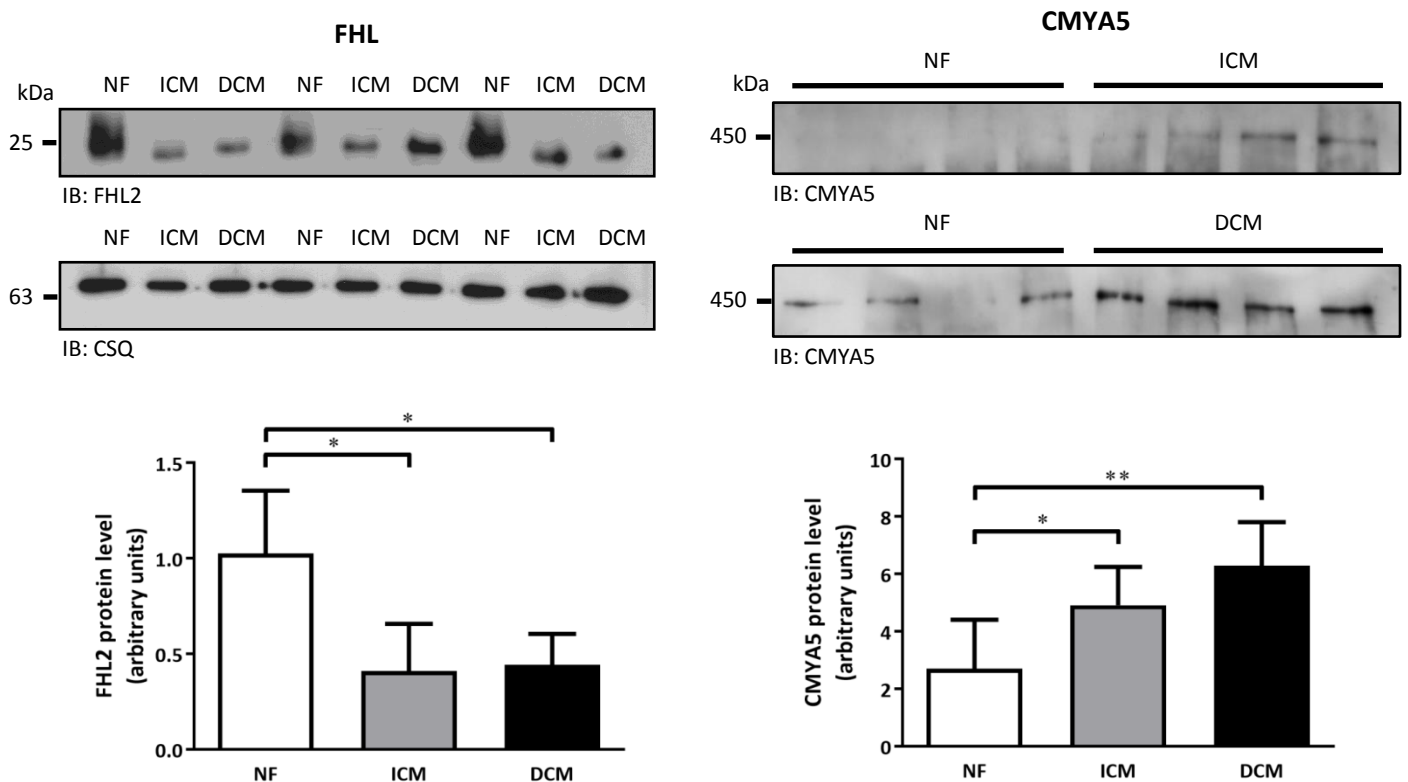


Figure 8: Protein levels of FHL2 and CMYA5 in NF, ICM and DCM human heart samples

FHL2 and CMYA5 protein levels were assessed by western immunoblotting using respective antibodies. Protein loading for FHL2 was assessed by immunoblotting for calsequestrin (CSQ). Due to technical challenges for blotting of large proteins, ICM and DCM samples for CMYA5 were tested in two separate runs. Each run was performed with four NF samples as control. The results were merged in the according bar chart with ICM and DCM expressed relatively to their corresponding controls. For CMYA5 no loading control was performed due to the high molecular mass of CMYA5 of 450 kDa.

Bar charts summarize the data of the western immunoblots. * $p < 0.05$; ** $p < 0.01$; FHL2 N=3; CMYA5 N=4

3.2 PCR cloning and protein expression of recombinant CMYA5 moieties

3.2.1 PCR

To confirm the CMYA5-FHL2 interaction using independent methodology and to map the region of FHL2 interaction on CMYA5, we generated eight non-overlapping cDNA moieties for recombinant protein expression. Human *CMYA5* cDNA was cloned from NF human heart tissue. Primers were designed and used to clone eight constructs from genomic human cDNA for subsequent insertion into a bacterial protein expression vector allowing recombinant protein expression and purification. Each construct consisted of 1500 bp (translating into 500 aa). The slightly larger C-terminal moiety (1707 bp; 569 aa) unites all previously described functionally important protein binding domains of CMYA5 (Figure 9). This allowed the subcloning and subsequent expression of the entire *CMYA5* mRNA (Figure 10).



Figure 9: Schematic depiction of eight non-overlapping CMYA5 moieties

CMYA5 moieties #1 (aa 1-500; bp 1-1500) to #7 (aa 3001-3500; bp 10001-11500) comprise 500 aa (1500 bp), moiety #8 (aa 3501-4069; bp 11501-12207) comprises 569 aa (1707 bp) and contains the protein binding motifs BBC, FN3 I, FN3 II and SPRY.

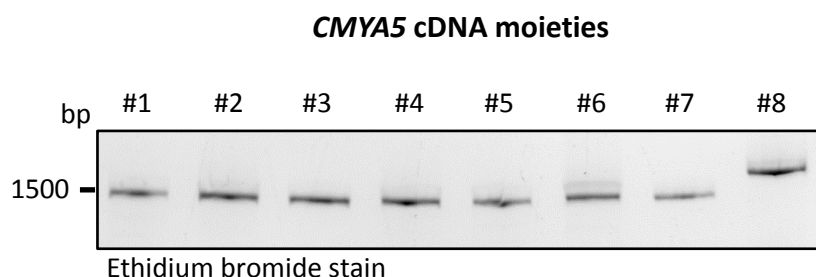


Figure 10: PCR amplification of *CMYA5* cDNA moieties

Agarose gel electrophoresis shows amplified cDNA moieties #1 (bp 1-1500) - #7 (bp 9001-11500) at the expected size of 1500 bp and moiety #8 (bp 11501-12207) at the expected larger size of 1707 bp.

3.2.2. Cloning of *CMYA5* cDNA moieties into *Champion*TM *pET 151 D-TOPO* vector and transformation into *One Shot*[®] *TOP10* chemically competent *E. coli*

The eight *CMYA5* cDNA sequences were cloned each into the *Champion*TM *pET151 D-TOPO* vector, containing a His₆-tag as well as a V5-epitope upstream of its multiple cloning site. After transformation into *One Shot*[®] *TOP10* chemically competent *E. coli* cells, five clones from each transformation were picked for plasmid DNA isolation. In order to verify correct ligation, analysis was performed via PCR using the same primers as for the cloning and plasmid DNA as templates with subsequent agarose gel electrophoresis (Figure 11) as well as spectrophotometrical determination of the DNA concentration. The sequences with correct sizes and highest DNA concentrations were sent for sequencing using the internal T7 promoter primer (see Appendix 2). Assessment of the sequencing results verified successful cloning of all eight sequences into the *Champion*TM *pET151 D-TOPO* vector.

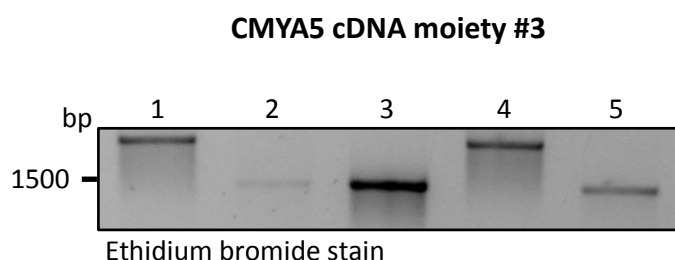


Figure 11: Example of plasmid DNA isolation of *CMYA5* moiety #3

Agarose gel electrophoresis of five PCR products derived from control PCR using the same primers as for cloning and the plasmids as template randomly picked for *CMYA* moiety #3. Clones 2, 3 and 5 display the expected molecular size of 1500 bp. Clones 1 and 4 migrate at a higher molecular size, indicating defective cloning. Clone 3 showed the highest DNA concentration spectrophotometrically and was sent for sequencing to Eurofins Genomics (see Appendix 2).

3.2.3 Recombinant protein expression

After confirmation of correctly inserted sequences, the vectors were transformed into One Shot[®] BL21 (DE3), chemically competent *E. coli* cells for recombinant protein expression. Expression was induced by IPTG and purification achieved by Ni/NTA agarose bead affinity chromatography. His₆-tagging of the recombinant proteins enables selection of targeted proteins by Ni/NTA agarose beads. We were able to express and purify seven out of eight recombinant CMYA5 moieties, lacking moiety #6 (aa 2501-3000; Figure 12).

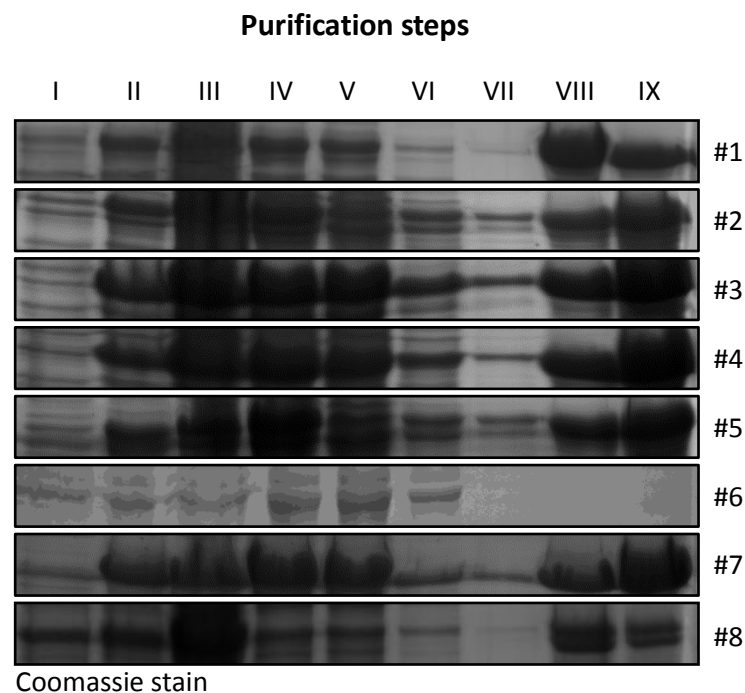


Figure 12: Induction and purification of recombinant CMYA5 protein moieties

Coomassie stained SDS-PAGE highlight the presence of the recombinant proteins during different steps of the purification procedure. (I) shows protein expression before induction. After induction (II) and cell lysis, the lysate was sonicated (III) and cleared by centrifugation (IV). It was bound to Ni/NTA columns, the flow through (V) and two washing steps (VI, VII) were collected before elution was performed (VIII). The final step was overnight dialysis of the eluate (IX).

All moieties except #6 were successfully induced and purified of the cells and show high protein levels in the final protein solution (dialysed eluate). Moiety #6 shows expression after induction but does not bind sufficiently to the column and could thus not be purified.

The electrophoresis shows irregular migration pattern for all moieties that is shown in Figure 13 and was assessed by western immunoblot analysis using an anti-V5 antibody.

For displayed molecular sizes see Figure 13.

In the absence of a suitable antibody that could recognise all CMYA5 moieties and to test for correct recombinant protein expression, SDS-PAGE and western immunoblot analysis was performed using an anti-V5 antibody. All proteins analyzed showed gel electrophoresis migration patterns that deviated from the expected calculated molecular mass of about 55 kDa (or 60 kDa, respectively, for the C-terminal moiety #8; Figure 13) and suggests an impact of the protein folding or posttranslational modifications of the proteins on the migration pattern. Although inconsistent migration patterns indicate larger inserts, the sequencing confirmed the correct insert sequences and the presence of a stop codon. The strong anti-V5 signal in western immunoblot analysis indicates expression of the proteins of interest. All recombinant protein concentrations were measured by Bradford assay. Moiety #8 showed lowest concentration and was subsequently concentrated using Centricon[®] centrifugal filter devices YM-30.

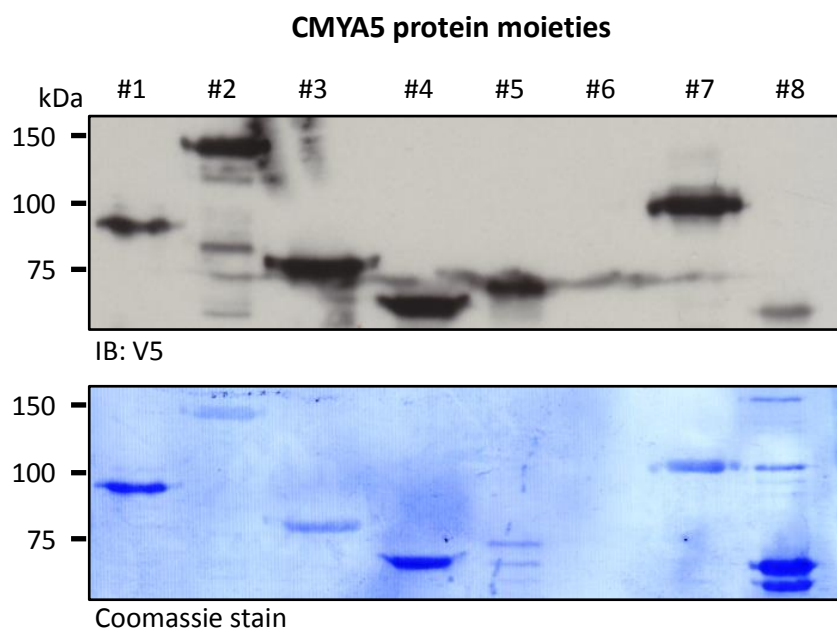


Figure 13: SDS-PAGE and western immunoblot analysis of recombinant protein expression

Upper panel: Western immunoblot analysis of eight recombinant CMYA5 moieties using an anti-V5 primary antibody. The calculated molecular mass is about 55 kDa for moieties #1 - #7 and about 60 kDa for moiety #8. Moiety #6 was not successfully purified. Moieties #1 - #7 display different migration patterns in SDS-PAGE with moiety #2 migrating highest at around 150 kDa.

Lower panel: Corresponding Coomassie stained PVDF membrane for total protein staining.

3.3 Investigation of the FHL2-CMYA5 interaction

3.3.1 Pull-down assays

Pull-down assays were performed in order to test GST-FHL2 binding to the recombinant CMYA5 protein moieties and to identify the interaction domain that is able to bind to FHL2. In order to do so, recombinant GST-tagged FHL2 was pre-bound to glutathione-*S*-sepharose beads via its GST-tag and the respective recombinant CMYA5 moieties were added afterwards. In order to exclude unspecific binding of CMYA5 moieties to GST or to the beads, control samples were included, in which recombinantly expressed CMYA5 proteins were incubated with pre-bound recombinant GST or beads only (\emptyset), respectively (Figure 14).

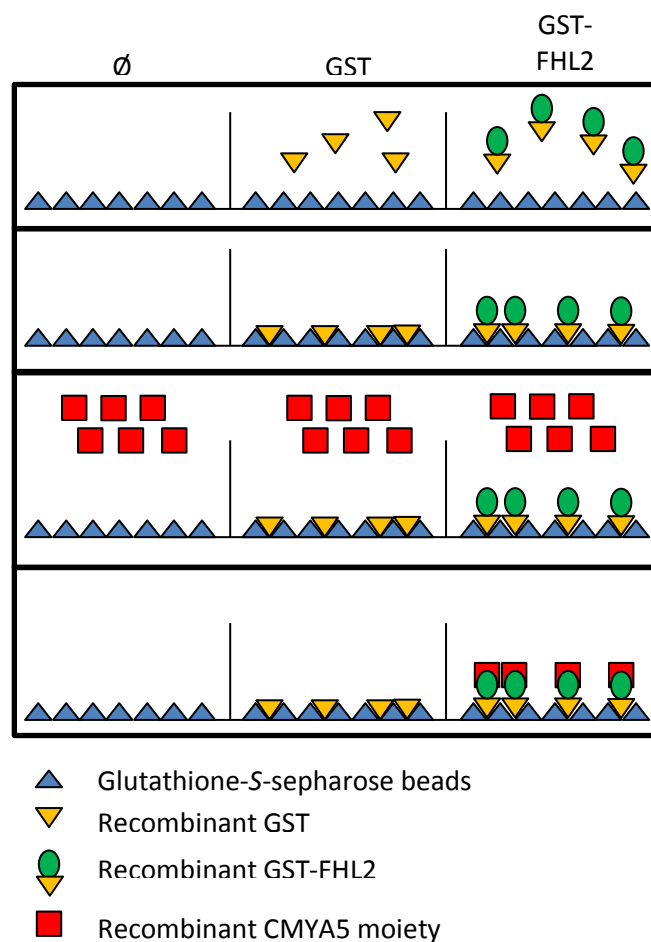


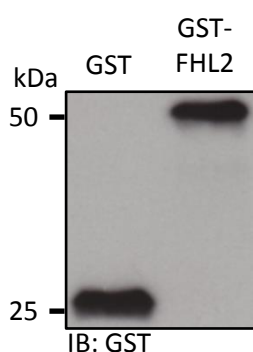
Figure 14: Schematic depiction of pull-down assays

GST or GST-FHL2 was bound to glutathione-*S*-sepharose beads. Empty beads (\emptyset) were used as additional control. Recombinant V5-tagged CMYA5 moieties were subsequently added. After washing, binding of the CMYA5 protein moieties was analyzed via western immunoblot analysis using an anti-V5 antibody. The depicted scheme shows an overview of the experimental setup.

GST controls bind strongly to the glutathione-*S*-sepharose beads. Loading of GST and GST-FHL2 in the pull-down assays was comparable as shown by western immunoblotting using an anti-GST antibody (see Figure 15A).

Our data demonstrate that both, the N- and C-terminal protein moieties, moiety #1 (N-terminal) and moiety #8 (C-terminal), bind to FHL2 significantly stronger than controls with recombinant GST or beads only (\emptyset). Observed binding of moieties #2 - #7 was not increased compared to these controls and they were therefore excluded as possible interaction domains for FHL2 (Figure 15B).

A.



B.

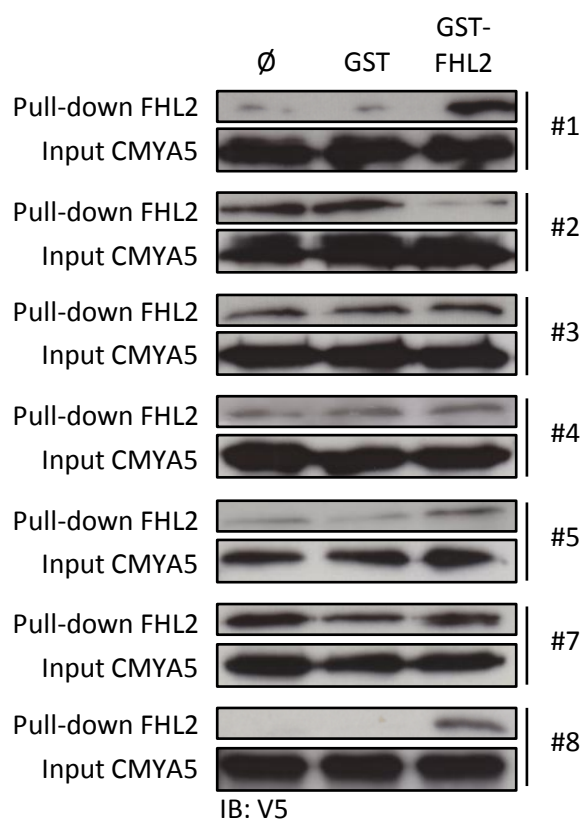


Figure 15: FHL2 binding ability of recombinant CMYA5 moieties

(A) Equal binding of recombinant GST and GST-tagged FHL2 to the glutathione-*S*-sepharose beads was tested separately by western immunoblotting using an anti-GST antibody. The pull-down fraction is displayed.

(B) GST pull-down assays show the ability of N-terminal CMYA5 moiety #1 and C-terminal CMYA5 moiety #8 to bind to FHL2. Recombinant V5-tagged CMYA5 moieties were incubated with GST-tagged FHL2 and tested by western immunoblotting using an anti-V5 antibody. Incubation with recombinant GST or beads alone were used as a negative control (\emptyset). For displayed molecular masses see Figure 13.

After verification of the C-terminus as a putative interaction region for FHL2, we speculated that the FN3 regions might play a pivotal role since several FN3 containing proteins have been identified already as FHL2 binding partners, such as titin and cMyBP-C^{93, 121}. We therefore designed primers to clone this particular region as described for the CMYA5 moieties and expressed that region in order to use it in additional refined pull-down assays (see Table 15).

Table 15: Primers for directional cloning of CMYA5's FN3 regions

aa	Forward primer	Reverse primer
3695 - 3907	CACCATGGCGAGCCGCGA TAGCAAC	TCACATTAGAGGTTTCAGA AAGAGA

Experiments performed using the recombinantly expressed FN3 region were able to show that indeed this protein domain of CMYA5, containing only the two FN3 regions was equally able to bind FHL2 as shown for the larger protein moiety #8 hinting towards these regions as crucially important or at least favorable for FHL2 binding to CMYA5 (see Figure 16).

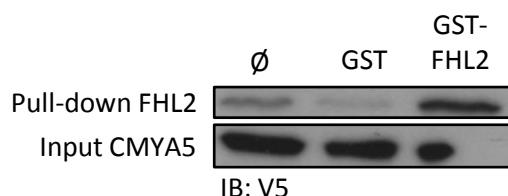


Figure 16: FHL2 binding ability of the FN3 region of CMYA5

GST pull-down assays show the ability of the FN3 region of CMYA5 to bind FHL2. Recombinant V5-tagged CMYA5 moieties were incubated with GST-tagged FHL2 and tested by western immunoblotting using an anti-V5 antibody. Incubation with recombinant GST or beads alone were used as negative controls (∅).

3.3.2 Identification of the FHL2 binding sites of CMYA5 by peptide array

To further confirm and define the exact sites of interaction within the relevant recombinant CMYA5 moieties #1 and #8, the N- and C-terminal regions of CMYA5 were used to inspire peptide arrays. In these arrays, 25 aa comprising peptides were synthesized with a 5 aa overlap covering aa 1-500 (N-terminus) and aa 3501-4069 (C-terminus) of CMYA5 and investigated for their ability to bind to FHL2. The peptides were spotted onto nitrocellulose

membranes and incubated with recombinant GST-FHL2. Recombinant GST alone was used as a negative control to exclude false positive interactions. The membranes were analyzed with an anti-GST antibody (Figure 17).

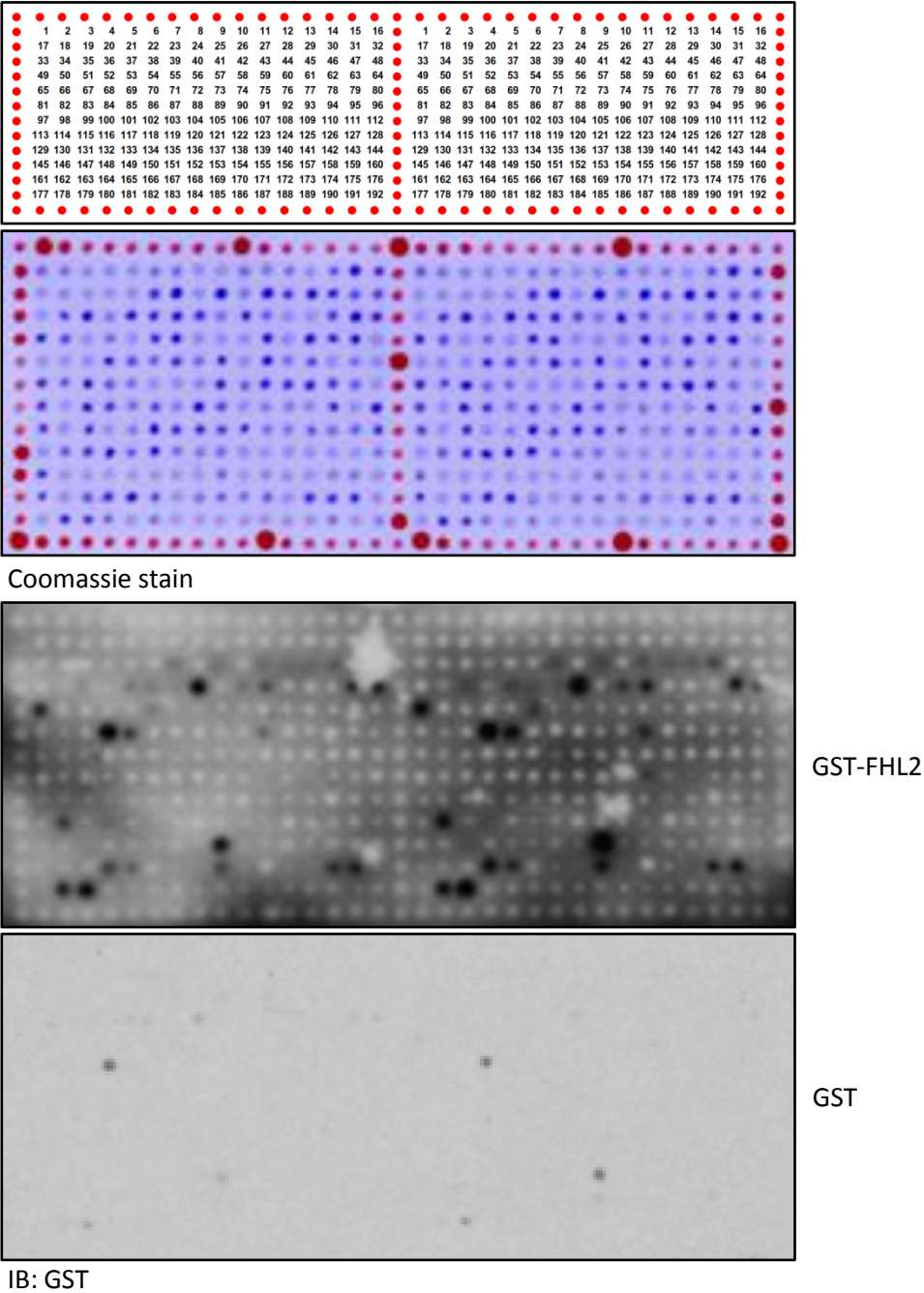


Figure 17: Results of the peptide array

Upper panel: Positioning of each peptide on the nitrocellulose membrane. Each peptide was tested twice. The red dots represent a frame that is used by the spotting machine for orientation.

Middle panel: Coomassie-stained nitrocellulose membrane after spotting of the peptides.

Lower two panels: Detection of signals after incubation of the peptides with GST-FHL2, or GST, respectively, and subsequent testing with anti-GST antibody.

After processing the nitrocellulose membranes, it was revealed that various peptides in the middle regions of moieties #1 and #8 were capable of FHL2 binding, indicated by black spots. As depicted in Figure 18, out of the four described structural domains of CMYA5, the TRIM-like region, the two FN3 regions as well as the SPRY domain, but not the B-box coiled-coil (yellow), comprise FHL2 binding peptides, represented by black spots, thus indicating a possible interaction face. Also, certain peptides based on the N-terminal fraction of CMYA5 showed interaction. FHL2 is the first protein that was shown as a putative interaction partner for the N-terminal portion of CMYA5.

The last 14 peptides, comprising the C-terminal 90 amino acids, could not be synthesized and were not tested for a FHL2 interaction. For a detailed spotting plan see Appendix 4.

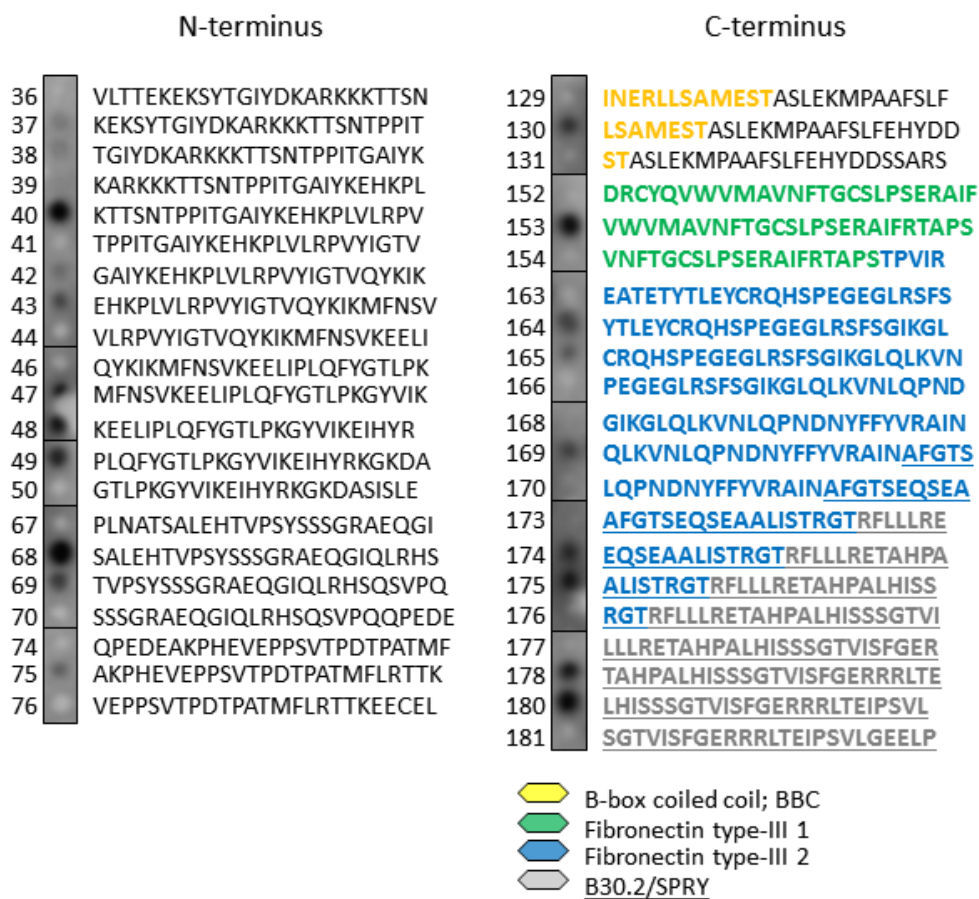


Figure 18: Overview of the peptide array results

Numerous synthesised peptides show GST-FHL2 interaction. The N-terminal 500 aa (moiety #1) of CMYA5 contain several peptide sequences with potential FHL2 interaction, indicated by black spots. Within the C-terminal TRIM-like region of CMYA5, both FN3 regions and the SPRY domain, but not the B-box domain, contain peptides with FHL2 binding affinity. The position of the 25-mers within the 500 aa sequence is indicated on the left side of the sequence, see the detailed spotting plan in Appendix 4.

3.4 Subcellular localization of CMYA5 and FHL2 in ARVM

In order to investigate a potential co-localization of CMYA5 and FHL2 in a native environment, immunofluorescence and subsequent confocal microscopy were performed in ARVM using an antibody against the C-terminus of CMYA5 as well as an antibody against FHL2. Antibodies that recognize the established Z-disc marker protein α -actinin or cMyBP-C, which is known to localize in the A-band of the C-zones of the sarcomere, were used as references.

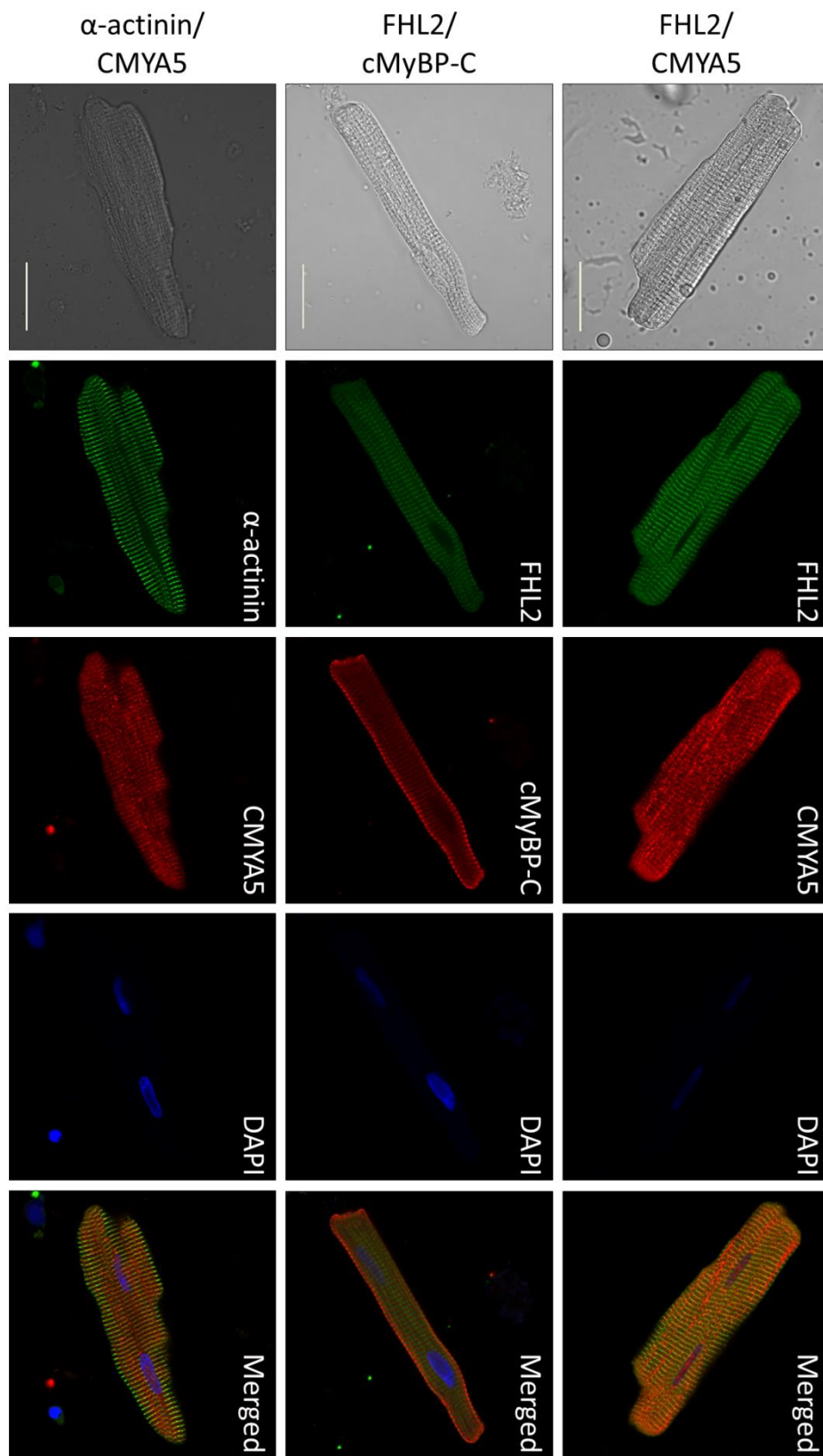
Whilst α -actinin is localized to the Z-disc as a single band, cMyBP-C is organized in doublet-appearing structures representing the C-zones of sarcomeric A-bands (Figure 19A).

When compared to the reference proteins, FHL2 shows a regular single striation pattern with a Z-disc localization within sarcomeres. This is revealed by co-staining with cMyBP-C as shown by the 2D-signal density report that revealed alternate sarcomeric expression, confirming Z-disc localization of FHL2 within the myofilament lattice.

CMYA5 also shows a striated pattern and sarcomeric localization, however, additional nuclear staining and faint longitudinal bands were detectable. In order to allow conclusions regarding the sarcomeric localization of CMYA5 within the sarcomere, ARVM were co-stained with an α -actinin antibody. CMYA5 shows a similar localization pattern as α -actinin and 2D-signal profiling reveals a signal overlay, indicating partial Z-disc localization for the C-terminus of CMYA5 (Figure 19B).

Co-staining of FHL2/CMYA5 and subsequent 2D-signal profiling revealed close proximity of FHL2 and CMYA5 in Z-disc vicinity (Figure 19B).

A.



B.

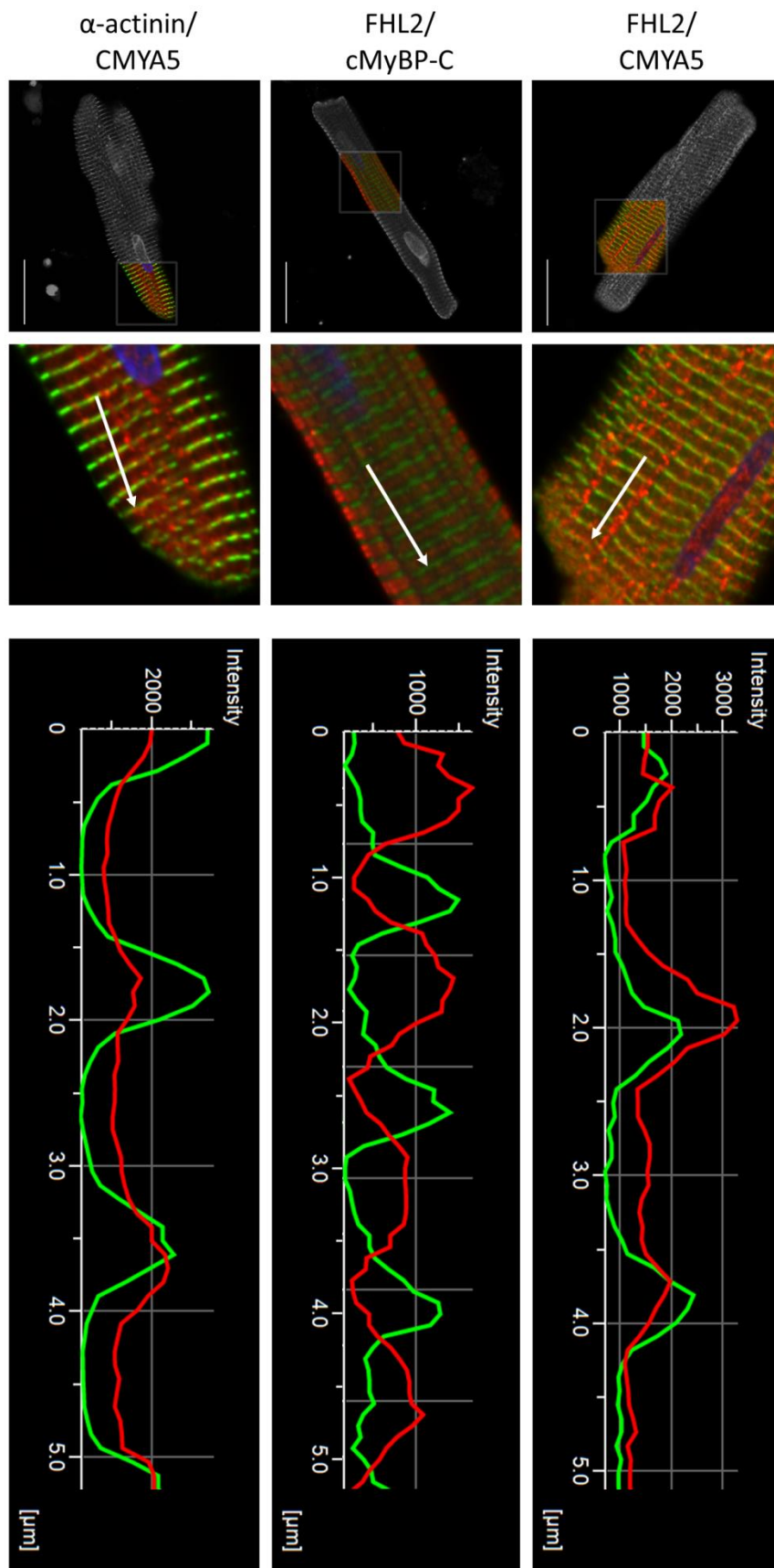


Figure 19: Subcellular localization of FHL2 and CMYA5

(A) Intracellular localization pattern of FHL2 and CMYA5. Immunofluorescence was performed in ARVM using antibodies against FHL2, CMYA5, α -actinin and c-MyBP-C. Nuclear counterstaining was performed with DAPI. All images of the same column are acquired with identical laser settings. Scale bars: 25 μ m

(B) Co-localization of FHL2 and CMYA5. Signal intensity was digitally analyzed over a distance of 10 μ m (white arrows). Results for the first 5 μ m are shown.

Upper panel: Intensity scans show co-localization of FHL2 and CMYA5.

Middle panel: cMyBP-C resides in the C-zone of the A-band and shows alternate localization to FHL2 in the sarcomere.

Lower panel: As cardiac Z-disc marker and interaction partner of CMYA5, α -actinin co-staining shows CMYA5 localization potentially occurs near the Z-disc.

3.5 Analysis of CMYA5 and FHL2 co-localization by Duolink[®] technology

Analysis by immunofluorescence and confocal microscopy suggests a subcellular co-localization of FHL2 and CMYA5, but definitive conclusions regarding their interaction in the cellular environment cannot be drawn by this method. Therefore, Duolink[®] assays were established to investigate the proximity of the FHL2-CMYA5 interaction.

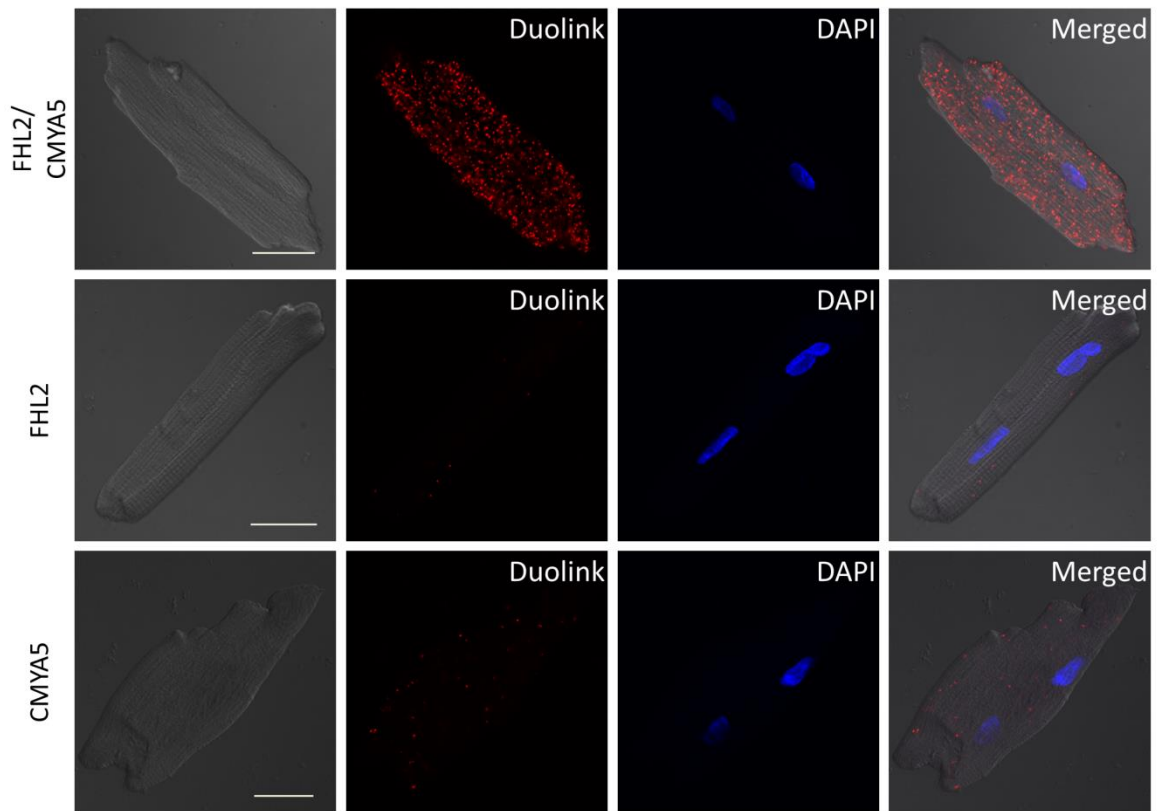
Initially, primary antibodies against FHL2 and CMYA5 were used. Subsequently, incubation with secondary Duolink[®] anti-rabbit and anti-mouse antibodies was performed. These carry DNA oligomers allowing ligation and subsequent rolling circle amplification with fluorescently labelled nucleotides. In the case that both antibodies of both species are coming in direct vicinity, they produce a fluorescent signal that can be visualized by confocal microscopy and thus provides a positive correlate for protein interaction in a cellular environment.

As this method is prone for false positive signals, as described in the respective methods section, control experiments were performed at the same time by labelling either one of the proteins of interest separately to exclude secondary antibody (PLA probes) cross reactivity.

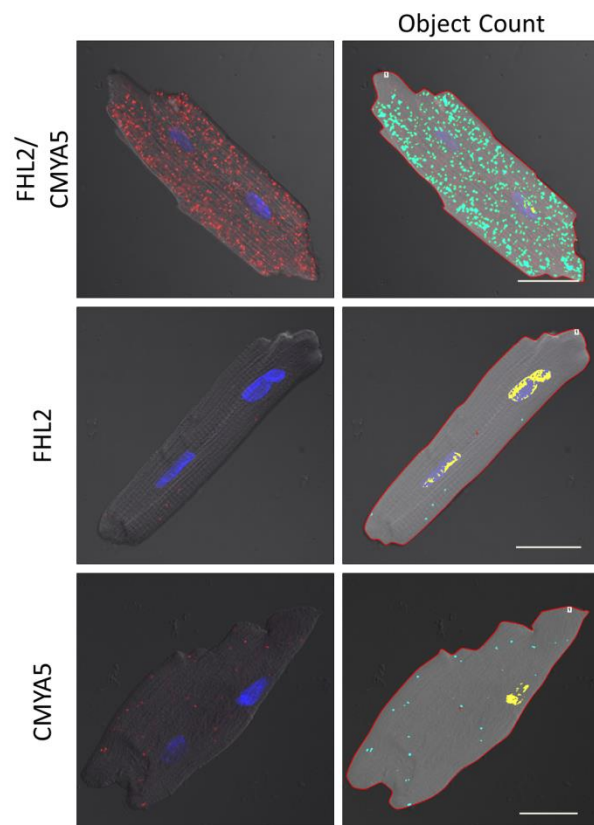
FHL2 and CMYA5 co-staining revealed strong subcellular co-localization of these proteins throughout ARVM, visualized by red fluorescing dots, whereas controls do not display secondary antibody cross-reaction (see Figure 20A). Quantification of the proximity ligation signals was performed by digital object counting. The signals obtained when cells were co-stained were significantly enhanced in comparison to the negative controls, suggesting indeed an interaction of FHL2 and CMYA5 (Figure 20B/C).

Additional Z-stack imaging was performed to demonstrate the protein interaction in a 3D context throughout the entire intracellular compartment (Figure 20D).

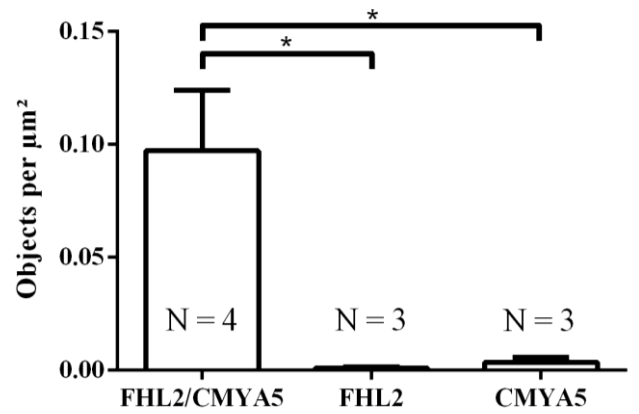
A.



B.



C.



D.

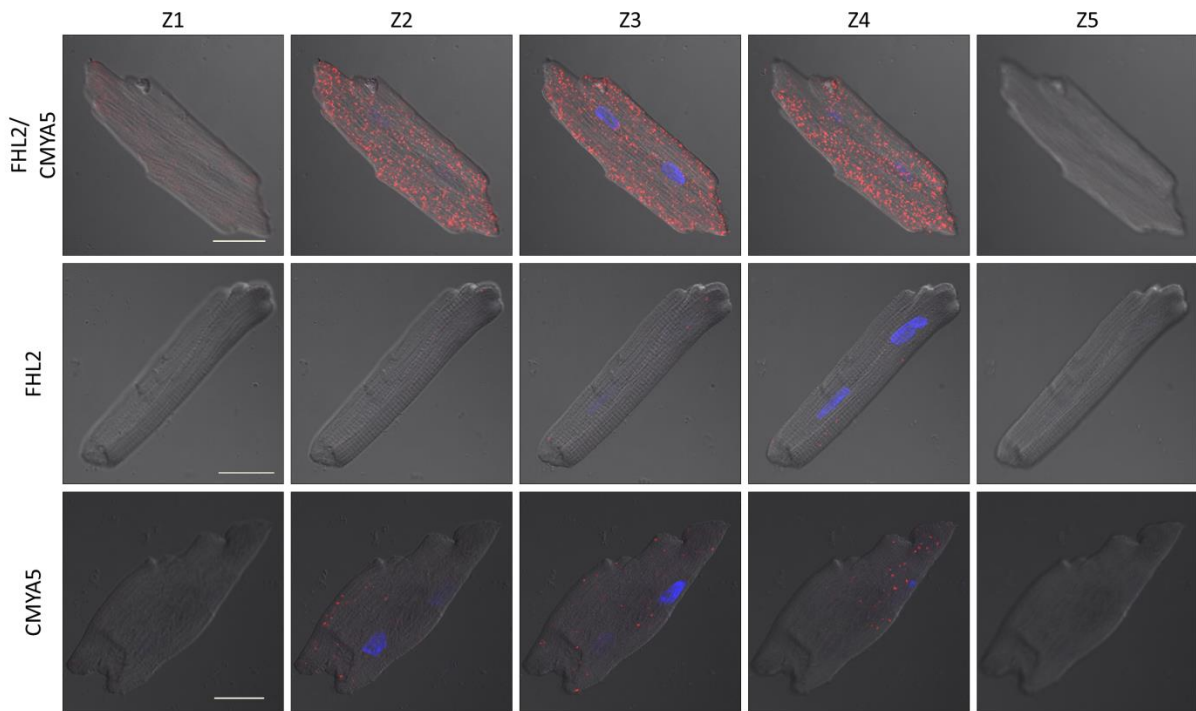


Figure 20: FHL2-CMYA5 co-localization in ARVM

(A) Duolink[®] assay of ARVM co-stained with anti-FHL2 and anti-CMYA5. ARVM were co-stained with primary antibodies against FHL2 and CMYA5 and DNA oligomer-carrying secondary antibodies. The DNA oligomers were ligated and amplified in the presence of fluorescently labelled nucleotides and signal for co-localization. The left column shows images acquired with a transmission detector, the middle two columns show single channel images for the Duolink[®] signal as well as DAPI imaging for nuclear counterstaining and the right column shows merged images. Cells that were co-stained with FHL2 and CMYA5 antibodies show a strong Duolink[®] signal indicating co-localization of these proteins in ARVM. Cells incubated with single primary antibodies and both PLA probes were used as negative controls and do not display significant signal intensity for Duolink[®] signals. Importantly, all images of the same column are acquired with identical laser settings.

(B) Digital object count for Duolink[®] images. Merged signal images were used for digital Duolink[®] signal object counts and are displayed in the left column. The digitally processed images are shown in the right column. The areas taken into account are displayed in brighter grey and surrounded by red lines. A signal intensity threshold was defined automatically and the respective areas were scanned for signals above that level. Each counted signal is displayed as turquoise spot. DAPI signals are processed as yellow areas and are not taken into account. ARVM co-labelled with FHL2 and CMYA5 display much higher numbers of signals than negative controls.

(C) Quantification and statistical analysis of Duolink[®] object counts. Nearly 0.1 objects per μm^2 were counted for co-labelled ARVM and almost none for negative controls.

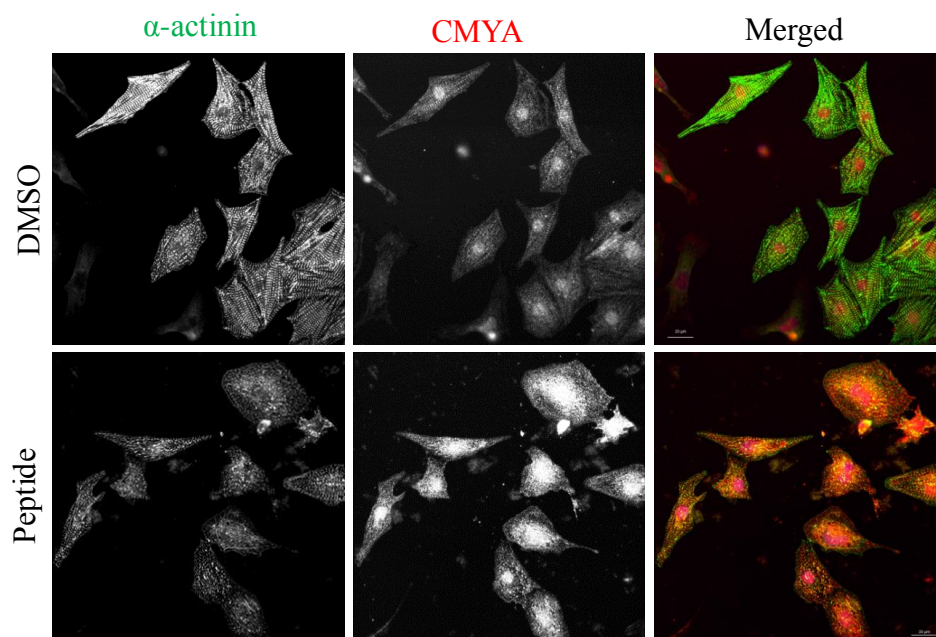
(D) 3D-analysis of co-localization of CMYA5 and FHL2. Z-stack imaging was performed to verify 3D distribution of Duolink[®] signals. Each cell was scanned in Z-orientation and 10 images were acquired with defined intervals. Every second image is displayed. The red fluorescence is distributed equally throughout the ARVM that were co-stained with FHL2 and CMYA5 antibodies, and the absence of signal was confirmed for both negative controls. * $p < 0.05$; co-labelled ARVM: N=4; negative controls: N=3; scale bars: 25 μm .

3.6 Cell surface area measurements of neonatal rat ventricular myocytes exposed to peptides in order to disrupt the FHL2-CMYA5 interaction in response to neurohumoral stimulation

NRVM were isolated from 0-3 day neonatal Wistar rats. Cells were exposed for 3 h with vehicle (DMSO) or a myristoylated FHL2-CMYA5 peptide (rat sequence: LQISSNGTVISFSERRRLTEIPSVL). Subsequently, cells were exposed to (PE) for 48 h to mimic chronic neurohumoral stimulation. Subsequently, cells were fixed and stained with antibodies against α -actinin and CMYA5 for confocal analysis and determination of the cell surface (Figure 21A).

This revealed that cells exposed to the peptide exhibited a significantly smaller cell surface area in response to the neurohumoral intervention, when compared to DMSO treated control cells (Figure 21B), suggesting a functional importance of the FHL2-CMYA5 interaction in pro-hypertrophic cell growth.

A.



B.

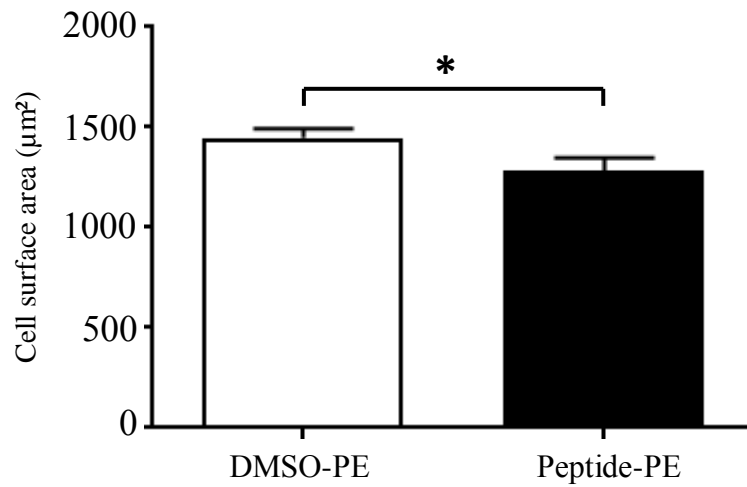


Figure 21: Effect of peptide treatment of NRVM on cell surface area in response to phenylephrine

Neonatal rat ventricular myocytes were pre-treated for 3h with vehicle (DMSO) or 10 µM myristoylated peptide and then stimulated with 3 µM PE for 48 h. Cells were then fixed in 4% (v/v) PFA, stained with antibodies against α -actinin (green) and CMYA5 (red) and analyzed by confocal microscopy.

(A) Representative confocal images (B) Cell surface measurements were performed using Image J software. Bar charts display data from the DMSO control group (white; n=107 cells) and the peptide intervention group (black; n=81 cells). Treatment with peptides led to a significantly smaller increase in cell surface area in response to PE when compared to control cells.

* $p < 0.05$.

4 Discussion

4.1 FHL2 and CMYA5 mRNA and protein expression is differentially regulated in human end-stage heart failure

In our investigations, we were able to show that protein expression levels of FHL2 are reduced in ventricular human samples from patients with end-stage heart failure due to ICM and DCM when compared to NF donor heart samples by western immunoblot analysis. Whilst *FHL2* mRNA levels were not significantly reduced, there was a trend towards lower mRNA levels in failing samples detectable that could be attributed to small n-numbers. These findings are in accordance with previously published work, which showed not only that protein levels are reduced, but also FHL2 mislocalisation in heart failure¹²². Whether the underlying molecular mechanisms originate from changes in transcriptional regulation, protein stability or expression remains elusive and certainly warrants further investigations.

It was shown that various sarcomeric proteins, such as cardiac troponin T, cTnI or myosin heavy chain 7 (MYH7) show isoform shifts to the fetal isoform during HF development¹²³. More importantly, it has been shown that HF development is characterized by reactivation of the fetal gene program¹²⁴. Increased FHL1 protein levels¹²⁵ in HF while FHL2 levels are decreased are probably also a result of this transcriptional shift.

FHL2 is part of an anti-hypertrophic response to chronic β -adrenergic stimulation as it was shown that transgenic FHL2 expression has an anti-hypertrophic effect on cardiac myocytes¹⁰². Pathologically, chronic adrenergic signaling is an important contributor for the development of HF as seen in ICM and DCM³⁸. During cardiac remodeling, boosted activation of anti-hypertrophic feedback mechanisms is strongly needed such as the inhibitory action of FHL2 on CaN-regulated hypertrophic transcription and nuclear ERK signaling¹⁰⁴. That means when FHL2 protein levels decline, this molecular brake can no longer prevent pro-hypertrophic remodeling. Therefore, prolonged neurohumoral stimulation is at the threshold of physiological to pathological cardiac adaptation. It can be speculated that downregulation of FHL2 might promote the development of HF. Whether reduced levels of FHL2 correlate with disease progression or can even be considered as causative remains subject of speculation, but the fact, that levels of CMYA5 protein expression increase in HF argue against a general reduction of anti-hypertrophic gene expression in cardiomyopathy. Therefore downregulation of FHL2 might be considered more cause than effect of HF progression.

Methodically, western immunoblotting of large proteins like CMYA5 is technically challenging. We were not able to analyze both ICM and DCM samples at the same time as NF

samples, but we minimized the risk of false results by repeating the experiment with as many samples as we were able to generate and using similar conditions for CMYA5 and FHL2 blotting. Unfortunately, human samples have a limited availability in general. These limitations of large proteins were ultimately reason for us to generate smaller fractions of the target protein for the investigation of the interaction with FHL2. We also used two different CMYA5 antibodies, one provided by Derek Blake¹⁰⁵ and one commercial antibody by Invitrogen (Catalog # PA5-21170). Also, analysis of mRNA levels supports the results of protein levels.

Samples were analyzed for mRNA and protein expression levels of CMYA5 and displayed enhanced CMYA5 mRNA levels in ICM samples and higher levels of protein expression in both DCM and ICM samples compared to NF heart samples.

It is conceivable that CMYA5 expression is upregulated as a response to pro-hypertrophic growth as it is known to upregulate its own expression under conditions of enhanced MEF2 activity such as during HF. This would emphasize a potential role as part of an anti-hypertrophic feedback mechanism. Again, cause and effect could not be determined conclusively in this thesis, but the scarce knowledge leads to the assumption of CMYA5 having an anti-hypertrophic impact, taking into consideration, that AngII or PE infusion increase CMYA5 expression¹¹⁰, presumably as feedback, and CaN function is hindered by CMYA5 in skeletal muscle, possibly by scaffolding CaN in a protective manner¹¹⁵.

However, if higher levels of total CMYA5 are in fact protective remains elusive. On one hand, above-mentioned compartmentalization is one key to protein function and CMYA5 localization in HF has not been investigated. As this work shows, FHL2 and CMYA5 are interacting on a protein level, therefore lack of FHL2 in heart failure might very well have negative consequences on CMYA5 localization. On the other hand, hypertrophy itself might be responsible for higher CMYA5 protein levels by requiring more sarcomeres without increasing the relative effect of CMYA5 per cell. Taking both into account, upregulation of CMYA5 might be the response of cardiac myocytes to antagonize pathological signaling, whilst no beneficial effect on CMYA5 function can be observed, or even results in higher disorganization of the sarcomeric apparatus.

Furthermore, the comparison of end stage HF to NF samples does not take HF progression into account. The condition cannot be seen as on-off switch, but as a progressive condition with constant changes in cardiac myocyte properties on the way to complete failure. Analyzing hearts in compensated stages of eccentric or dilated cardiomyopathy is just as

important as comparing it to physiological hypertrophic growth but acquiring human samples for these conditions is impossible.

4.2 *FHL2 and CMYA5 expression is upregulated by pro-hypertrophic stimuli*

MEF2, a transcription factor downstream of the Ca^{2+} /calmodulin kinase signaling axis (CaMK)¹²⁶, stimulates expression of both FHL2 and CMYA5 as part of the so-called excitation-transcription coupling^{90, 109}. CaMK activation occurs, mediated by calmodulin, at high amplitude of intracellular Ca^{2+} as a response to hypertrophic stimuli, i.e. β -AR signaling or pressure overload¹²⁶⁻¹²⁸. Besides its direct effect on CMYA5 and FHL2 expression, there is evidence that MEF2 also acts indirectly by enhancing SRF¹²⁹, which is known as an important TF contributing to hypertrophy development¹³⁰ and is established to drive FHL2 expression⁸⁷. Also, the pro-hypertrophic CaN/NFAT pathway is activated by increased intracellular Ca^{2+} concentrations, although rather responding to sustaining slight increases of intracellular Ca^{2+} ¹²⁷. NFAT is not known to directly increase expression of FHL2 or CMYA5, but MEF2 is also targeted by CaN, albeit to a lesser extent than by CaMK¹³¹.

Why total FHL2 levels are reduced in HF although transcriptional activities are elevated, not just for MEF2 and SRF, but also for p53¹³², remains subject to future investigation. Whether *FHL2* transcription is overall reduced by yet unknown factors or enhanced protein degradation occurs during HF needs to be further explored.

Another study revealed *in vivo* stimulation with AngII or PE as favorable to increase CMYA5 expression in cardiac myocytes¹¹⁰.

Considering their possible anti-hypertrophic function *in vivo* and reduction of pathological cardiac growth, it can be hypothesized that MEF2 driven expression of FHL2 and CMYA5 acts as negative feedback in times of hypertrophic stimulation of cardiac myocytes. In line with these findings, *Fhl2*^{-/-} mice seem to show normal cardiac development and function under basal condition, but an exaggerated hypertrophic growth after chronic β -AR stimulation¹⁰².

Interestingly, in another study, pressure overload, simulated by TAC-surgery, did not have a differential effect on hypertrophy development in *Fhl2*^{-/-} mice⁷⁶, raising the question of a selective role of FHL2 in antagonizing the neuro-humoral pathway of hypertrophic signaling.

Our own studies with CMYA5/FHL2-interaction disrupting peptides in NRVM revealed decreased hypertrophic growth after adrenergic stimulation. However, this study is very preliminary. We did not establish proof of actual disruption of the CMYA/FHL2-interaction in the presence of the peptides. Furthermore, long-term effects were not investigated.

Nevertheless the results suggest that future studies are required to proof or discount CMYA5/FHL2-interaction as pro- or anti-hypertrophic. A proper experimental setup, in which the interaction is diminished, but individual functions are preserved would be the first step for further investigations.

4.3 FHL2 and CMYA5 are associated with sarcomeric structures of cardiac myocytes

Both, FHL2 and CMYA5 do not show enzymatic activity. For CMYA5, various interaction partners are established, some of them hinting towards a potential role in maintaining structural integrity of the sarcomeric apparatus. Z-disc proteins α -actinin and desmin as well as dystrophin are established binding partners of CMYA5^{108, 109, 113, 114}. The individual purposes of each interaction are not fully understood yet, but it can be hypothesized that CMYA5 is one of many proteins localized primarily around the Z-disc stabilizing the sarcomere internally and tethering it to the sarcolemma besides functioning as a signaling hub in its role as AKAP. In line with this hypothesis is the finding of elevated CMYA5 levels in hypertrophy of cardiac myocytes. Generally, the relative amount of sarcomeres increases during hypertrophy and this requires more proteins to keep the structural integrity intact¹³³.

Also, titin binds to CMYA5, while it is additionally an established FHL2 interaction partner. Both proteins have interaction sites in the M-line region of titin, with an additional binding site for FHL2 in the N2B region^{93, 107}. The cardiac specific N2B spring element of titin is phosphorylated by PKA after β -AR stimulation, leading to a reduction in passive tension¹³⁴. Although no binding of CMYA5 to this region is known, this important physiological modification may depend on CMYA5 anchoring PKA to its substrate.

FHL2 is known to tether metabolic enzymes such as MM-CK, PFK, adenylate kinase and AC to the regions of high energy consumption in the sarcomere^{93, 122}. PFK-2 has been shown to become phosphorylated *in vitro*¹³⁵, thus providing more energy by glycolysis and PKA directly phosphorylates and thereby inhibits the catalytic activity of the cardiac isoform type V of AC¹³⁶, presumably as negative feedback on cAMP cycling. Tethering these metabolic enzymes to titin and their regulation by phosphorylation may depend on the interaction between FHL2 and CMYA5 as scaffolding proteins, and on the ability of CMYA5 to anchor PKA and locate it in vicinity to its substrates.

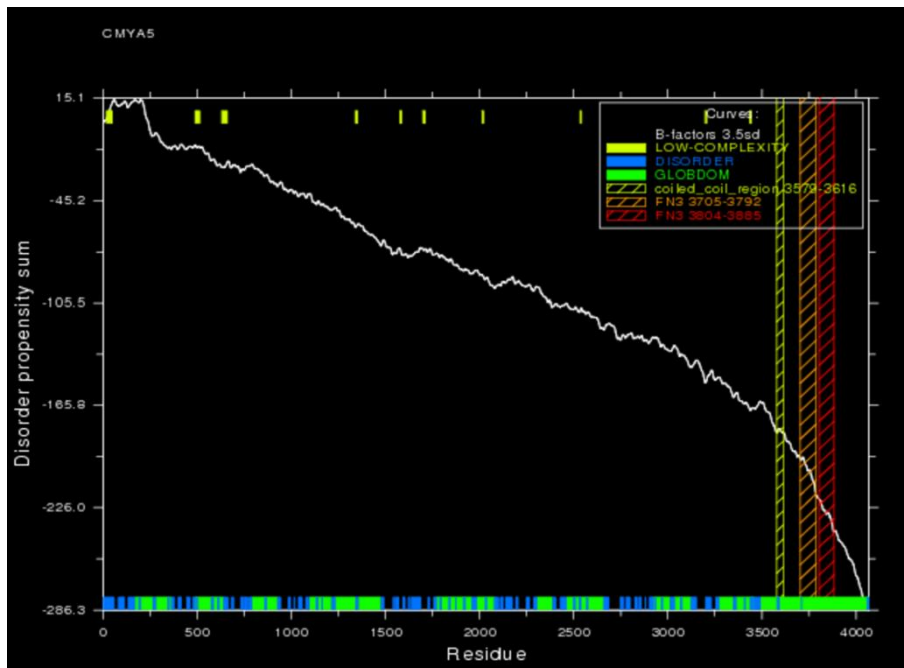
4.4 CMYA5 is an intrinsically disordered protein (IDP) and could be a flexible linker

CMYA5 is a large protein, comprising more than 4000 aa. Despite its large molecular mass, all protein interactions investigated so far are described to occur at the C-terminal end.

Considering its role as a PKA anchoring protein, it can be hypothesized that the middle region of CMYA5 contains no protein binding interfaces, but may act as flexible linker to enable part of the protein to bind to target proteins in different locations, whilst N-and C-terminus being structurally embedded in the sarcomeric apparatus.

Intrinsically disordered proteins (IDP), such as small ubiquitin-like modifier¹³⁷ have been known for some years already and their abundance seems higher than estimated in the past¹³⁸. They vary in length and aa sequence, but are similar in aa composition, more precisely in the amount of polar, uncharged amino acids. Many computational prediction tools have been established over the years, among others Globprot2¹³⁹. When running the CMYA5 amino acid sequence through Globprot2, it reveals disordered regions throughout the aa sequence, whilst predicting order for the C-terminal region (Figure 22). As comparison also the FHL2 sequence was run through the software and displays a high level of order throughout the LIM domains.

A.



B.

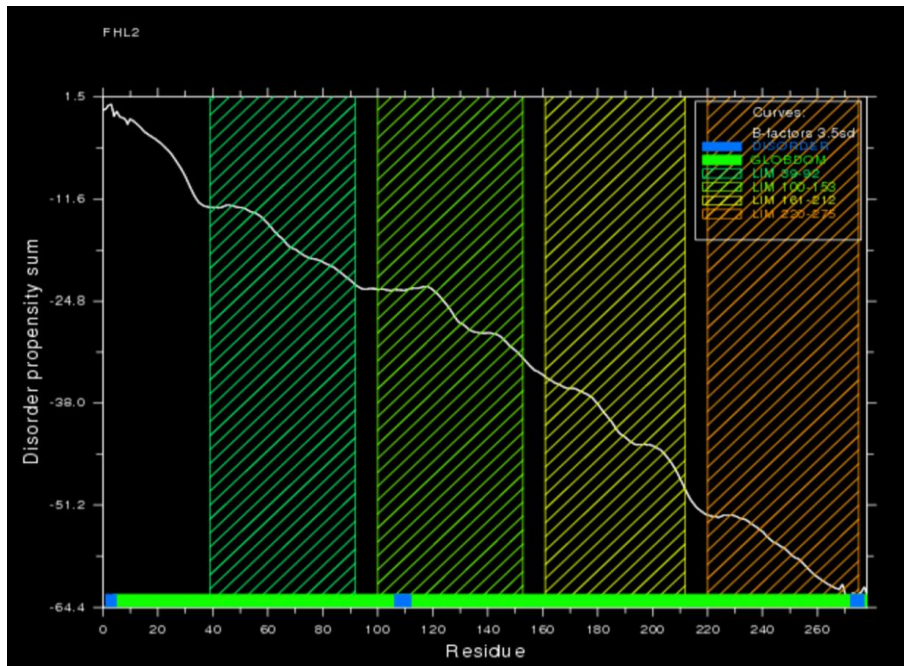


Figure 22: Globprot2 results for the amino acid sequences of CMYA5 and FHL2

Globprot2 analysis of (A) CMYA5 and (B) FHL2

Computational sequence analysis of the CMYA5 primary structure reveals a high number of regions with low order, indicated by blue bars at the bottom, whilst the C-terminal end is dominated by predictions of order, indicated by green bars. Three of the four described C-terminal domains are recognized by the program. In contrast to CMYA5, analysis of the FHL2 primary structure shows a high level of order and four LIM-domains are recognized by the program.

The four domains described for protein binding are all located at the C-terminus, the region of highest evolutionary conservation. The middle region of CMYA5 varies greatly among different species, not just in composition, but also in length¹¹¹. Interestingly, also parts of the N-terminal amino acid sequence are conserved, which could indicate specific functions for that region as well. Our findings on FHL2 binding to the N-terminal domain of CMYA5 might be the first of many protein interaction discoveries.

When analyzing our CMYA5 deletion moieties, we experienced an unusual migration pattern in gel electrophoresis with our constructs #1 - #7 appearing at a higher molecular mass than estimated by the number of aa. This characteristic has been described for certain IDP in the past, amongst others the murine norovirus NS1-2 protein¹⁴⁰.

Therefore, it can be hypothesized that CMYA5 is anchored to the sarcomeric apparatus near the Z-disc by its C-terminal binding domains but remains partially flexible in order to acquire

different interaction partners that are not in close vicinity and to act flexible to changes in mechanical stretch. The hypothesis of CMYA5 being disordered, however, has still to be confirmed by additional methods like nuclear magnetic resonance spectroscopy or electron spin resonance and more N-terminal interactions have yet to be found.

4.5 FHL2 and CMYA5 are interaction partners in cardiac myocytes

We employed alternate methodologies in order to prove that the interaction between FHL2 and CMYA5 occurs in a native cardiac myocyte environment. First hints were provided by a yeast-2-hybrid screen our group had performed. In order to confirm the protein interaction, we produced eight recombinant deletion moieties of the large original protein CMYA5 to use in GST pull-down experiments. Of all successfully cloned cDNA fragments, we were able to purify seven different protein moieties (lacking moiety #6). After verification of their aa sequence, we pre-bound them via His₆-tag to appropriate beads and incubated with recombinant GST-tagged FHL2. Our results indicate binding of FHL2 to the N-terminal and C-terminal regions of CMYA5 (#1 and #8).

The C-terminal moiety #8 contains two FN3 regions which are known to bind FHL2, for instance in the interaction with integrin β 4 binding protein⁹⁵, which is described to contain two FN3 regions (NCBI Gene ID: 3692). These domains in CMYA5 were also candidates for FHL2 binding. We were able to show that recombinant proteins containing all four binding domains of CMYA5 (moiety #8), but also just both FN3 regions were equally able to bind to FHL2. Further fragmentation of the C-terminus into 25 aa containing peptides moiety using peptide arrays confirmed FHL2 affinity for both FN3 regions of CMYA5. On top of that, certain peptides representing the SPRY domain display enhanced FHL2 binding affinities.

Additional to the C-terminal interaction, the N-terminal moiety #1 shows FHL2 binding in pull-down assays. Up to date no protein interaction has been described for this domain of CMYA5. However, it was shown *in vitro* that CMYA5 is a PKA substrate and phosphorylation occurs near the N-terminal end¹¹².

The function of the CMYA5-FHL2 interaction is currently subject to intense investigation. Considering their inability to immediately participate enzymatically in signal transduction, it can be hypothesized that their role is in structural stabilization of the costameric apparatus and targeting of proteins that rely on a defined cellular localization.

The additional interaction at the N-terminus of CMYA5 needs to be investigated in future experiments. Its evolutionary conservation leads to the assumption that protein binding occurs N-terminally as well as C-terminally, but specific binding partners had so far not been

identified. It is interesting that the interaction occurs at both ends of CMYA5 and questions whether more than one molecule of FHL2 is part of a full interactome. The outcome of this interaction could well lead to three-dimensional changes of the CMYA5 structure and thus might influence interaction with other binding partners. Also, two independently existing interactions are possible, fulfilling different molecular tasks.

4.6 FHL2-CMYA5 interaction occurs near the sarcomeric Z-disc of cardiac myocytes

To determine the subcellular localization of CMYA5 and FHL2, we performed immunofluorescence and confocal microscopy in ARVM targeting both proteins. To put their distribution into context, we co-stained for established sarcomeric proteins cMyBP-C and α -actinin. Both proteins of interest show a striated expression pattern. This emphasizes their potential role in contributing to the maintenance of structural integrity of the cardiac myocyte sarcomere.

We showed that CMYA5 is located primarily at the Z-disc. Although FHL2 localizes to various subcellular regions, depending on the tissue, in cardiac myocytes it was found mainly at the Z-disc⁹³. Immunofluorescence signals for CMYA5 do not exclude nuclear regions and are more blurry than for FHL2. This can be at least partially explained with lower antibody specificity since high quality commercial antibodies targeting CMYA5 had not been established at the time when experiments were conducted. Nevertheless, clear striations and Z-disc localization of CMYA5 confirm the putative relationship with FHL2 in a sarcomeric context. Digital analysis for co-stained FHL2 and CMYA5 showed a distinct signal overlay for their subcellular localization as well.

The Z-disc is the site of polarity reversal of the actin filaments¹⁴¹, made up of a plethora of different proteins interacting in a defined area, visible as a dense line under the microscope. Its main function is to transmit tension during every contraction. But besides that, most of the proteins that are part of the Z-disc fulfil numerous other tasks, as for instance telethonin, a protein that essentially binds together the N-termini of two adjacent titin molecules, which represents the strongest protein-protein interaction observed to date^{142, 143}. Telethonin also participates in the regulation of myocardial hypertrophy by interacting with calsarcin-1¹⁴⁴, which is a mediator of calcineurin activity¹⁴⁵. It is additionally linked to the regulation of G-protein coupled receptor signaling¹⁴⁶.

Moreover, Z-discs of cardiac muscle cells are quite different to that of fast skeletal muscle cells, mainly in thickness. Cardiac myocytes contain 6 layers of Z-discs, instead of a 2 layer

Z-disc in fast skeletal muscle cells, providing more resistance to distortion during muscle activity¹⁴⁷.

The accepted roles of FHL2 and CMYA5 specifically in Z-disc function have not been investigated, but the various costameric protein interactions revealed for CMYA5^{107, 113} suggest that it is localized at the junction of intra-/intersarcomeric and extrasarcomeric structures of cardiac myocytes, connecting sarcomeric structures to the cell membrane. FHL2 is believed to be more flexible in the intracellular context. To fulfill its diverse tasks, it must relocate to different intracellular sites and interact with different partners. Its primarily sarcomeric distribution around Z-discs in our experiments might result from a primary localization of FHL2 in that region, with the ability to translocate towards other regions upon stimulation. CMYA5 might be its main anchor, and even responsible for negative feedback on FHL2 translocation, in that context.

Functional analysis of stimulated cells remains obligatory in order to shed light on a possible translocation of FHL2 or CMYA5 under different conditions. Also, disease models show changes in total protein levels of both proteins, with CMYA5 levels increasing and FHL2 decreasing in end stage HF. To speculate about loss or gain of protein function under these extreme conditions, it remains crucial to analyze localization of both proteins in a HF model, especially in different stages of HF in order to understand the dynamics of protein function. To further increase representation of *in vivo* processes at one point, models of human cardiac myocytes, preferably in form of engineered heart tissue involving human induced pluripotent stem cell-derived cardiac myocytes, could be established to analyze FHL2 and CMYA5 functions.

5 Conclusions

The molecular network sustaining cardiac myocyte function is fine-tuned to fulfill the diverse adaptations to different physical circumstances, ranging from deep sleep to extreme physical strain, and permanent flawless performance is required. In order to do so, protein-protein interactions of yet unknown complexity are essential.

The aim of this work was to shed light on one particular interaction. With different molecular techniques we were able to show that FHL2 and CMYA5 physically interact in ARVM in Z-disc vicinity.

FHL2 has been shown to exert various cellular functions, depending on tissue expression. In a cardiac context, its anti-hypertrophic effect under chronic adrenergic stimulation should be highlighted. CMYA5, discovered just a few years ago, is a muscle-specific AKAP, with structural functions in the sarcomere. Initial clues for their physical interaction and similarities in anti-hypertrophic activity, as indicated by their repressing effects on the pathological pro-hypertrophic CaN/NFAT pathway show a possible importance and interdependency of both proteins for their physiological function. For this thesis, we concentrated methodically on verification and mapping of the interaction in cardiac myocytes using various biochemical methods, molecular biology and imaging techniques. We also provide pilot data on putative functional consequences of this interaction in an NRVM model exposed to chronic neurohumoral stimulation in the presence of peptides in order to mask the protein-binding interface.

Heart failure remains one of the main challenges in health research in the 21st century. Despite advances in pharmacological interventions and extracorporeal life support systems, the disease-promoting western life style and the increasing life expectancy demand the development of individualized treatment. Therefore, fundamental understanding of cardiac myocyte physiology and pathophysiology is the foundation for necessary improvement in heart failure therapy. This thesis is the groundwork for future experiments uncovering these mechanisms.

Our group is currently working on a model of disrupted interaction between FHL2 and CMYA5, whilst leaving individual protein functions intact, using small interfering peptides. To establish this model and to show functional consequences of pathologically changed interaction between FHL2 and CMYA5 in *in vivo* experiments is of great interest in order to find specific pharmacological or even genetic targets for hypertrophy and heart failure treatment.

I Abstract

Four-and-a-half-LIM domains 2 (FHL2) is a non-enzymatic protein that is expressed primarily in skeletal muscle and in heart tissue. FHL2 acts as a transcriptional co-factor and can modulate protein function and localization upon binding. Interestingly, FHL2 was shown to exert anti-hypertrophic effects in cardiac myocytes by interaction with extracellular signal-regulated kinase 2 and preventing its nuclear translocation.

Previous work in the group identified cardiomyopathy-associated protein 5 (CMYA5) as a potential novel cardiac interaction partner of FHL2. CMYA5 is a muscle-specific A-kinase anchoring protein with restricted expression to skeletal and heart muscle that participates in the regulation of the subcellular compartmentalization of cyclic adenosine monophosphate-dependent protein kinase. It is of interest that CMYA5, similar to FHL2, represses the pathological pro-hypertrophic Calcineurin/Nuclear factor of activated T-cells pathway.

The aim of this dissertation was to verify the interaction between CMYA5 and FHL2 and to investigate the functional consequences of this interaction in cardiac myocytes.

Initially, to identify the interaction interface, eight V5-tagged recombinant protein fragments of CMYA5 were generated and used in *in vitro* pull-down experiments with glutathione S-transferase-tagged FHL2. This mapped the interaction within the N-terminal and C-terminal regions of CMYA5. Additionally, a peptide array was carried out for these regions and identified various 25 amino acids peptides within both of them that displayed strong affinity to FHL2.

In order to investigate the subcellular localization of the CMYA5-FHL2 interaction, immunocytochemistry for FHL2 and CMYA5 and subsequent confocal microscopy were performed in isolated adult rat ventricular myocytes and revealed co-localization of FHL2 and CMYA5 at the sarcomeric Z-disc. These observations were further corroborated by Duolink[®] technology.

To study the functional consequences of the FHL2-CMYA5 interaction, neonatal rat ventricular myocytes were exposed to phenylephrine in the presence of a peptide that mimics the FHL2-CMYA5 interface to disrupt the interaction. Measurements revealed a reduction in cell surface size in peptide treated cells suggesting a pro-hypertrophic function of this interaction.

Taken together, the data from this dissertation confirm a functionally important interaction between FHL2 and CMYA5 in cardiac myocytes that warrants further investigations.

Zusammenfassung

Four-and-a-half-LIM domains 2 (FHL2) ist ein hauptsächlich in Skelettmuskel und Herzmuskel exprimiertes Protein ohne enzymatische Aktivität. FHL2 fungiert unter anderem als Transkriptions-Co-Faktor und verändert sowohl Eigenschaften als auch die Lokalisation verschiedener Proteine durch seine Bindung. Interessanterweise hemmt FHL2 durch eine Interaktion mit extracellular signal-regulated kinase 2 dessen Migration in den Zellkern und übt somit antihypertrophe Effekte in Kardiomyozyten aus.

Im Vorfeld zu dieser Arbeit hat unsere Gruppe bereits cardiomyopathy-associated protein 5 (CMYA5) als möglichen Bindungspartner von FHL2 identifiziert. CMYA5 ist ein ebenfalls in Herz- und Skelettmuskelzellen exprimiertes Protein, das die cyclic adenosine monophosphate abhängige protein kinase A bindet und somit dessen intrazelluläre Verteilung steuert. CMYA5, genau wie FHL2, reduziert die Wirkung der pathologischen Calcineurin/Nuclear factor of activated T-cells Signalkaskade. Dies bedeutet, dass CMYA5 eine Rolle in der kardialen Hypertrophieentwicklung spielen könnte.

Das Ziel der vorliegenden Arbeit war es, die Interaktion zwischen CMYA5 und FHL2 zu verifizieren und daraus resultierende Folgen für deren zelluläre Funktionen in Kardiomyocyten zu untersuchen. Um die Lokalisation der Interaktion innerhalb der Proteine zu identifizieren wurden zunächst acht V5-gekoppelte rekombinante Proteinfragmente von CMYA5 generiert und in *in vitro* pull-down Experimenten mit Glutathione S-transferase-gekoppeltem FHL2 getestet. Dies zeigte die Bindung von FHL2 sowohl zum C-Terminus, als auch zum N-Terminus von CMYA5. Zusätzlich wurde ein Protein Array durchgeführt, das mehrere 25 Aminosäuren umfassende Peptide dieser Regionen als starke FHL2 Bindungspartner identifizierte. Um die zelluläre Lokalisation zu bestimmen, wurden immunzytochemische Verfahren und konfokale Mikroskopie von Kardiomyozyten aus adulten Ratten durchgeführt. Hierbei zeigte sich eine Co-Lokalisation beider Proteine nahe der Z-Scheibe kardialer Sarkomere. Diese Ergebnisse wurden mithilfe von Duolink[®]-Technologie bestätigt.

Um die funktionellen Konsequenzen der Interaktion zu untersuchen, wurden neonatale Ventrikelmuskelzellen von Ratten Phenylephrin ausgesetzt während Peptide die Bindungsstellen für die Proteininteraktion blockierten. Messungen der Zelloberfläche zeigten eine Vergrößerung der mit Peptiden behandelten Zellen und suggerieren somit eine prohypertrophe Funktion der Interaktion.

Zusammenfassend bestätigen die Daten dieser Dissertation eine funktionell bedeutende Proteinbindung zwischen FHL2 und CMYA5, die weiterer Untersuchungen bedarf.

II List of abbreviations

α -MHC	α -Myosin heavy chain
aa	Amino acid
AC	Adenylate cyclase
ADK	Adenylate kinase
AngII	Angiotensin II
AKAP	A-kinase anchoring protein
APS	Ammonium persulfate
AR	Adrenoceptor
ARVM	Adult rat ventricular myocytes
ATP	Adenosine triphosphate
BBC	B-Box coiled coil
BLOC-1	Biogenesis of lysosome-related organelles complex
bp	Base pair
BSA	Bovine serum albumin
CaMK	Ca ²⁺ /calmodulin-dependent kinase
cAMP	Cyclic adenosine monophosphate
CaN	Calcineurin
cDNA	Complementary DNA
CMYA5	Cardiomyopathy-associated 5
cMyBP-C	Cardiac myosin binding protein C
CSQ	Calsequestrin
cTnC	Cardiac troponin C
cTnI	Cardiac troponin I
DAPI	4',6-diamidino-2-phenylindole
DCM	Dilated cardiomyopathy
ddH ₂ O	Distilled water
DMEM	Dulbecco's Modified Eagle Medium
DMSO	Dimethyl sulfoxide
DNA	Deoxyribonucleic acid
dNTP	Deoxy-nucleotide triphosphate
DPBS	Dulbecco's phosphate-buffered saline
ECL	Enhanced chemiluminescence
EDTA	Ethylenediaminetetraacetic acid

EGTA	Ethylene glycol tetraacetic acid
ERK	Extracellular signal-regulated kinase
ex/em	Excitation/emission
FHL2	Four-and-a-half LIM domains 2
FMOC	Fluorenylmethoxycarbonyl
FN3	Fibronectin type III
GATA	GATA-binding factor
GPCRs	G-protein-coupled receptors
GST	Glutathione <i>S</i> -transferases
GTP	Guanosine-5'-triphosphate
HAND1	Heart- And Neural crest Derivatives-expressed protein 1
HF	Heart failure
His ₆	6x Histidine
HUGO	Human genome organisation
ICM	Ischaemic cardiomyopathy
IDP	Intrinsically disordered proteins
IF	Immunofluorescence
IPTG	Isopropyl β-D-1-thiogalactopyranoside
LB	Lysogeny broth
LIM	LIN-11; ISL-1; MEC-3
LRO	Lysosome related organelles
LTCC	L-type Ca ²⁺ channels
MAKAP	Muscle specific AKAP
MAPK	Mitogen-activated protein kinase
MEF2	Myocyte enhance factor 2
MEK	MAPK/ERK kinase
minK	Minimal potassium
MM-CK	Muscle specific creatine kinase
mRNA	Messenger RNA
NCBI Gene ID	National Center for Biotechnology Information Gene Identity
NF	Non-failing
NFAT	Nuclear factor of activated T-cells
NGS	Non-specific goat serum
Ni/NTA	Nickel/nitrilotriacetic acid

NRVM	Neonatal rat ventricular myocytes
OD ₆₀₀	Optical density at 600 nm
PCR	Polymerase chain reaction
PE	Phenylephrine
PFK	Phosphofructokinase
PKA	CAMP-dependent protein kinase
PKD	Protein kinase D
PLA	Proximity ligation assay
PLB	Phospholamban
PVDF	Polyvinylidene fluoride
RII α /I	Regulatory subunit II α /I
RING	Really interesting new gene
RNA	Ribonucleic acid
RT-PCR	Reverse transcription polymerase chain reaction
RTK	Receptor tyrosine kinase
RyR2	Ryanodine receptor 2
SDS-PAGE	Sodium dodecyl sulfate polyacrylamide gel electrophoresis
SERCA2a	Sarco/endoplasmatic reticulum Ca ²⁺ -ATPase 2a
SK1	Sphingosine kinase-1
SPRY	SP1A and ryanodine receptor
SR	Sarcoplasmic reticulum
SRF	Serum response factor
SSC	Saline sodium citrate
TAC	Transverse aortic constriction
TAE	Tris base, acetic acid, EDTA
TEMED	N,N,N',N'-tetramethylethylenediamine
TF	Transcription factor
TFA	Trifluoroacetic acid
TFMSA	Trifluoromethanesulfonic acid
TIPS	Triisopropylsilyl
TRIM	Tripartite motif
Tris	Tris(hydroxymethyl)aminomethane
TTBS	Tris-buffered saline + Tween 20
WB	Western immunoblotting

III List of figures

Figure 1: Development of the in-hospital morbidity rate of heart failure in Germany from 1995 – 2012

Figure 2: Examples for PKA substrates in cardiac myocytes after β -adrenergic stimulation

Figure 3: Schematic summarizing ERK1/2 signaling events in the heart.

Figure 4: Conserved topology of the LIM domain

Figure 5: Map of the pET151/D-TOPO® vector

Figure 6: Exemplary depiction of peptide synthesis for the N-terminal fraction of CMYA5 moiety #1

Figure 7: FHL2 and CMYA5 mRNA expression analysis in human ventricular cardiac tissue

Figure 8: Protein levels of FHL2 and CMYA5 in NF, ICM and DCM human heart samples

Figure 9: Schematic depiction of eight non-overlapping CMYA5 moieties

Figure 10: PCR amplification of *CMYA5* cDNA moieties

Figure 11: Example of plasmid DNA isolation of *CMYA5* moiety #3

Figure 12: Induction and purification of recombinant *CMYA5* protein moieties

Figure 13: SDS-PAGE and western immunoblot analysis of recombinant protein expression

Figure 14: Schematic depiction of pull-down assays

Figure 15: FHL2 binding ability of recombinant *CMYA5* moieties

Figure 16: FHL2 binding ability of the FN3 region of *CMYA5*

Figure 17: Results of the peptide array

Figure 18: Overview of the peptide array results

Figure 19: Subcellular localization of FHL2 and *CMYA5*

Figure 20: FHL2-*CMYA5* co-localization in ARVM

Figure 21: Effect of disrupting peptides on NRVM cell size after stimulation with phenylephrine

Figure 22: Globprot2 results for the amino acid sequences of *CMYA5* and FHL2

IV List of tables

Table 1: Gene Family - A-kinase anchoring proteins

Table 2: FHL2 binding partners

Table 3: Alphabetical list of chemicals and reagents

Table 4: Alphabetical list of buffers and their composition

Table 5: List of commercial kits

Table 6: List of primary antibodies

Table 7: List of secondary antibodies for western immunoblotting

Table 8: List of secondary antibodies for immunofluorescence

Table 9: Alphabetical list of consumables

Table 10: Alphabetical list of equipment

Table 11: List of software

Table 12: Composition of SDS-PAGE gels with different polyacrylamide concentrations

Table 13: Primers for directional cloning of *CMYA5* moieties

Table 14: Dyes and laser settings used in immunofluorescence/Duolink® assay

Table 15: Primers for directional cloning of *CMYA5*'s FN3 regions

V Bibliography

1. Venes D, Taber CW. *Taber's cyclopedic medical dictionary*. Philadelphia: F.A. Davis; 2013.
2. Dolgin M. Nomenclature and criteria for diagnosis of diseases of the heart and great vessels. 1994:xiv, 334 p.
3. Deutscher herzbericht 2014. 2015
4. Young DR, Reynolds K, Sidell M, et al. Effects of physical activity and sedentary time on the risk of heart failure. *Circulation. Heart failure*. 2014;7:21-27
5. Prevalence of insufficient physical activity 2008. *Global Health Observatory Data*. 2011
6. He J, Ogden LG, Bazzano LA, et al. Risk factors for congestive heart failure in us men and women: Nhanes i epidemiologic follow-up study. *Arch Int Med*. 2001;161:996-1002
7. Heidenreich PA, Albert NM, Allen LA, et al. Forecasting the impact of heart failure in the united states: A policy statement from the american heart association. *Circulation. Heart failure*. 2013;6:606-619
8. Roger VL, Weston SA, Redfield MM, et al. Trends in heart failure incidence and survival in a community-based population. *Jama*. 2004;292:344-350
9. Hall JE. *Guyton and hall textbook of medical physiology*. Philadelphia, PA: Elsevier; 2016.
10. Schmidt RF, Thews G. *Human physiology*. Berlin ; New York: Springer-Verlag; 1989.
11. Vassilatis DK, Hohmann JG, Zeng H, et al. The g protein-coupled receptor repertoires of human and mouse. *Proceedings of the National Academy of Sciences of the United States of America*. 2003;100:4903-4908
12. Lodish HF. *Molecular cell biology. 4th edition*. New York: W.H. Freeman; 2000.
13. Xiao RP. Beta-adrenergic signaling in the heart: Dual coupling of the beta2-adrenergic receptor to g(s) and g(i) proteins. *Sci STKE*. 2001;2001:re15
14. Rockman HA, Koch WJ, Lefkowitz RJ. Seven-transmembrane-spanning receptors and heart function. *Nature*. 2002;415:206-212
15. Wang GY, McCloskey DT, Turcato S, et al. Contrasting inotropic responses to alpha1-adrenergic receptor stimulation in left versus right ventricular myocardium. *American journal of physiology. Heart and circulatory physiology*. 2006;291:H2013-2017
16. Levick JR. *An introduction to cardiovascular physiology*. London: Hodder Arnold; 2010.
17. Evans DL. Cardiovascular adaptations to exercise and training. *Vet Clin North Am Equine Pract*. 1985;1:513-531
18. Tao L, Bei Y, Zhang H, et al. Exercise for the heart: Signaling pathways. *Oncotarget*. 2015;6:20773-20784
19. Gauthier C, Seze-Goismier C, Rozec B. Beta 3-adrenoceptors in the cardiovascular system. *Clin Hemorheol Microcirc*. 2007;37:193-204
20. Brodde OE, Michel MC. Adrenergic and muscarinic receptors in the human heart. *Pharmacol Rev*. 1999;51:651-690
21. Granneman JG. The putative beta4-adrenergic receptor is a novel state of the beta1-adrenergic receptor. *Am J Physiol Endocrinol Metab*. 2001;280:E199-202
22. Lodish HF. *Molecular cell biology*. New York: W.H. Freeman-Macmillan Learning; 2016.
23. Lymperopoulos A, Rengo G, Koch WJ. Adrenergic nervous system in heart failure: Pathophysiology and therapy. *Circulation research*. 2013;113:739-753
24. Eschenhagen T. Is ryanodine receptor phosphorylation key to the fight or flight response and heart failure? *The Journal of clinical investigation*. 2010;120:4197-4203
25. Pavoine C, Defer N. The cardiac beta2-adrenergic signaling a new role for the cpla2. *Cell Signal*. 2005;17:141-152
26. Mochizuki N, Ohba Y, Kiyokawa E, et al. Activation of the erk/mapk pathway by an isoform of rap1gap associated with g alpha(i). *Nature*. 1999;400:891-894
27. Ramos JW. The regulation of extracellular signal-regulated kinase (erk) in mammalian cells. *Int J Biochem Cell Biol*. 2008;40:2707-2719

28. Lorenz K, Schmitt JP, Schmitteckert EM, et al. A new type of erk1/2 autophosphorylation causes cardiac hypertrophy. *Nature medicine*. 2009;15:75-83
29. Rose BA, Force T, Wang Y. Mitogen-activated protein kinase signaling in the heart: Angels versus demons in a heart-breaking tale. *Physiol Rev*. 2010;90:1507-1546
30. Bueno OF, De Windt LJ, Tymitz KM, et al. The mek1-erk1/2 signaling pathway promotes compensated cardiac hypertrophy in transgenic mice. *The EMBO journal*. 2000;19:6341-6350
31. Exton JH. Mechanisms involved in alpha-adrenergic phenomena. *Am J Physiol*. 1985;248:E633-647
32. Li X, Zhu L, Yang A, et al. Calcineurin-nfat signaling critically regulates early lineage specification in mouse embryonic stem cells and embryos. *Cell Stem Cell*. 2011;8:46-58
33. Nemer G, Nemer M. Cooperative interaction between gata5 and nf-atc regulates endothelial-endocardial differentiation of cardiogenic cells. *Development*. 2002;129:4045-4055
34. Horsley V, Pavlath GK. Nfat: Ubiquitous regulator of cell differentiation and adaptation. *The Journal of cell biology*. 2002;156:771-774
35. Bourajjaj M, Armand AS, da Costa Martins PA, et al. Nfatc2 is a necessary mediator of calcineurin-dependent cardiac hypertrophy and heart failure. *The Journal of biological chemistry*. 2008;283:22295-22303
36. Bueno OF, Wilkins BJ, Tymitz KM, et al. Impaired cardiac hypertrophic response in calcineurin abeta -deficient mice. *Proceedings of the National Academy of Sciences of the United States of America*. 2002;99:4586-4591
37. McMurray JJV, Pfeffer MA. Heart failure. *The Lancet*. 2005;365:1877-1889
38. Eschenhagen T. Beta-adrenergic signaling in heart failure - adapt or die. *Nature medicine*. 2008;14:485-487
39. Borbely A, van der Velden J, Papp Z, et al. Cardiomyocyte stiffness in diastolic heart failure. *Circulation*. 2005;111:774-781
40. van Heerebeek L, Borbely A, Niessen HW, et al. Myocardial structure and function differ in systolic and diastolic heart failure. *Circulation*. 2006;113:1966-1973
41. Gandhi MS, Kamalov G, Shahbaz AU, et al. Cellular and molecular pathways to myocardial necrosis and replacement fibrosis. *Heart failure reviews*. 2011;16:23-34
42. Creemers EE, Pinto YM. Molecular mechanisms that control interstitial fibrosis in the pressure-overloaded heart. *Cardiovascular research*. 2011;89:265-272
43. Freedman NJ, Lefkowitz RJ. Anti-beta(1)-adrenergic receptor antibodies and heart failure: Causation, not just correlation. *The Journal of clinical investigation*. 2004;113:1379-1382
44. Lohse MJ, Engelhardt S, Danner S, et al. Mechanisms of beta-adrenergic receptor desensitization: From molecular biology to heart failure. *Basic research in cardiology*. 1996;91 Suppl 2:29-34
45. Ungerer M, Parruti G, Bohm M, et al. Expression of beta-arrestins and beta-adrenergic receptor kinases in the failing human heart. *Circulation research*. 1994;74:206-213
46. Luttrell LM. 'Location, location, location': Activation and targeting of map kinases by g protein-coupled receptors. *J Mol Endocrinol*. 2003;30:117-126
47. McDonald PH, Chow CW, Miller WE, et al. Beta-arrestin 2: A receptor-regulated mapk scaffold for the activation of jnk3. *Science*. 2000;290:1574-1577
48. Brodde OE, Hillemann S, Kunde K, et al. Receptor systems affecting force of contraction in the human heart and their alterations in chronic heart failure. *J Heart Lung Transplant*. 1992;11:S164-174
49. Engelhardt S, Hein L, Wiesmann F, et al. Progressive hypertrophy and heart failure in beta1-adrenergic receptor transgenic mice. *Proceedings of the National Academy of Sciences of the United States of America*. 1999;96:7059-7064
50. Gheorghide M, Colucci WS, Swedberg K. Beta-blockers in chronic heart failure. *Circulation*. 2003;107:1570-1575
51. Port JD, Bristow MR. Altered beta-adrenergic receptor gene regulation and signaling in chronic heart failure. *Journal of molecular and cellular cardiology*. 2001;33:887-905

52. Lowes BD, Gilbert EM, Abraham WT, et al. Myocardial gene expression in dilated cardiomyopathy treated with beta-blocking agents. *The New England journal of medicine*. 2002;346:1357-1365
53. Frey N, McKinsey TA, Olson EN. Decoding calcium signals involved in cardiac growth and function. *Nature medicine*. 2000;6:1221-1227
54. Abraham WT, Gilbert EM, Lowes BD, et al. Coordinate changes in myosin heavy chain isoform gene expression are selectively associated with alterations in dilated cardiomyopathy phenotype. *Mol Med*. 2002;8:750-760
55. Gorelik J, Wright PT, Lyon AR, et al. Spatial control of the betaar system in heart failure: The transverse tubule and beyond. *Cardiovascular research*. 2013;98:216-224
56. Nikolaev VO, Moshkov A, Lyon AR, et al. Beta2-adrenergic receptor redistribution in heart failure changes camp compartmentation. *Science*. 2010;327:1653-1657
57. Ianoul A, Grant DD, Rouleau Y, et al. Imaging nanometer domains of beta-adrenergic receptor complexes on the surface of cardiac myocytes. *Nat Chem Biol*. 2005;1:196-202
58. Steinberg SF, Brunton LL. Compartmentation of g protein-coupled signaling pathways in cardiac myocytes. *Annu Rev Pharmacol Toxicol*. 2001;41:751-773
59. Kinderman FS, Kim C, von Daake S, et al. A dynamic mechanism for akap binding to rii isoforms of camp-dependent protein kinase. *Molecular cell*. 2006;24:397-408
60. Gold MG, Lygren B, Dokurno P, et al. Molecular basis of akap specificity for pka regulatory subunits. *Molecular cell*. 2006;24:383-395
61. Skroblin P, Grossmann S, Schafer G, et al. Mechanisms of protein kinase a anchoring. *International review of cell and molecular biology*. 2010;283:235-330
62. Rababa'h A, Singh S, Suryavanshi SV, et al. Compartmentalization role of a-kinase anchoring proteins (akaps) in mediating protein kinase a (pka) signaling and cardiomyocyte hypertrophy. *Int J Mol Sci*. 2014;16:218-229
63. Pare GC, Bauman AL, McHenry M, et al. The makap complex participates in the induction of cardiac myocyte hypertrophy by adrenergic receptor signaling. *Journal of cell science*. 2005;118:5637-5646
64. Gao T, Yatani A, Dell'Acqua ML, et al. Camp-dependent regulation of cardiac l-type ca²⁺ channels requires membrane targeting of pka and phosphorylation of channel subunits. *Neuron*. 1997;19:185-196
65. McConnell BK, Popovic Z, Mal N, et al. Disruption of protein kinase a interaction with a-kinase-anchoring proteins in the heart in vivo: Effects on cardiac contractility, protein kinase a phosphorylation, and troponin i proteolysis. *The Journal of biological chemistry*. 2009;284:1583-1592
66. A-kinase anchor proteins. 2015
67. Diviani D, Dodge-Kafka KL, Li J, et al. A-kinase anchoring proteins: Scaffolding proteins in the heart. *American journal of physiology. Heart and circulatory physiology*. 2011;301:H1742-1753
68. Therrien M, Michaud NR, Rubin GM, et al. Ksr modulates signal propagation within the mapk cascade. *Genes Dev*. 1996;10:2684-2695
69. Zhong L, Chiusa M, Cadar AG, et al. Targeted inhibition of ankrd1 disrupts sarcomeric erk-gata4 signal transduction and abrogates phenylephrine-induced cardiomyocyte hypertrophy. *Cardiovascular research*. 2015;106:261-271
70. Mikhailov AT, Torrado M. The enigmatic role of the ankyrin repeat domain 1 gene in heart development and disease. *Int J Dev Biol*. 2008;52:811-821
71. Schmeichel KL, Beckerle MC. The lim domain is a modular protein-binding interface. *Cell*. 1994;79:211-219
72. Dawid IB, Breen JJ, Toyama R. Lim domains: Multiple roles as adapters and functional modifiers in protein interactions. *Trends in genetics : TIG*. 1998;14:156-162
73. Kadmas JL, Beckerle MC. The lim domain: From the cytoskeleton to the nucleus. *Nat Rev Mol Cell Biol*. 2004;5:920-931

74. McCabe A, Hashimoto K, Hall WW, et al. The four and a half lim family members are novel interactants of the human t-cell leukemia virus type 1 tax oncoprotein. *Journal of virology*. 2013;87:7435-7444
75. Brown S, Coghill ID, McGrath MJ, et al. Role of lim domains in mediating signaling protein interactions. *IUBMB life*. 2001;51:359-364
76. Chu PH, Ruiz-Lozano P, Zhou Q, et al. Expression patterns of fhl/slim family members suggest important functional roles in skeletal muscle and cardiovascular system. *Mechanisms of development*. 2000;95:259-265
77. Lardenois A, Chalmel F, Demougin P, et al. Fhl5/act, a crem-binding transcriptional activator required for normal sperm maturation and morphology, is not essential for testicular gene expression. *Reprod Biol Endocrinol*. 2009;7:133
78. Morgan MJ, Madgwick AJ. The fourth member of the fhl family of lim proteins is expressed exclusively in the testis. *Biochemical and biophysical research communications*. 1999;255:251-255
79. Shathasivam T, Kislinger T, Gramolini AO. Genes, proteins and complexes: The multifaceted nature of fhl family proteins in diverse tissues. *Journal of cellular and molecular medicine*. 2010;14:2702-2720
80. Lee SM, Tsui SK, Chan KK, et al. Chromosomal mapping, tissue distribution and cdna sequence of four-and-a-half lim domain protein 1 (fhl1). *Gene*. 1998;216:163-170
81. Gramolini AO, Kislinger T, Alikhani-Koopaei R, et al. Comparative proteomics profiling of a phospholamban mutant mouse model of dilated cardiomyopathy reveals progressive intracellular stress responses. *Mol Cell Proteomics*. 2008;7:519-533
82. Gaussin V, Tomlinson JE, Depre C, et al. Common genomic response in different mouse models of beta-adrenergic-induced cardiomyopathy. *Circulation*. 2003;108:2926-2933
83. Sheikh F, Raskin A, Chu PH, et al. An fhl1-containing complex within the cardiomyocyte sarcomere mediates hypertrophic biomechanical stress responses in mice. *The Journal of clinical investigation*. 2008;118:3870-3880
84. Genini M, Schwalbe P, Scholl FA, et al. Subtractive cloning and characterization of dral, a novel lim-domain protein down-regulated in rhabdomyosarcoma. *DNA and cell biology*. 1997;16:433-442
85. Chan KK, Tsui SK, Lee SM, et al. Molecular cloning and characterization of fhl2, a novel lim domain protein preferentially expressed in human heart. *Gene*. 1998;210:345-350
86. Scholl FA, McLoughlin P, Ehler E, et al. Dral is a p53-responsive gene whose four and a half lim domain protein product induces apoptosis. *The Journal of cell biology*. 2000;151:495-506
87. Philippar U, Schrott G, Dieterich C, et al. The srf target gene fhl2 antagonizes rhoa/mal-dependent activation of srf. *Molecular cell*. 2004;16:867-880
88. Schafer K, Neuhaus P, Kruse J, et al. The homeobox gene lbx1 specifies a subpopulation of cardiac neural crest necessary for normal heart development. *Circulation research*. 2003;92:73-80
89. Johannessen M, Moller S, Hansen T, et al. The multifunctional roles of the four-and-a-half-lim only protein fhl2. *Cellular and molecular life sciences : CMLS*. 2006;63:268-284
90. Ewen EP, Snyder CM, Wilson M, et al. The mef2a transcription factor coordinately regulates a costamere gene program in cardiac muscle. *The Journal of biological chemistry*. 2011;286:29644-29653
91. Stathopoulou K, Cuello F, Candasamy AJ, et al. Four-and-a-half lim domains proteins are novel regulators of the protein kinase d pathway in cardiac myocytes. *The Biochemical journal*. 2014;457:451-461
92. Hill AA, Riley PR. Differential regulation of hand1 homodimer and hand1-e12 heterodimer activity by the cofactor fhl2. *Molecular and cellular biology*. 2004;24:9835-9847
93. Lange S, Auerbach D, McLoughlin P, et al. Subcellular targeting of metabolic enzymes to titin in heart muscle may be mediated by dral/fhl-2. *Journal of cell science*. 2002;115:4925-4936

94. Arimura T, Hayashi T, Matsumoto Y, et al. Structural analysis of four and half lim protein-2 in dilated cardiomyopathy. *Biochemical and biophysical research communications*. 2007;357:162-167
95. Wixler V, Geerts D, Laplantine E, et al. The lim-only protein dral/fhl2 binds to the cytoplasmic domain of several alpha and beta integrin chains and is recruited to adhesion complexes. *The Journal of biological chemistry*. 2000;275:33669-33678
96. Samson T, Smyth N, Janetzky S, et al. The lim-only proteins fhl2 and fhl3 interact with alpha- and beta-subunits of the muscle alpha7beta1 integrin receptor. *The Journal of biological chemistry*. 2004;279:28641-28652
97. Sun J, Yan G, Ren A, et al. Fhl2/slim3 decreases cardiomyocyte survival by inhibitory interaction with sphingosine kinase-1. *Circulation research*. 2006;99:468-476
98. Hayashi H, Nakagami H, Takami Y, et al. Fhl-2 suppresses vegf-induced phosphatidylinositol 3-kinase/akt activation via interaction with sphingosine kinase-1. *Arteriosclerosis, thrombosis, and vascular biology*. 2009;29:909-914
99. Pitson SM, Xia P, Leclercq TM, et al. Phosphorylation-dependent translocation of sphingosine kinase to the plasma membrane drives its oncogenic signaling. *J Exp Med*. 2005;201:49-54
100. Johnson KR, Becker KP, Facchinetti MM, et al. Pkc-dependent activation of sphingosine kinase 1 and translocation to the plasma membrane. Extracellular release of sphingosine-1-phosphate induced by phorbol 12-myristate 13-acetate (pma). *The Journal of biological chemistry*. 2002;277:35257-35262
101. Krishnamurthy G, Patberg KW, Obreztkhikova MN, et al. Developmental evolution of the delayed rectifier current ics in canine heart appears dependent on the beta subunit mink. *Heart rhythm : the official journal of the Heart Rhythm Society*. 2004;1:704-711
102. Kong Y, Shelton JM, Rothermel B, et al. Cardiac-specific lim protein fhl2 modifies the hypertrophic response to beta-adrenergic stimulation. *Circulation*. 2001;103:2731-2738
103. Purcell NH, Darwis D, Bueno OF, et al. Extracellular signal-regulated kinase 2 interacts with and is negatively regulated by the lim-only protein fhl2 in cardiomyocytes. *Molecular and cellular biology*. 2004;24:1081-1095
104. Hojajev B, Rothermel BA, Gillette TG, et al. Fhl2 binds calcineurin and represses pathological cardiac growth. *Molecular and cellular biology*. 2012;32:4025-4034
105. Benson MA, Tinsley CL, Blake DJ. Myospryn is a novel binding partner for dysbindin in muscle. *The Journal of biological chemistry*. 2004;279:10450-10458
106. Walker MG. Pharmaceutical target identification by gene expression analysis. *Mini Rev Med Chem*. 2001;1:197-205
107. Sarparanta J, Blandin G, Charton K, et al. Interactions with m-band titin and calpain 3 link myospryn (cmya5) to tibial and limb-girdle muscular dystrophies. *The Journal of biological chemistry*. 2010;285:30304-30315
108. Kouloumenta A, Mavroidis M, Capetanaki Y. Proper perinuclear localization of the trim-like protein myospryn requires its binding partner desmin. *The Journal of biological chemistry*. 2007;282:35211-35221
109. Durham JT, Brand OM, Arnold M, et al. Myospryn is a direct transcriptional target for mef2a that encodes a striated muscle, alpha-actinin-interacting, costamere-localized protein. *The Journal of biological chemistry*. 2006;281:6841-6849
110. Nakagami H, Kikuchi Y, Katsuya T, et al. Gene polymorphism of myospryn (cardiomyopathy-associated 5) is associated with left ventricular wall thickness in patients with hypertension. *Hypertension research : official journal of the Japanese Society of Hypertension*. 2007;30:1239-1246
111. Sarparanta J. Biology of myospryn: What's known? *Journal of muscle research and cell motility*. 2008;29:177-180
112. Reynolds JG, McCalmon SA, Tomczyk T, et al. Identification and mapping of protein kinase a binding sites in the costameric protein myospryn. *Biochimica et biophysica acta*. 2007;1773:891-902

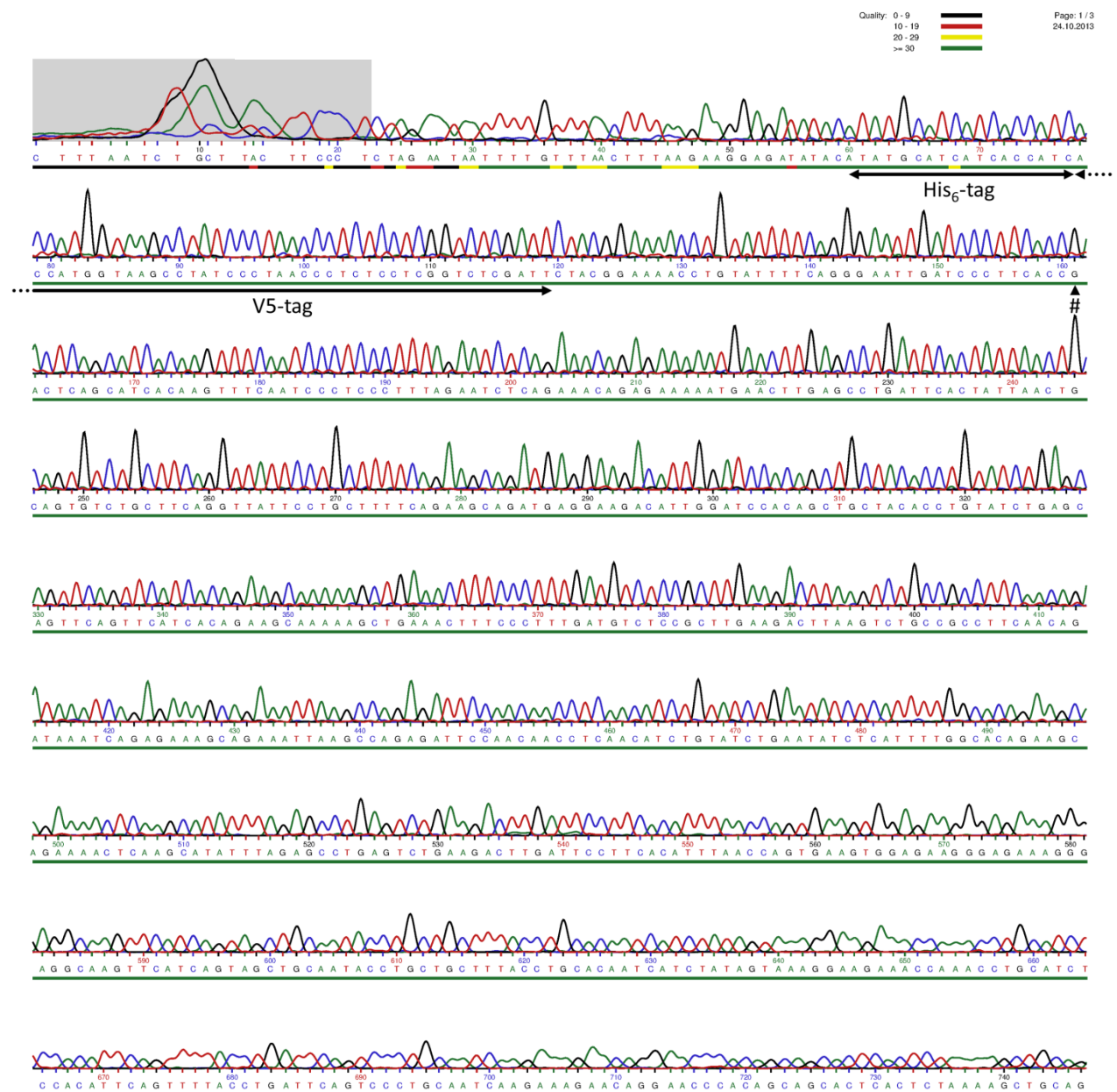
113. Reynolds JG, McCalmon SA, Donaghey JA, et al. Deregulated protein kinase a signaling and myospryn expression in muscular dystrophy. *The Journal of biological chemistry*. 2008;283:8070-8074
114. Tsoupri E, Capetanaki Y. Myospryn: A multifunctional desmin-associated protein. *Histochemistry and cell biology*. 2013;140:55-63
115. Kielbasa OM, Reynolds JG, Wu CL, et al. Myospryn is a calcineurin-interacting protein that negatively modulates slow-fiber-type transformation and skeletal muscle regeneration. *FASEB journal : official publication of the Federation of American Societies for Experimental Biology*. 2011;25:2276-2286
116. Bolger GB, Baillie GS, Li X, et al. Scanning peptide array analyses identify overlapping binding sites for the signaling scaffold proteins, beta-arrestin and rack1, in camp-specific phosphodiesterase pde4d5. *The Biochemical journal*. 2006;398:23-36
117. Frank R. The spot-synthesis technique. Synthetic peptide arrays on membrane supports-- principles and applications. *J Immunol Methods*. 2002;267:13-26
118. Cuello F, Bardswell SC, Haworth RS, et al. Protein kinase d selectively targets cardiac troponin i and regulates myofilament ca²⁺ sensitivity in ventricular myocytes. *Circulation research*. 2007;100:864-873
119. Zimmermann WH, Fink C, Kralisch D, et al. Three-dimensional engineered heart tissue from neonatal rat cardiac myocytes. *Biotechnol Bioeng*. 2000;68:106-114
120. Schneider CA, Rasband WS, Eliceiri KW. Nih image to imagej: 25 years of image analysis. *Nat Methods*. 2012;9:671-675
121. Tskhovrebova L, Trinick J. Titin: Properties and family relationships. *Nat Rev Mol Cell Biol*. 2003;4:679-689
122. Bovill E, Westaby S, Crisp A, et al. Reduction of four-and-a-half lim-protein 2 expression occurs in human left ventricular failure and leads to altered localization and reduced activity of metabolic enzymes. *J Thorac Cardiovasc Surg*. 2009;137:853-861
123. Kong SW, Hu YW, Ho JW, et al. Heart failure-associated changes in rna splicing of sarcomere genes. *Circ Cardiovasc Genet*. 2010;3:138-146
124. Thum T, Galuppo P, Wolf C, et al. Micrnas in the human heart: A clue to fetal gene reprogramming in heart failure. *Circulation*. 2007;116:258-267
125. Hwang DM, Dempsey AA, Wang RX, et al. A genome-based resource for molecular cardiovascular medicine: Toward a compendium of cardiovascular genes. *Circulation*. 1997;96:4146-4203
126. Passier R, Zeng H, Frey N, et al. Cam kinase signaling induces cardiac hypertrophy and activates the mef2 transcription factor in vivo. *The Journal of clinical investigation*. 2000;105:1395-1406
127. Dolmetsch RE, Lewis RS, Goodnow CC, et al. Differential activation of transcription factors induced by ca²⁺ response amplitude and duration. *Nature*. 1997;386:855-858
128. Colomer JM, Mao L, Rockman HA, et al. Pressure overload selectively up-regulates ca²⁺/calmodulin-dependent protein kinase ii in vivo. *Mol Endocrinol*. 2003;17:183-192
129. Lin Q, Lu J, Yanagisawa H, et al. Requirement of the mads-box transcription factor mef2c for vascular development. *Development*. 1998;125:4565-4574
130. Paradis P, MacLellan WR, Belaguli NS, et al. Serum response factor mediates ap-1-dependent induction of the skeletal alpha-actin promoter in ventricular myocytes. *The Journal of biological chemistry*. 1996;271:10827-10833
131. Bueno OF, van Rooij E, Molkentin JD, et al. Calcineurin and hypertrophic heart disease: Novel insights and remaining questions. *Cardiovascular research*. 2002;53:806-821
132. Song H, Conte JV, Jr., Foster AH, et al. Increased p53 protein expression in human failing myocardium. *J Heart Lung Transplant*. 1999;18:744-749
133. Richter GW, Kellner A. Hypertrophy of the human heart at the level of fine structure. An analysis and two postulates. *The Journal of cell biology*. 1963;18:195-206

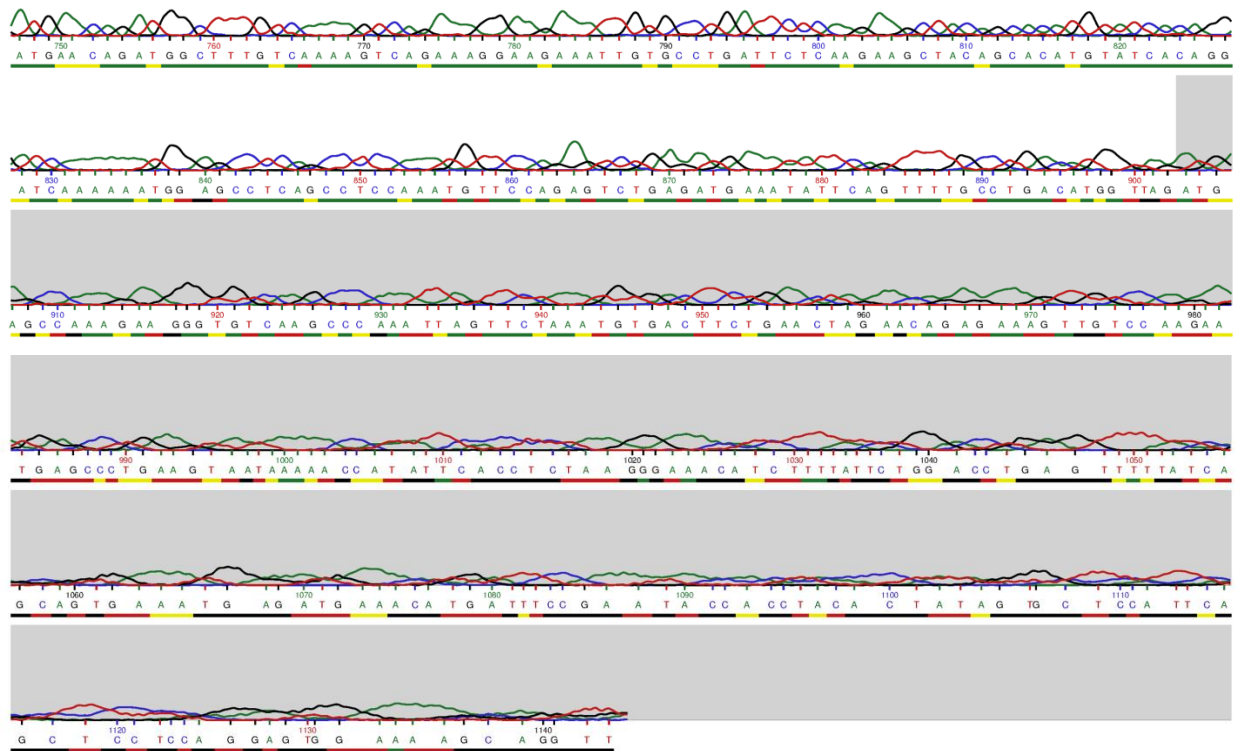
134. Yamasaki R, Wu Y, McNabb M, et al. Protein kinase a phosphorylates titin's cardiac-specific n2b domain and reduces passive tension in rat cardiac myocytes. *Circulation research*. 2002;90:1181-1188
135. Dihazi H, Kessler R, Eschrich K. Glucose-induced stimulation of the ras-camp pathway in yeast leads to multiple phosphorylations and activation of 6-phosphofructo-2-kinase. *Biochemistry*. 2003;42:6275-6282
136. Iwami G, Kawabe J, Ebina T, et al. Regulation of adenylyl cyclase by protein kinase a. *The Journal of biological chemistry*. 1995;270:12481-12484
137. Grana-Montes R, Marinelli P, Reverter D, et al. N-terminal protein tails act as aggregation protective entropic bristles: The sumo case. *Biomacromolecules*. 2014;15:1194-1203
138. Uversky VN, Oldfield CJ, Dunker AK. Intrinsically disordered proteins in human diseases: Introducing the d2 concept. *Annu Rev Biophys*. 2008;37:215-246
139. Globplot 2.3. 2016
140. Baker ES, Luckner SR, Krause KL, et al. Inherent structural disorder and dimerisation of murine norovirus ns1-2 protein. *PloS one*. 2012;7:e30534
141. Takahashi K, Hattori A. Alpha-actinin is a component of the z-filament, a structural backbone of skeletal muscle z-disks. *Journal of biochemistry*. 1989;105:529-536
142. Zou P, Pinotsis N, Lange S, et al. Palindromic assembly of the giant muscle protein titin in the sarcomeric z-disk. *Nature*. 2006;439:229-233
143. Bertz M, Wilmanns M, Rief M. The titin-telethonin complex is a directed, superstable molecular bond in the muscle z-disk. *Proceedings of the National Academy of Sciences of the United States of America*. 2009;106:13307-13310
144. Candasamy AJ, Haworth RS, Cuello F, et al. Phosphoregulation of the titin-cap protein telethonin in cardiac myocytes. *The Journal of biological chemistry*. 2014;289:1282-1293
145. Frey N, Olson EN. Calsarcin-3, a novel skeletal muscle-specific member of the calsarcin family, interacts with multiple z-disc proteins. *The Journal of biological chemistry*. 2002;277:13998-14004
146. Haworth RS, Cuello F, Herron TJ, et al. Protein kinase d is a novel mediator of cardiac troponin i phosphorylation and regulates myofilament function. *Circulation research*. 2004;95:1091-1099
147. Luther PK. The vertebrate muscle z-disc: Sarcomere anchor for structure and signaling. *Journal of muscle research and cell motility*. 2009;30:171-185

VI Appendices

Appendix 1: Sequencing of CMYA5 moiety #3 clone 3 by Eurofins Genomics

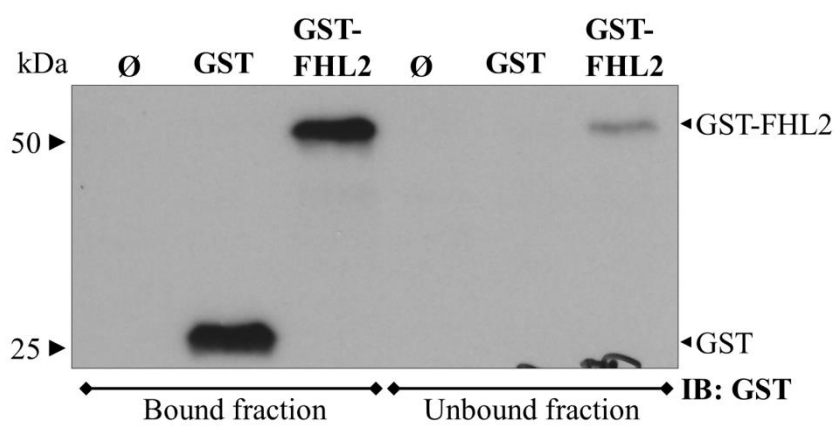
The available T7 promoter primer was used for sequencing of the construct. DNA sequences for the His₆- and V5-tag are indicated, as well as the first base for CMYA5 moiety #3 (#). Not all 1500 bp are covered by the sequencing. A second sample was sent for reverse sequencing using the available reverse T7 promoter primer by Eurofins Genomics to confirm the full sequence.





Appendix 2: Control for GST binding to glutathione-S-sepharose beads

An anti-GST antibody was used in western immunoblotting analysis to detect GST or GST-FHL2 in bound fraction. In the unbound fraction it was scarcely detectable.



Appendix 3: Detailed plan for peptide synthesis for the peptide array

CMYA5 moiety	Peptide number	Amino acid sequence
#1 (N-terminal)	1	MASRDSNHAGESFLGSDGDEEATRE
	2	SNHAGESFLGSDGDEEATRELETEE
	3	ESFLGSDGDEEATRELETEEESEGE
	4	SDGDEEATRELETEEESEGEEDETA
	5	EATRELETEEESEGEEDETAASEE
	6	LETEEESEGEEDETAASEEEEPDSR
	7	ESEGEEDETAASEEEEPDSRSLSDQD
	8	EDETAASEEEEPDSRSLSDQDEEGKI
	9	AESEEEEPDSRSLSDQDEEGKIKQEYI
	10	EPDSRSLSDQDEEGKIKQEYIISDPS
	11	LSDQDEEGKIKQEYIISDPSFSMVT
	12	EEGKIKQEYIISDPSFSMVTVQRED
	13	KQEYIISDPSFSMVTVQREDSGITW
	14	ISDPSFSMVTVQREDSGITWETNSS
	15	FSMVTVQREDSGITWETNSSRSSTP
	16	VQREDSGITWETNSSRSSTPWASEE
	17	SGITWETNSSRSSTPWASEESQTSG
	18	ETNSSRSSTPWASEESQTSGVCSRE
	19	RSSTPWASEESQTSGVCSREGSTVN
	20	WASEESQTSGVCSREGSTVNSPPGN
	21	SQTSGVCSREGSTVNSPPGNVSVFIV
	22	VCSREGSTVNSPPGNVSVFIVDEVKK
	23	GSTVNSPPGNVSVFIVDEVKKVRKRT
	24	SPPGNVSVFIVDEVKKVRKRTHKSKH
	25	VSVFIVDEVKKVRKRTHKSKHGSPL
	26	DEVKKVRKRTHKSKHGSPLRRKGN
	27	VRKRTHKSKHGSPLRRKGNRKRNS
	28	HKSKHGSPLRRKGNRKRNSFESQD

#1 (N-terminal)	29	GSPSLRRKGNRKRNSFESQDVPTNK
	30	RRKGNRKRNSFESQDVPTNKKGSPL
	31	RKRNSFESQDVPTNKKGSPLTSASQ
	32	FESQDVPTNKKGSPLTSASQVLTTE
	33	VPTNKKGSPLTSASQVLTTEKEKSY
	34	KGSPLTSASQVLTTEKEKSYTGIYD
	35	TSASQVLTTEKEKSYTGIYDKARKK
	36	VLTTEKEKSYTGIYDKARKKKTTSN
	37	KEKSYTGIYDKARKKKTTSNTPPIT
	38	TGIYDKARKKKTTSNTPPITGAIYK
	39	KARKKKTTSNTPPITGAIYKEHKPL
	40	KTTSNTPPITGAIYKEHKPLVLRPV
	41	TPPITGAIYKEHKPLVLRPVYIGTV
	42	GAIYKEHKPLVLRPVYIGTVQYKIK
	43	EHKPLVLRPVYIGTVQYKIKMFNSV
	44	VLRPVYIGTVQYKIKMFNSVKEELI
	45	YIGTVQYKIKMFNSVKEELIPLQFY
	46	QYKIKMFNSVKEELIPLQFYGTLPK
	47	MFNSVKEELIPLQFYGTLPKGYVIK
	48	KEELIPLQFYGTLPKGYVIKEIHYR
	49	PLQFYGTLPKGYVIKEIHYRKGKDA
	50	GTLPKGYVIKEIHYRKGKDASISLE
	51	GYVIKEIHYRKGKDASISLEPDLN
	52	EIHYRKGKDASISLEPDLNNSGSNT
	53	KGKDASISLEPDLNNSGSNTVSKTR
	54	SISLEPDLNNSGSNTVSKTRKLVAQ
	55	PDLNNSGSNTVSKTRKLVAQSIEDK
	56	SGSNTVSKTRKLVAQSIEDKVKEVF
	57	VSKTRKLVAQSIEDKVKEVFPPWRG
	58	KLVAQSIEDKVKEVFPPWRGALSKG

#1 (N-terminal)	59	SIEDKVKEVFPPWRGALSKGSESLT
	60	VKEVFPPWRGALSKGSESLTLMFSH
	61	PPWRGALSKGSESLTLMFSHEDQKK
	62	ALSKGSESLTLMFSHEDQKKIYADS
	63	SESLTLMFSHEDQKKIYADSPLNAT
	64	LMFSHEDQKKIYADSPLNATSALEH
	65	EDQKKIYADSPLNATSALEHTVPSY
	66	IYADSPLNATSALEHTVPSYSSSGR
	67	PLNATSALEHTVPSYSSSGRAEQGI
	68	SALEHTVPSYSSSGRAEQGIQLRHS
	69	TVPSYSSSGRAEQGIQLRHSQSV PQ
	70	SSSGRAEQGIQLRHSQSV PQQPEDE
	71	AEQGIQLRHSQSV PQQPEDEAKPHE
	72	QLRHSQSV PQQPEDEAKPHEVEPPS
	73	QSV PQQPEDEAKPHEVEPPSVTPDT
	74	QPEDEAKPHEVEPPSVTPDTPATMF
	75	AKPHEVEPPSVTPDTPATMFLR TTK
	76	VEPPSVTPDTPATMFLR TTKKEEC EL
	77	VTPDTPATMFLR TTKKEEC ELASPGT
	78	PATMFLR TTKKEEC ELASPGTAASEN
	79	LRTTKKEEC ELASPGTAASENDSSVS
	80	EELASPGTAASENDSSVSPSFAN
	81	ASPGTAASENDSSVSPSFANEV KKE
	82	AASENDSSVSPSFANEV KKEDVYSA
	83	DSSVSPSFANEV KKEDVYSAHHSIS
	84	PSFANEV KKEDVYSAHHSISLEAAS
	85	EVKKEDVYSAHHSISLEAASPGLAA
	86	DVYSAHHSISLEAASPGLAASTQDG
	87	HHSISLEAASPGLAASTQDGLDPDQ
	88	LEAASPGLAASTQDGLDPDQE QPDL

#1 (N-terminal)	89	PGLAASTQDGLDPDQEQPDLTSIER
	90	STQDGLDPDQEQPDLTSIERAEPVS
	91	LDPDQEQPDLTSIERAEPVSAKLTP
	92	EQPDLTSIERAEPVSAKLTPTHPSV
	93	TSIERAEPVSAKLTPTHPSVKGEKE
	94	AEPVSAKLTPTHPSVKGEKEENMLE
	95	AKLTPTHPSVKGEKEENMLEPSISL
	96	THPSVKGEKEENMLEPSISLSEPLM

#8 (C-terminal)	97	QKELKKSQIDTYCYTCKCPISATDK
	98	KSQIDTYCYTCKCPISATDKVFGTH
	99	TYCYTCKCPISATDKVFGTHKDHEV
	100	CKCPISATDKVFGTHKDHEVSTLDT
	101	SATDKVFGTHKDHEVSTLDTAISAV
	102	VFGTHKDHEVSTLDTAISAVKVQLA
	103	KDHEVSTLDTAISAVKVQLAEFLEN
	104	STLDTAISAVKVQLAEFLENLQEKS
	105	AISAVKVQLAEFLENLQEKSLRIEA
	106	KVQLAEFLENLQEKSLRIEAFVSEI
	107	EFLLENLQEKSLRIEAFVSEIESFFN
	108	LQEKSLRIEAFVSEIESFFNTIEEN
	109	LRIEAFVSEIESFFNTIEENCSKNE
	110	FVSEIESFFNTIEENCSKNEKRLEE
	111	ESFFNTIEENCSKNEKRLEEQNEEM
	112	TIEENCSKNEKRLEEQNEEMMKKVL
	113	CSKNEKRLEEQNEEMMKKVLAQYDE
114	KRLEEQNEEMMKKVLAQYDEKAQSF	
115	QNEEMMKKVLAQYDEKAQSFEEVKK	
116	MKKVLAQYDEKAQSFEEVKKKKMEF	
117	AQYDEKAQSFEEVKKKKMEFLHEQM	

#8 (C-terminal)	118	KAQSFEEVKKKKMEFLHEQMVHFLQ
	119	EEVKKKKMEFLHEQMVHFLQSMDTA
	120	KKMEFLHEQMVHFLQSMDTAKDTLE
	121	LHEQMVHFLQSMDTAKDTLETIVRE
	122	VHFLQSMDTAKDTLETIVREAEELD
	123	SMDTAKDTLETIVREAEELDEAVFL
	124	KDTLETIVREAEELDEAVFLTSFEE
	125	TIVREAEELDEAVFLTSFEEINERL
	126	AEELDEAVFLTSFEEINERLLSAME
	127	EAVFLTSFEEINERLLSAMESTASL
	128	TSFEEINERLLSAMESTASLEKMPA
	129	INERLLSAMESTASLEKMPAAFSLF
	130	LSAMESTASLEKMPAAFSLFEHYDD
	131	STASLEKMPAAFSLFEHYDDSSARS
	132	EKMPAAFSLFEHYDDSSARSDQMLK
	133	AFSLFEHYDDSSARSDQMLKQVAVP
	134	EHYDDSSARSDQMLKQVAVPQPPRL
	135	SSARSDQMLKQVAVPQPPRLEPQEP
	136	DQMLKQVAVPQPPRLEPQEPNSATS
	137	QVAVPQPPRLEPQEPNSATSTTIAV
	138	QPPRLEPQEPNSATSTTIAVYWSMN
	139	EPQEPNSATSTTIAVYWSMNKEDVI
	140	NSATSTTIAVYWSMNKEDVIDSFQV
	141	TTIAVYWSMNKEDVIDSFQVYCMEE
	142	YWSMNKEDVIDSFQVYCMEEPQDDQ
	143	KEDVIDSFQVYCMEEPQDDQEVNEL
	144	DSFQVYCMEEPQDDQEVNELVEEYR
	145	YCMEEPQDDQEVNELVEEYRLTVKE
146	PQDDQEVNELVEEYRLTVKESYCIF	
147	EVNELVEEYRLTVKESYCIFEDLEP	

#8 (C-terminal)	148	VEEYRLTVKESYCIFEDLEPDRCYQ
	149	LTVKESYCIFEDLEPDRCYQVWVMA
	150	SYCIFEDLEPDRCYQVWVMAVNFTG
	151	EDLEPDRCYQVWVMAVNFTGCSLPS
	152	DRCYQVWVMAVNFTGCSLPSERAIF
	153	VWVMAVNFTGCSLPSERAIFRTAPS
	154	VNFTGCSLPSERAIFRTAPSTPVIR
	155	CSLPSERAIFRTAPSTPVIRAEDCT
	156	ERAIFRTAPSTPVIRAEDCTVCWNT
	157	RTAPSTPVIRAEDCTVCWNTATIRW
	158	TPVIRAEDCTVCWNTATIRWRPTTP
	159	AEDCTVCWNTATIRWRPTTPEATET
	160	VCWNTATIRWRPTTPEATETYTLEY
	161	ATIRWRPTTPEATETYTLEYCRQHS
	162	RPTTPEATETYTLEYCRQHSPEGEG
	163	EATETYTLEYCRQHSPEGEGLRSFS
	164	YTLEYCRQHSPEGEGLRSFSGIKGL
	165	CRQHSPEGEGLRSFSGIKGLQLKVN
	166	PEGEGLRSFSGIKGLQLKVNLPND
	167	LRSFSGIKGLQLKVNLPNDNYFFY
	168	GIKGLQLKVNLPNDNYFFYVRAIN
	169	QLKVNLPNDNYFFYVRAINAFGTS
	170	LQPNDNYFFYVRAINAFGTSEQSEA
	171	NYFFYVRAINAFGTSEQSEAALIST
	172	VRAINAFGTSEQSEAALISTRGTRF
	173	AFGTSEQSEAALISTRGTRFLLRE
	174	EQSEAALISTRGTRFLLRETAHPA
	175	ALISTRGTRFLLRETAHPALHISS
	176	RGTRFLLRETAHPALHISSSGTVI
	177	LLRETAHPALHISSSGTVISFGER

#8 (C-terminal)	178	TAHPALHISSSGTVISFGERRRLTE
	179	LHISSSGTVISFGERRRLTEIPSVL
	180	SGTVISFGERRRLTEIPSVLGEELP
	181	SFGERRRLTEIPSVLGEELPSCGQH
	182	RRLTEIPSVLGEELPSCGQHYWETT
	183	IPSVLGEELPSCGQHYWETTVTDCP
	184	GEELPSCGQHYWETTVTDCPAYRLG
	185	SCGQHYWETTVTDCPAYRLGICSSS
	186	YWETTVTDCPAYRLGICSSSAVQAG
	187	VTDCPAYRLGICSSSAVQAGALGQG
	188	AYRLGICSSSAVQAGALGQGETSWY
	189	ICSSSAVQAGALGQGETSWYMHCS
	190	AVQAGALGQGETSWYMHCSSEPQRYT
	191	ALGQGETSWYMHCSSEPQRYTFFYSG
	192	ETSWYMHCSSEPQRYTFFYSGIVSDV

Acknowledgements

Firstly, I would like to express my sincere gratitude to my thesis adviser Prof. Friederike Cuello for her continuous support of my MD study and related research, for her patience, motivation, and immense knowledge. She continuously supervised this project with the highest passion and was always available in times of need.

The same gratitude belongs to my second supervisor on this project, Dr. Konstantina Stathopoulou. Her high scientific standards led to the results on which this thesis is built.

This work would not have been possible without the immense help of Angelika Piasecki. Her selfless effort in support of this and any other project of our group is unmatched.

Further thanks go to Nils Mangels, who helped acquiring images from ARVM that upgrade not just our knowledge about FHL2 and CMYA5 but also improve every presentation in a way that would not have been possible without him.

Also, many thanks to Prof. George Baillie and Jane Findlay from the Institute of Cardiovascular and Medical Sciences in Glasgow for their help with the peptide array.

I am grateful to the Institute of Experimental Pharmacology and Toxicology directed by Prof. Thomas Eschenhagen and especially to the AG Cuello for creating the most creative and supporting work environment possible and the financial support of my thesis.

Also, I want to thank the Deutsches Zentrum für Herz-Kreislaufforschung (DZHK) for financial and educative support of this project and for allowing me to travel to Glasgow and learn the method of peptide array on the spot.

I dedicate this work to my mother, who was my biggest fan and my toughest critic.

Lebenslauf wurde aus datenschutzrechtlichen Gründen entfernt

Eidesstattliche Versicherung

Ich versichere ausdrücklich, dass ich die Arbeit selbständig und ohne fremde Hilfe verfasst, andere als die von mir angegebenen Quellen und Hilfsmittel nicht benutzt und die aus den benutzten Werken wörtlich oder inhaltlich entnommenen Stellen einzeln nach Ausgabe (Auflage und Jahr des Erscheinens), Band und Seite des benutzten Werkes kenntlich gemacht habe.

Ferner versichere ich, dass ich die Dissertation bisher nicht einem Fachvertreter an einer anderen Hochschule zur Überprüfung vorgelegt oder mich anderweitig um Zulassung zur Promotion beworben habe.

Ich erkläre mich einverstanden, dass meine Dissertation vom Dekanat der Medizinischen Fakultät mit einer gängigen Software zur Erkennung von Plagiaten überprüft werden kann.

Unterschrift: